The links between the Seychelles- Chagos Thermocline Ridge and large scale climate modes and primary productivity; and the annual cycle of chlorophyll-a

Dilmahamod Ahmad Fehmi
DLMAHM001

Supervisors: Professor Chris Reason & Dr. Juliet Hermes

Submitted in the fulfilment of the requirements for the degree of
Master of Science (Ocean and Climate Dynamics)

Department of Oceanography

Faculty of Science

University of Cape Town

February 2014

PLAGIARISM DECLARATION

I know the meaning of plagiarism and declare that all of the work in the dissertation, save for that which is properly acknowledged, is my own. Aside from guidance from my supervisors, I have received no assistance, except as acknowledged.

SIGNATURE: _____

DATE: _____

Acknowledgement

The writing of this thesis has been one of the most significant academic challenges I have ever had to face. I would like to thank all people who have helped and inspired me during this project.

First and foremost, I would like to express my overwhelming gratitude to my supervisors Professor Chris Reason and Dr. Juliet Hermes. Their excellent guidance, supervision, valuable advice and support made this an enjoyable and challenging project.

I would like to thank Dr. Olivier Maury for providing me with the model output data and for helping me with my countless questions; and Jock Currie for his precious help with data and his guidance.

Much appreciation must go to Vincent Guri who remained extremely patient throughout innumerable questions of Matlab and guidance into scripts, besides good company and friendship.

Thank you to Lekraj Etwarysing, Mthetho Sovara, Beenesh Motah, my classmates, all those in Oceanography department at UCT and everyone else for the valuable discussions, kind assistance and awesome company during the writing-up of this thesis.

Most importantly, none of this would have been possible without the love and patience of my Dad and Mum, my little brother Zehree and my sister Rushda. Thank you for all the good conversations, (mostly over Skype) and for boosting me up. They have been a constant source of love, concern, support and strength all these years and I would like to express my heart-felt gratitude to them.

ABSTRACT

The Seychelles-Chagos Thermocline Ridge (SCTR) is a region of upwelling present at 55°E-90°E and 5°S-12°S in the southwest tropical Indian Ocean. It is a region of strong ocean-atmosphere interactions due to the high variability of the thermocline depth caused by the local Ekman pumping. Sea-viewing Wide Field-of-view Sensor (SeaWiFS) has shown high variability of surface chlorophyll-a (SChl-a) in the SCTR region. The Indian Ocean Dipole (IOD) and El Niño Southern Oscillation (ENSO) have also driven significant interannual variation of the depth of 20°C isotherm (D20) and SChl-a in the southern tropical Indian Ocean. A 50-years hindcast (RUN58-07) from a coupled bio-physical model was used to study the SChl-a concentration on an annual time scale and the interannual variability of D20 and SChl-a in the SCTR in response to IOD and ENSO events. Initial analysis revealed a high over-estimation of SChl-a in the 50-year run. Therefore, a 44-years hindcast (RUN58-01) of the same coupled model was taken into consideration. Comparisons with observations show that the RUN58-07 reproduces the D20 and SSH better than the RUN58-01 but the RUN58-01 shows better agreement with SeaWiFS. Results reveal that the SCTR exhibits an annual cycle of SChl-a concentration, with a peak in austral winter (June-August) due to the strong south-easterlies, increasing wind stirring and induced upwelling. Vertical sections of the SCTR also indicate that an increase in surface concentration in austral winter is compensated by a decrease in subsurface phytoplankton blooms. Composite figures show that IOD events exhibit a greater influence on the subsurface and surface variability in the SCTR region. The IOD deepens and shoals the D20 in the SCTR and eastern Indian Ocean respectively whereas ENSO displays a weaker and less-extensive influence on the D20. The spatial distribution of SChl-a in the Indian Ocean is completely disrupted by IOD during which the SCTR becomes oligotrophic whereas the eastern Indian Ocean becomes highly productive. ENSO, however, does not display any significant biogeochemical signature in the SCTR. This study should improve our understanding of the interannual variability of the thermocline depth and chlorophyll-a in the SCTR region; and for the optimization of the management of fishery resources and marine ecosystems.

Table of Contents

List of Figures

List of Tables

1 Introduction

The Seychelles Chagos Thermocline Ridge (SCTR), in the western Indian Ocean, is a region of upwelling which is known to be one of the centres of strong ocean-atmosphere interaction and it is characterised by a strong Ekman pumping. It is found between the latitudes 5°S and 12°S, and longitudes 55°E and 90°S. A deflection in the south-easterly trade winds over the equator during austral winter and the north-easterly winds during austral summer forms a cyclonic circulation which is responsible for this upwelling region (Vialard et al., 2009). Previous studies have demonstrated that the thermocline depth has strong variability and it is influenced by many factors such as westward-propagating oceanic Rossby Waves (Masumoto and Meyers, 1998; Hermes and Reason, 2008; Yokoi et al., 2008) and eastward-propagating Madden-Julian Oscillation on intraseasonal time scales (Duvel and Vialard, 2007). Oceanic and atmospheric variability at multiple time scales is frequent in the SCTR.

The variability of the SCTR can have significant impacts in many nearby regions. Annamalai et al. (2005) showed that the start of the Indian summer monsoon can be delayed by about 1 week if the sea surface temperature anomaly (SSTA) is positive in the SCTR, as this is associated with a slowing in the northward migration of the Inter-tropical Convergence Zone (ITCZ). Such a delay may influence climatic conditions in many countries in Asia (Vecchi and Harrison, 2004; Izumo et al., 2008; Yokoi et al., 2008). Rainfall in East Africa is also influenced by the variability of the SSTA in SCTR (Goddard and Graham, 1999; Black et al., 2003; Ummenhofer et al., 2009). Ocean variability in this region can also have a direct impact on the weather and climate, in particular cyclogenesis in the tropical South Indian Ocean (Jury et al., 1999; Xie et al., 2002; Malan et al., 2014). Hence, it is fundamental to investigate the physical processes taking place there.

Large-scale modes of climate variability such as the El Niño Southern Oscillation (ENSO) and the Indian Ocean Dipole (IOD) play an important role in the surface and subsurface variability in the Indian Ocean. These specific climate modes are known to influence the sea surface temperature (SST) and wind regimes in the Indian Ocean. Oceanic Rossby waves are also triggered during ENSO and IOD, hence influencing the thermocline depth in the SCTR. Therefore, it is essential to understand how the variability of the thermocline depth is impacted during and after El Niño-Southern Oscillation (ENSO) and Indian Ocean Dipole (IOD) events.

Studying the variation of primary productivity (chlorophyll-a) has become an important aspect of understanding and predicting the biological part of oceans. It is of the upmost importance since high primary productivity (high concentration of chlorophyll-a) will tend to attract more fish such as tuna, since food is abundant. The Southwest Indian Ocean (SWIO) is a region of relatively high biodiversity and has numerous important fish resources. Compared to the surrounding waters, in the upwelling SCTR region, deep nutrient-rich waters are brought to the euphotic zone, enhancing primary productivity, even though it is not as productive as coastal waters. However, the spatial distribution of the chlorophyll-a is disrupted during large scale climate modes (IOD and ENSO). This variability due to the forcing of the climate modes need to be understood so as to conserve and optimise the utilisation of fish stocks.

In this study, the impacts of the physics on the ecosystem will be considered and ultimately emphasis will be put on how the surface chlorophyll-a in the SCTR region varies on the annual time scale.

Primary productivity by marine phytoplankton is an indicator of marine ecosystem health and it support fisheries. Hence, this study will be of relevance for the successful management of the marine ecosystems and ecological processes in the region.

1.1 Research Aims

The aims of the study are to use both a coupled bio-physical model and remote sensing data to investigate the variability of the depth of the 20°C isotherm (D20; a commonly used proxy of thermocline depth in tropical waters) and surface chlorophyll-a (SChl-a) in the Seychelles-Chagos Thermocline Ridge (SCTR) during the Indian Ocean Dipole and El Niño Southern Oscillation events. The annual cycle of the SChl-a in the SCTR and its forcing will also be appraised.

1.2 Specific Objectives

- Validate the physical and biogeochemical part of the coupled bio-physical model (NEMO-PISCES) using remotely-sensed data from Archiving, Validation and Interpretation of Satellite Oceanographic data (AVISO); and Sea-Viewing Wide Field-of-view Sensor (SeaWiFS).

- Assess the variability of the upper layers of chlorophyll-a in the SCTR region on an annual time scale with an overview of its vertical distribution.

- Assess the annual cycle of D20 in the SCTR.

- Create composites of SST, D20 and SChl-a anomalies during pure positive and negative IODs and ENSOs events to investigate their impacts.

2 Literature Review

2.1 Indian Ocean

The Indian Ocean, compared to the Atlantic, Pacific and Southern oceans is the smallest one and has the highest mean sea surface temperature on Earth. Unlike the Atlantic and the Pacific Oceans, it is unique since it is land-locked by the presence of Asia as its northern boundary. The Asian landmass prevents northward heat export from the tropics to the high latitudes in the Indian Ocean unlike in the North Atlantic and North Pacific, but it does connect to the Southern Ocean in the south. Owing to this unique geography, there is an asymmetry in the Indian Ocean's structure and circulation (Qasim, 1998) which also drives the strong monsoon circulation. This monsoon cycle drives the seasonal evolution of the Indian Ocean's currents and the location of the upwelling regions (Hong et al., 2012). The interactions of the tropical Indian Ocean with the atmosphere influence the climate on both regional and global scales (Schott et al., 2009).

The wind system in the Indian Ocean north of about 15°S is entirely different from other oceans (Siedler et al., 2001). It is the only ocean which has westerly annual-mean winds on the equator. The equatorial thermocline is flat and deep due to the lack of steady equatorial upwelling resulting from these weak winds (Xie et al., 2002). However, upwelling occurs in the North Indian Ocean, more precisely off the coast of Somalia, Arabia and India and this usually occurs only during the summer monsoon; and in the Southern Hemisphere near the termination of the south-east trades as well as along the Sumatran/Javan west coast (Schott et al., 2002).

2.2 Oceanic Circulation in Indian Ocean

The main circulation of the Indian Ocean is shown in figure 1. The South Equatorial Current (SEC) is a westward flowing current which is largely supplied from the Indonesian Throughflow (ITF). At the east coast of Madagascar, it splits up to form the Northeast and Southeast Madagascar Currents (NEMC and SEMC). On approaching the coast of northern Mozambique, the NEMC splits into the Mozambique Channel eddy flow to its south and the northward flowing East African Coastal Current (EACC). The SEMC may also partly retroflect and generate eddies that may drift westwards towards the southern Mozambique Channel. The striking seasonal reversal of the Somali current can be observed when comparing Figure 1 with Figure 2. This drastic modification is due to the changes in the wind stress curl over the tropical Indian Ocean associated with the monsoon. Another seasonally reversing current is the Southwest/Northeast Monsoon Current south of India/Sri Lanka (Schott et al., 2009). During the austral winter (SW Monsoon), the Somali current flows towards the north which turns into a southward flow in austral summer (NE Monsoon). This southward flow of the Somali current then supplies the South Equatorial Countercurrent (SECC) which flows east across the whole Indian Ocean

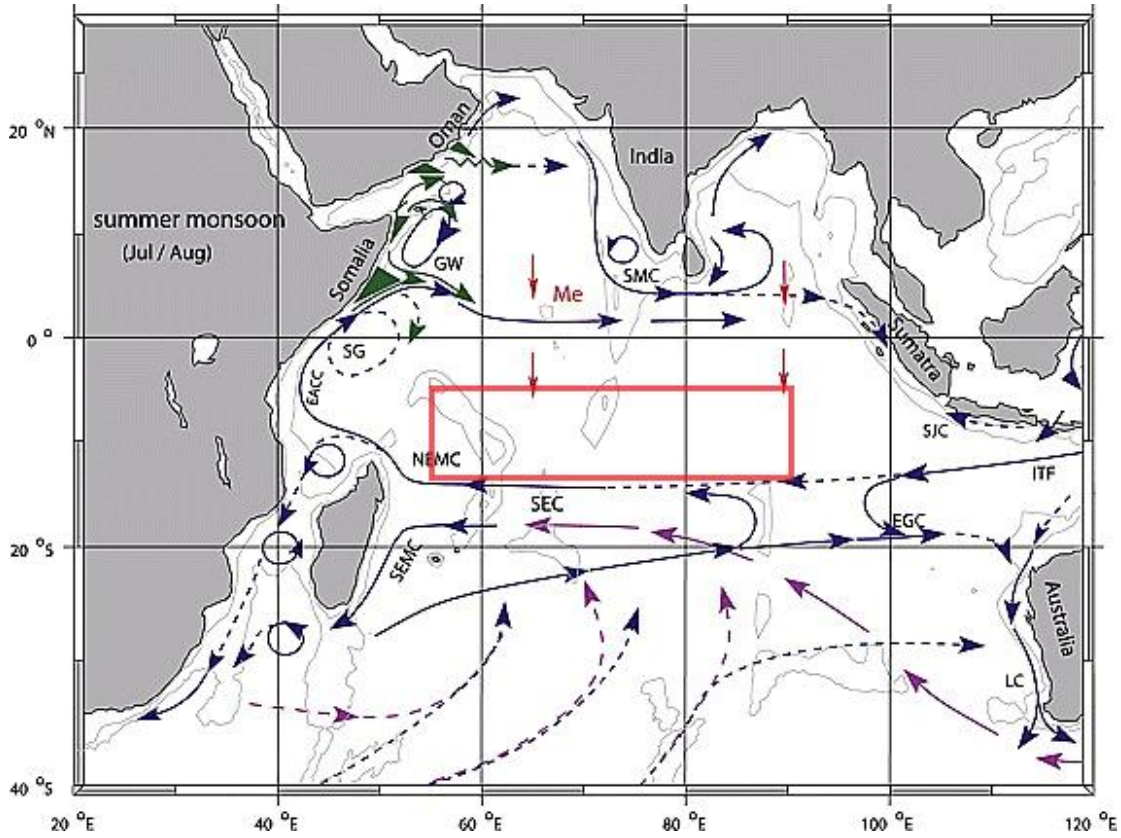

Figure 1: Schematic representation of identified current branches during the summer (southwest) monsoon. Current branches indicated are the South Equatorial Current (SEC), South Equatorial Countercurrent (SECC), Northeast and Southeast Madagascar Current (NEMC and SEMC), East African Coastal Current (EACC), Somali Current (SC), Southern Gyre (SG) and Great Whirl (GW) and associated upwelling wedges (green shades), Southwest and Northeast Monsoon Currents (SMC and NMC), South Java Current (SJC), East Gyral Current (EGC), and Leeuwin Current (LC). The subsurface return flow of the supergyre is shown in magenta. Depth contours shown are for 1000 m and 3000 m (grey). Updated representations are from SMC01; red vectors (Me) show directions of meridional Ekman transports. ITF indicates Indonesian Throughflow. The Seychelles-Chagos Thermocline Ridge (SCTR) is shown by the red box (Picture adapted from Schott et al., 2009).

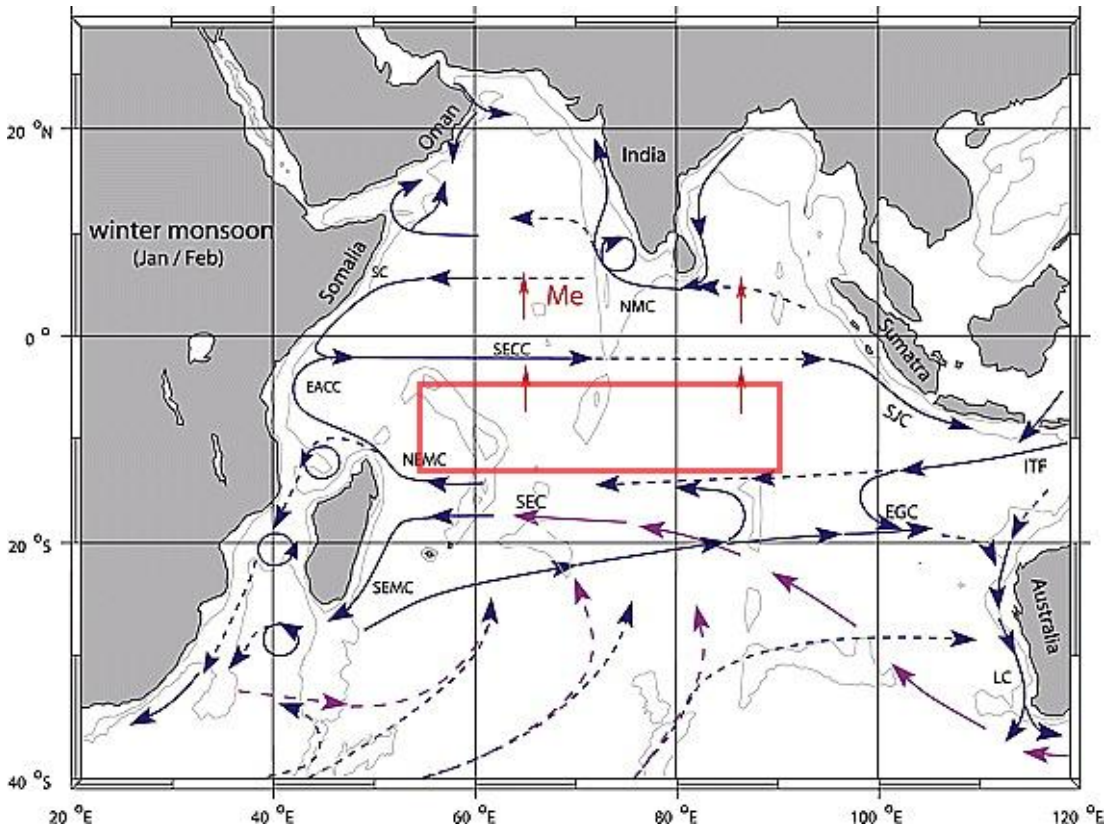

Figure 2: Same as figure 1 but for the winter (northeast monsoon) (Picture adapted from Schott et al., 2009).

2.3 Monsoonal Circulation of the tropical Indian Ocean

Studies of the monsoonal circulation of the wind stress fields in the tropical Indian Ocean have previously been done by Schott and McCreary (2001); and Tomczak and Godfrey (2003). South-easterlies are present throughout the year south of about 10°S except in austral winter where these extends further north and are stronger.

In austral summer, the south-easterlies only extend to around 13°S with monsoonal westerlies between 5°S and 11°S (Hermes and Reason, 2008). From March to May, the south-easterlies strengthen and shift northward. They reach their maximum strength and northward position during austral winter and in September to November, they remain strong.

However, in April and October, westerlies are present on the equator although they are not visible in seasonal means (Hermes and Reason, 2008).

2.4 Thermocline Domes in the world

The temperature of sea water typically decreases as the depth increases, except at high latitudes. The thermocline is a region where there is a rapid decrease of temperature over a relatively small change in depth. In some parts of the ocean, there are regions where the negative temperature gradient over a certain range of depth is larger compared to the surrounding areas, forming a thermocline dome or ridge. Such domes are present in all oceans over the world and they have been relatively well documented. For example, the Guinea Dome is found in the tropical North Atlantic Ocean at approximately 12°N, 22°W (e.g., Busalacchi and Picaut, 1983; Siedler et al., 1992; Yamagata and Izuka, 1995); the Angola Dome in the tropical South Atlantic Ocean at approximately 9°S, 9°E (e.g., Busalacchi and Picaut, 1983; Waconge and Piton, 1992; Yamagata and Iizuka, 1995); the Costa Rica Dome situated in the North Pacific Ocean at 9°N, 90°W (e.g., Umatani and Yamagata, 1991; Fiedler, 2002) and the Mindanao Dome which is located at 7°N, 130°E in the Pacific Ocean (e.g., Masumoto and Yamagata, 1991; Tozuka et al., 2002; Suzuki et al., 2005). Other studies have also proposed the presence of seasonal thermal domes in the northern Indian Ocean: the Sri Lanka dome and the Bay of Bengal dome (Vinayachandran and Yamagata, 1998), and a Peru dome in the South Pacific Ocean (Siedler et al., 1992). Figure 3 shows the location of some of these domes. They are usually shoaling upwelling in the west-east regions of an ocean except for the Mindanao dome which is located in the western northern Pacific Ocean (Hermes and Reason, 2008).

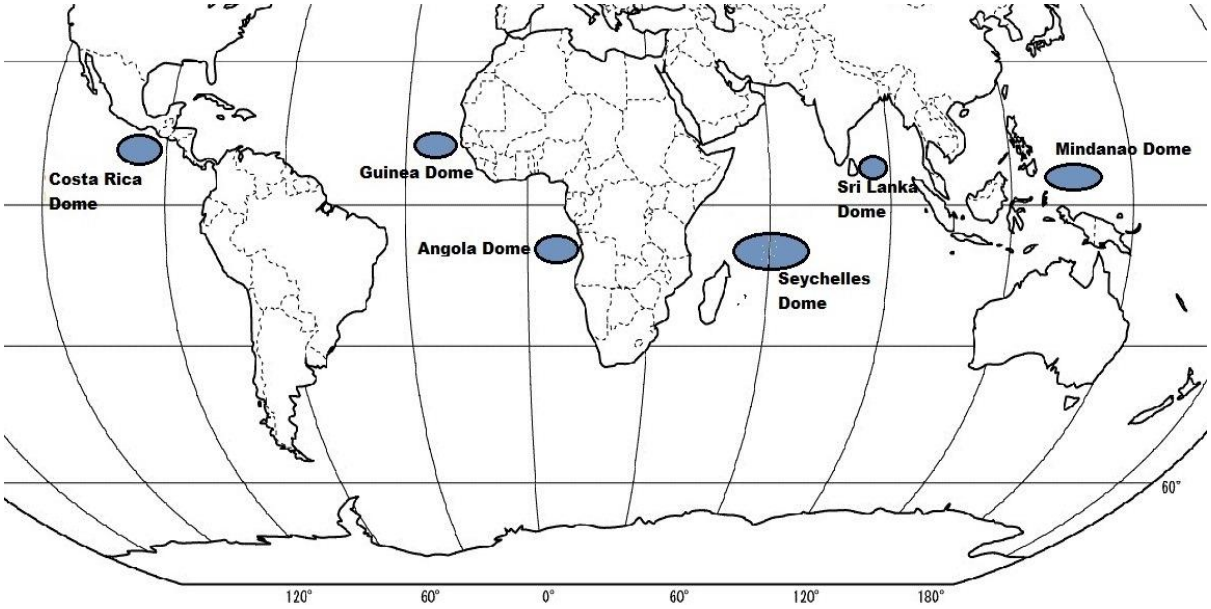

Figure 3: Location of thermocline domes in the world

2.5 Seychelles-Chagos Thermocline Ridge (SCTR)

During their research, Woodberry et al. (1989) and McCreary et al. (1993) were the first to establish that an upwelling region is present around the Republic of Seychelles in the southwest tropical Indian Ocean (SWTIO). It is found between the latitudes 5°S and 12°S, and longitudes 55°E and 90°S. Different names have been given to this specific area such as Seychelles Dome (SD; Yokoi et al., 2008), Seychelles-Chagos Thermocline Ridge (SCTR; Hermes and Reason, 2008) and the Thermocline Ridge of the Indian Ocean (TRIO; Vialard et al., 2009). However controversy existed as to whether this upwelling region forms part of a dome or part of a larger feature. Hermes & Reason (2008) showed that the thermocline has two regions of relative maximum which sometimes appear linked. The thermocline in the SCTR has also been shown to have strong seasonal and interannual variability. Recently, there has been increased interest in the SCTR region because the ocean-atmosphere interaction there can have significant climatic consequences (Goddard and Graham, 1999; Alexander et al., 2002; Black et al., 2003; Ummenhofer et al., 2009; Xie et al., 2009).

The surface winds and subsurface currents in the tropical South Indian Ocean play an essential role in the formation of SCTR. The south-easterly trade winds exhibit a striking reversal north of 10°S. In austral winter, they are deflected when crossing the equator and form the Somali jet along the East African highlands and feeding into the SW monsoon. In austral summer, a low-level westerly jet is formed between the equator and 10°S when the north-easterly monsoonal winds are deflected while crossing the equator. Where this flow converges into the south-easterly trades, cyclonic circulation wind stress curl occurs which is responsible for the formation of the SCTR (Hermes and Reason, 2008; Vialard et al., 2009). The surface currents also play an important role in the upwelling process in this region. To the south of the SCTR, the Ekman transport associated with the easterly-winds is southwards whereas that associated with the monsoonal westerlies to the north of the SCTR is northward. Thus, a surface current divergence in the upper ocean is induced by the wind stress curl and beta effect, leading to upwelling and a shoaling of the thermocline. On the other hand, the thermocline deepens whenever there is Ekman convergence since downwelling occurs.

A more detailed study of the SCTR including its annual cycle and its remote and local forcing was done by Hermes and Reason in 2008 using the Regional Ocean Modeling System (ROMS). The 20°C isotherm was used as a proxy for thermocline depth. One of the main outcomes was that the term "ridge" was more appropriate than "dome". This is because there are two main regions of upwelling with the most predominant one at 5°S-10°S, 45°E-60°E and the secondary region between 75°E-80°E; and these two domains are occasionally linked to each other. As a result, these authors suggested that the name 'Seychelles-Chagos Thermocline Ridge' was more appropriate (Hermes and Reason, 2008). The study showed that the SCTR is more pronounced in the western tropical Indian Ocean (between 50°E-60°E and 3°S-8°S) from December to March with the minimum depth of the thermocline being approximately 70m and that a secondary dome appeared in the eastern part (75°E-80°E) during March to May. From

June to August, a ridge is formed which link the two domes with shallower thermoclines in the west and as from September to November, the thermocline deepens in the south (7°S-10°S) but shoals in the north (3°S-7°S).

Major upwelling regions can generally be detected from the annual-mean sea surface temperature (SST) since they lead to a minimum in local SST. However this is not the case in the SCTR because the upwelled water does not reach the surface (Xie et al., 2002). Enhanced interannual variations of SST due to the shallow thermocline in the SCTR showed that a strong relationship exists between SST and thermocline depth. The shoaling and deepening of the thermocline influence the amount of upwelling and mixing and therefore the SST.

The seasonal variation of the SCTR is mainly controlled by semiannual forcing due to the two components of local Ekman upwelling. The first component is proportional to the planetary beta and the zonal wind stress and the other is proportional to the wind stress curl (Yokoi et al., 2008). Rossby waves have been well studied in the southern Indian Ocean and have been shown toinfluence the depth of the thermocline in the south west tropical Indian Ocean (SWTIO) (Masumoto and Meyers, 2008). Xie et al. (2002) showed that along 10°S, 64% of the total variance associated with Rossby waves is influenced by ENSO, while the cooling off the coast of Sumatra due to the IOD also contributes to the variability. Rao and Behera (2005) and Yu et al. (2005) used partial correlation analysis to study the Rossby waves north and south of 10°S. They found that north of 10°S, anomalous Ekman pumping related to IOD influence Rossby waves; whereas in the south, these are influenced by ENSO, especially after IOD events are terminated in December. These findings were supported by Currie et al. (2013). A study on the interannual variations of the SCTR by Hermes and Reason (2008) and Tozuka et al. (2010) showed that the arrival of downwelling (upwelling) Rossby waves and anomalous local Ekman downwelling (upwelling) cause the thermocline ridge to be anomalously weak (strong). These

studies indicated that Rossby waves as well as local Ekman upwelling play an important role in the SCTR.

2.6 El Niño Southern Oscillation (ENSO)

El Niño Southern Oscillation (ENSO) is a much studied large scale ocean-atmosphere interaction. It is the largest mode of interannual climate variability, influencing global weather and climate. An El Niño occurs about every 2 to 7 years in the tropical Pacific Ocean and it is distinguished from other climate phenomena by its predictability, strength and worldwide influence (Van Oldenborgh et al., 2005). It usually develops together with the Southern Oscillation which is an atmospheric pressure oscillation pattern across the tropical Indian and Pacific Oceans (McPhaden et al., 2006).

Air-sea interactions are key to El Niño which is characterised by anomalously warm surface waters in the central and eastern Pacific Ocean (Figure 4) associated with positive sea level anomalies and corresponding negative anomalies SST in the western Pacific Ocean. During an El Niño year, low pressure anomalies occur over northern Australia and Indonesia whereas high pressure anomalies form over the Pacific and western coast of South America. This causes the easterly winds to be reduced or sometimes reversed leading to the generation of downwelling Kelvin waves, a reversal in the pressure gradient in the upper ocean across the Pacific, and a relaxation of upwelling in the central and eastern parts. A positive feedback (Bjerknes feedback) allows SST anomalies in the central Pacific and westerly wind anomalies in the western and central Pacific to mutually strengthen. This positive feedback loop is counteracted by a delayed negative feedback (Jin and An, 1999), caused by the Sverdrup circulation associated with the change in zonal pressure gradient during ENSO which tends to induce an upper ocean divergence out of the equatorial stripe.

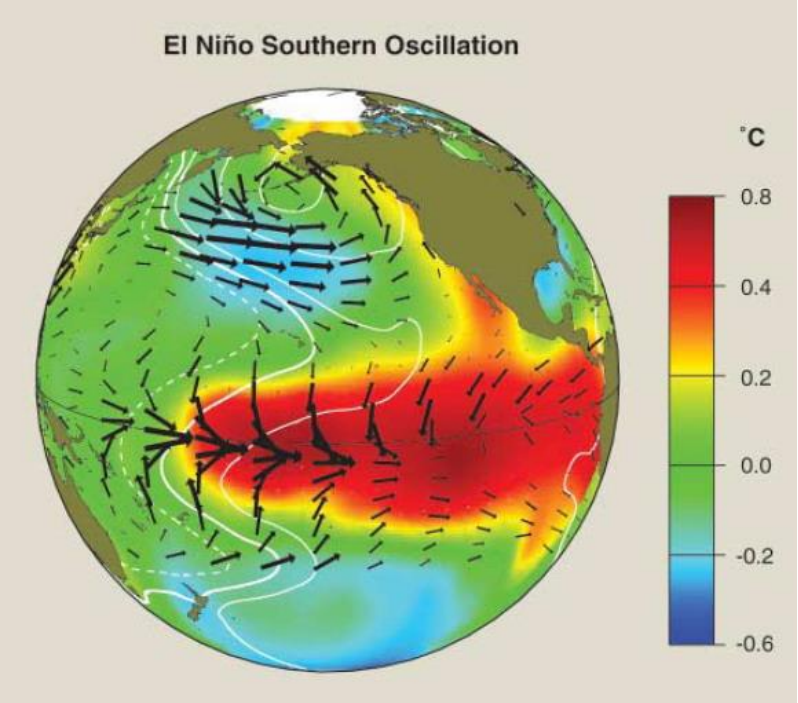

Figure 4: El Nino SST anomalies (colour shading), surface atmospheric pressure (contours), and surface wind stress (vectors) in the Pacific Ocean (McPhaden et al., 2006).

This shallows the thermocline and hence result in a phase change of ENSO. The rise of the thermocline in these specific regions initiates westward propagating deep ocean Rossby waves. When these waves reach Indonesia, they are reflected back as eastward propagating upwelling equatorial Kelvin waves which travel much faster compared to the Rossby waves. When these equatorial waves reach the eastern Pacific Ocean, they shoal the thermocline and hence, cold deep waters are upwelled. This process will therefore cool the surface temperature and shut off the El Niño event (Glebushko, 2004) and potentially trigger a La Niña event. The magnitude and duration of an ENSO event is controlled by the Bjerknes' feedback and Kelvin waves' propagation (McPhaden et al., 2006). It tends to be phase locked to the annual cycle beginning in April-May. Typically, it reaches its climax between November and December and dissipates by March-April of the next year (Trenberth, 1997; Vialard et al., 2009).

During ENSO years, the tropical convection changes and hence disturbs the atmospheric circulation. The eastward shift of the Walker circulation have direct effects on wind patterns,

near-surface air temperature, downward surface shortwave, and distribution of clouds and rainfall (Alexander et al., 2002) which eventually influence the SST, mixed layer depth (MLD) as well as ocean currents. This so-called atmospheric bridge causes a basin-wide warming of the Indian Ocean (Klein et al., 1999; Reason et al., 2000) and the North Atlantic Ocean (Enfield and Mayer, 1997).

Convection is reduced in the equatorial Indian Ocean and western Pacific Ocean during ENSO events. Anomalous westerlies and easterlies occur in the eastern Pacific Ocean and in the Indian Ocean respectively (Nigam and Shen, 1993; Klein et al., 1999; Lau and Nath, 2000) as well as related changes in branches of the Walker circulation (Venzke et al., 2000; Reason et al., 2000; Du et al., 2009). Changes in surface heat fluxes, especially cloud-induced solar radiation fluxes and wind-induced latent heat fluxes occur (Klein et al., 1999; Reason et al., 2000).

Anomalous anti-cyclonic wind stress curl is formed in the tropical south-eastern Indian Ocean during when El Niño reaches its mature phase (Schott et al., 2009). Owing to this forcing, a downwelling Rossby waves is formed, propagating westward from the south-eastern Indian Ocean (Perigaud and Delecluse, 1993; Masumoto and Meyers, 1998; Chambers et al., 1999). Previous studies have shown that this westward propagating Rossby waves cause the thermocline to deepen in the western Indian Ocean but this deepening is not as intense as it is during positive IOD since ENSO is known to mostly affect the thermocline depth south of 10°S (Rao and Behera, 2005; Yu et al., 2005; Xie et al., 2002).

2.7 Indian Ocean Dipole (IOD)

The sea surface temperature (SST) anomaly patterns due to ENSO are known to be one of the two distinct interannual SST variations in the tropical Indian Ocean (Pan & Oort 1983; Wallace et al., 1998; Saji and Yamagata, 2003**)**. When in its positive phase, the second type of variability consists of negative SST anomalies in the southeast tropical Indian Ocean (90°E-110°E and 0°-10°S) and positive SST anomalies in the western tropical Indian Ocean (50°E-70° and 10°N-10°S) and is known as the Indian Ocean Dipole mode (IOD) (Saji et al., 1999).

Prior to the discovery of the IOD, the Indian Ocean was believed to be mainly passive (Murtugudde and Busalacchi, 1999; Saji et al., 1999; Webster et al., 1999). The oceanic and atmospheric interactions of the IOD are distinctive; hence it is an independent mode of variability although it can often co-occur with ENSO (Yamagata et al., 2004; Schott et al., 2009). Compared to ENSO, IOD has a shorter lifetime which lasts approximately 6 months. Its signature starts to be visible in May-June, reaching its climax in October and decays by the end of the year (Saji et al., 1999). Hence, it is also seasonally phase-locked, in this case to the annual cycle of the Indian Ocean (Vinayachandran et al., 2002) and its seasonality itself suggests the influence of ocean dynamics (Schott et al., 2009).

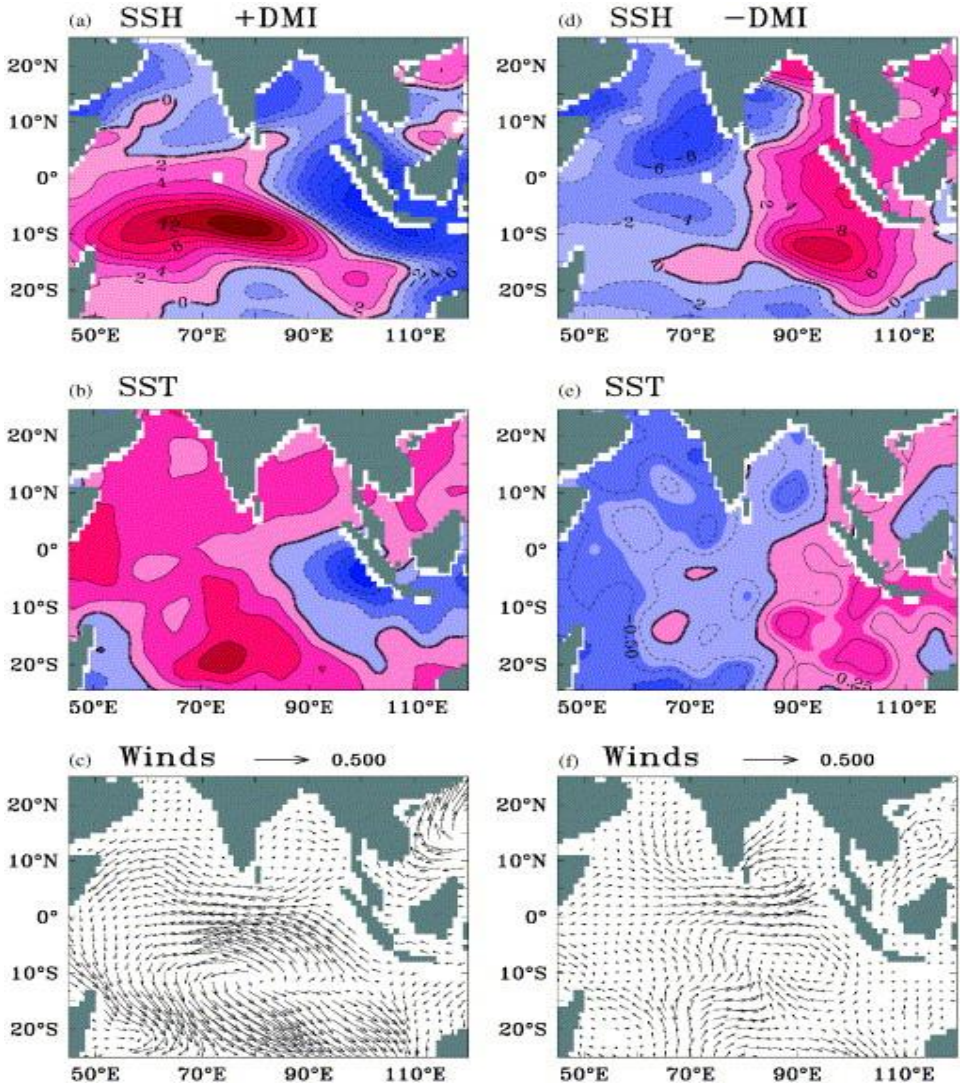

Figure 5: Composite anomalies during positive dipole mode events (left panels) (+DMI) and negative dipole mode events (right panels) (-DMI) Vinayachandran et al. (2002).

There exist positive and negative phases of the Indian Ocean Dipole mode (Vinayachandran et al., 2002) with a reversal in the SST anomaly pattern across the Indian Ocean. The SST anomalies during the positive phase of IOD are associated with equatorial easterly wind anomalies and alongshore wind anomalies off Sumatra favourable to upwelling (Figure 5; left panels). The changes in sea surface temperature involve different processes for the eastern part of the Indian Ocean compared to the western. Enhancement of the strong south-easterlies off the coast of Sumatra are responsible for the negative SSTA (Hong et al., 2008) by causing anomalous surface latent heat flux and vertical temperature advection (Li et al., 2002, 2003;

Drbohlav et al., 2007; Sun et al., 2010). However in the western Indian Ocean, easterly anomalies account for suppressed eastward transport and evaporation. Around 10°S, local upwelling is also restrained by the westward propagating Ekman ridge (Prasad and McCliean, 2004). These responses, together with meridional and vertical temperature advections, contribute to the above average SST in the western part (Li et al., 2002,2003; Drbohlav et al., 2007; Hong et al., 2008; Sun et al., 2010). However, the SST anomalies persist longer in the western part compared to the eastern part of the Indian Ocean during the IOD event.

Sea level anomalies also accompany the positive event with lower and higher than average sea surface height in the eastern and western part of the Indian Ocean respectively (Figure 5; left panels) (Chambers et al., 1999). During the negative phase, this pattern reverses although it is much weaker compared to the positive phase (Vinayachandran et al., 2002).

Figure 5 summarises the SST, sea surface height (SSH) and wind regimes during IOD events (Vinayachandran et al., 2002). Positive IOD events (left panels; 1997, 1994 and 1982) and negative events (right panels; 1996, 1993 and 1984) were chosen to make the observed September-November composite anomalies. The shades in reds show positive SST and SSH anomalies whereas those in blue show negative SST and SSH anomalies.

The zonal anomaly patterns in SST and SSH result from the easterly equatorial anomaly winds which raise the thermocline in the eastern part due to upwelling and deepen the thermocline in the western part, with off-equatorial Rossby wave responses also playing a role (e.g. Feng and Meyers, 2003; Murtugudde et al., 2000; Rao et al., 2002). Murtugudde et al. (2000) stated that eastward propagating Kelvin waves, formed by the equatorial easterly wind anomalies, also contribute to the shoaling of the thermocline off Sumatra.

Previous works have shown that the IOD has considerable impacts on both local and remote regions (Izumo et al., 2010; Yamagata et al., 2002). Saji et al. (1999) reported that the IOD

phenomenon is associated with precipitation anomalies and that it can cause severe floods and droughts in eastern Africa and Indonesia respectively. Birkett et al. (1999) also reported that during the positive IOD phase, there is anomalous convection and rainfall over the eastern Africa and western Indian Ocean.

However, using an ocean general circulation model and in situ upper-ocean temperature data, Suryachandra et al. (2001) showed that unlike the Pacific Ocean, SST variability in the Indian Ocean is controlled by ENSO whereas for subsurface variability, the dipole mode is dominant.

2.8 Primary Productivity

Phytoplankton are microscopic plants that form a key component of the marine ecosystem (Falkowski and Raven, 1997) and they are responsible for marine primary productivity (Hong et al., 2012). Through photosynthesis, they convert carbon dioxide to organic carbon, and hence they provide energy and fixed organic matter to the entire marine food web (Huan et al., 2006). An important pigment, chlorophyll-a, is responsible for phytoplankton photosynthesis and its concentration has been used as a proxy for marine primary biomass for decades (Chen and Gao, 2000).

Spatial and temporal distribution of Chl-a have become an important aspect in the study of the biology and biogeochemical processes of the oceans. Understanding the physical processes that are responsible for its variability is also fundamental since many coastal nations' economies depend on their biological productivity through fishery resources and marine industries (Schott et al., 2009). Spatial variability of phytoplankton will also modulate the population of zooplankton, and hence fish. This modulation will also affect the breeding of seabirds (Ramos et al., 2006; Monticelli et al., 2007).The launch of the SeaWiFS (Sea-Viewing Wide Field-of-view Sensor) satellite provided scientists with surface chlorophyll-a concentration data that has

led to the study of Chl-a concentration variability on a global scale. However, during the operating time of SeaWiFS (18th September 1997 to 11th December 2010), only two clear IODs and the well documented 1997/98 El Niño event have occurred. The study of Chl-a variability due to these climate modes has therefore been restricted (Meyers et al., 2007; Song et al., 2008). Fortunately, longer-term hindcasts of physical-biogeochemical models are helping with studies of seasonal and interannual variability with better resolution.

It is known that small variability in the mean sea surface temperature in the southern Tropical Indian Ocean (STIO) can significantly influence the regional biodiversity and climate (Schott et al., 2009). Two unique features of the Indian Ocean contribute to its distinctive biogeochemical processes as compared to the Pacific and Atlantic Ocean. It is land-locked in the northern part by Asia and this hinders the thermocline ventilation in the north. The second feature is the strong annual monsoon cycle that influences the ocean currents and the locations of upwelling (Hong et al., 2012). These physical responses induce a unique biogeochemical variability in the Indian Ocean (Wiggert et al., 2006). Interannual variability associated with ENSO and IOD strongly contributes to the basin-wide surface chlorophyll-a variability (Saji et al., 1999; Webster et al., 1999; Murtugudde et al., 2000).

The biogeochemical processes in the SCTR have received far less attention than the physical processes. Vinayachandran and Saji (2008) reported that during MJO events, entrainment of chlorophyll occurred from the deep chlorophyll maximum (DCM) (Kawamiya and Oschilies, 2001), and Jayakumar et al. (2011) who showed that an out-of-phase relationship exists between Ekman pumping and intra-seasonal cooling events in SCTR confirmed it. Resplandy et al., (2009) found that the surface blooms that occur in the SCTR during austral summer Madden-Julian Oscillation (MJO) events are not only due to the entrainment of chlorophyll from the subsurface but also from the entrainment of nutrients from the subsurface. During these events, the thermocline shoals bringing nutrient rich waters near the surface and causing

the mixed layer depth to shoal. Together with strong wind variations, these create the perfect condition for photosynthesis and ultimately surface blooms occur.

Ekman convergence formed between 3°S and 10°S and between 8°S and 15°S due to wind stress curl anomalies associated with IOD and ENSO forcing respectively generate Rossby waves that entrain phytoplankton to the surface during austral summer and this can be detected in global ocean colour data (Jayakumar and Gnanaseelan, 2012).

Currie et al. (2013) studied the variability of surface chlorophyll-a and integrated chlorophyll-a concentration in the Indian Ocean basin, with one of their study regions being the SCTR. They showed that during ENSO there is a weak and delayed biological response in the SCTR, with lower than normal integrated chlorophyll-a concentration. However, no significant signature is observed in surface chlorophyll-a. The most significant signature in SCTR occurs during IOD with negative anomalies of surface and integrated chlorophyll-a concentration. No clear asymmetry is observed between positive and negative chlorophyll-a anomalies, the most significant anomaly (negative) being related to IOD or co-occurring IOD and ENSO.

2.9 Research Questions

Many studies have been done regarding the physical (Xie et al., 2002; Masumoto and Meyers, 2008; Yokoi et al., 2008; Hermes and Reason, 2008; Tozuka et al., 2010) and biogeochemical aspects of the SCTR (Resplandy et al., 2009; Jayakumar and Gnanaseelan, 2012; George et al., 2012; Currie et al., 2013).

However, in spite of all these studies, the processes driving the variability of surface chlorophyll-a on an annual time scale has been investigated to some extent by Resplandy et al. (2009). This is fundamental since high chlorophyll content in a specific region plays a part in

attracting large fish such as tuna fleets and consequently, fishery resources will be optimized. However, it should be noted that the thermocline depth variations also influence the catch of large fish, as these can dive below the seine nets in the water is not too cold. It also acts as an indicator of marine ecosystem health; hence management of marine ecosystem and ecological processes will be successful.

During climate mode events such as the Indian Ocean Dipole and El Niño Oscillation, the circulation and properties, including chlorophyll-a concentrations, of the Indian Ocean are disturbed. Understanding how the chlorophyll-a patterns vary during these events is very important for fishery resources and marine ecosystems.

In order to achieve these goals, the following questions need to be addressed:

1. How does the surface chlorophyll-a concentration and its vertical distribution vary on an annual time scale in the Seychelles-Chagos Thermocline Ridge?

2. How are the 20°C isotherm and surface chlorophyll-a concentration influenced during large scale climate events such as El Niño Southern Oscillation (ENSO) and Indian Ocean Dipole (IOD)

3 DATA

Two runs of the same model have been used in this study. They are both based on the NEMO-PISCES model but they differ in some parameterizations and the resolution. One of the models has been run from 1958 to 2001, which we will refer as RUN58-01 and the other from 1958 to 2007, referred as RUN58-07.The framework of the NEMO-PISCES coupled model will first be described and ultimately the difference between the two runs.

3.1 Ocean model

The ocean general circulation model (OGCM) Nucleus for European Modelling of the Océan Parallélisé (OPA-NEMO) is the physical ocean model used in this study. The model is coupled to the dynamic-thermodynamic sea ice model developed at the University of Louvain – La Neve (Fichefet and Morales Maqueda, 1997). This global ORCA2 configuration has 30 vertical levels, from 10 m at the surface to a depth of 500m. In the first 125m, there are 12 depth levels. OPA-NEMO uses a free-surface formulation (Roullet and Madec, 2000) and it makes the Boussinesq and hydrostatic approximations.

Using the equation of state of Jacket and McDougall (1995), density is computed from potential temperature, salinity and pressure. Lateral mixing is performed along isopycnals. A turbulent closure scheme which is based on the vertical turbulent kinetic energy equation and which has been shown to perform well in the tropics (Blanke and Delescluse, 1993) has been used in the parameterization of vertical mixing.

Previous studies have been validated using both coupled modes (Lengaigne et al., 2006; Lengaigne and Vecchi, 2010) and uncoupled modes (Cravatte et al., 2007; Lengaigne et al., 2002) with different forcing strategies. Ocean structures such as currents, temperature and sea

level in the tropics and interannual variations of heat content in the Pacific Ocean (Lengaigne et al., 2012) have been accurately simulated by the OGCM, as well as the mixed layer depth (De Boyer Montégut et al., 2007; Keerthi et al., 2012) and sea level (Nidheesh et al., 2012) in the Indian Ocean.

The ocean general circulation model is coupled with the Pelagic Interaction Scheme for Carbon and Ecosystem Studies (PISCES) biogeochemical model (Aumont and Bopp, 2006; Aumont et al., 2008) which is derived from the Hamburg Model of Carbon Cycle version 5 (HAMOCC5) (Aumont et al., 2003). PISCES can replicate the marine biological productivity and the cycles of carbon as well as the main nutrients (Phosphorous, Nitrogen, Silicate and Iron). It was built on the assumption that growth of phytoplankton is directly restricted by availability in nutrients (Monod, 1942) and it was intended for a wide range of spatial and temporal scales, including global scale quasi-steady state simulations (Aumont and Bopp, 2006).

The model has 24 components as shown in Figure 6. It includes three non-living compartments which are semi-labile dissolved organic matter and two sizes (small and big) of sinking particles; and four living compartments which are represented by two phytoplankton size classes (nanophytoplankton and diatoms) and two zooplankton size classes (microzooplankton and mesozooplankton). The phytoplankton growth is limited by five nutrients namely nitrate (NO_3), ammonium (NH_4), phosphate (PO_4), silicate (SiO_4) and Iron (Fe). The ratios between C, N and P are kept constant at the values proposed by Takahashi et al. (1985) for all living compartments. The internal contents in Si of diatoms and Fe in both phytoplankton groups are prognostically simulated as a function of light level and external concentrations in nutrients (Aumont and Blopp, 2006). A modified version of the photoadaptation model by Geider et al.,

(1998) is used to model the Chl/C ratio. Constant elemental ratios of zooplankton are maintained.

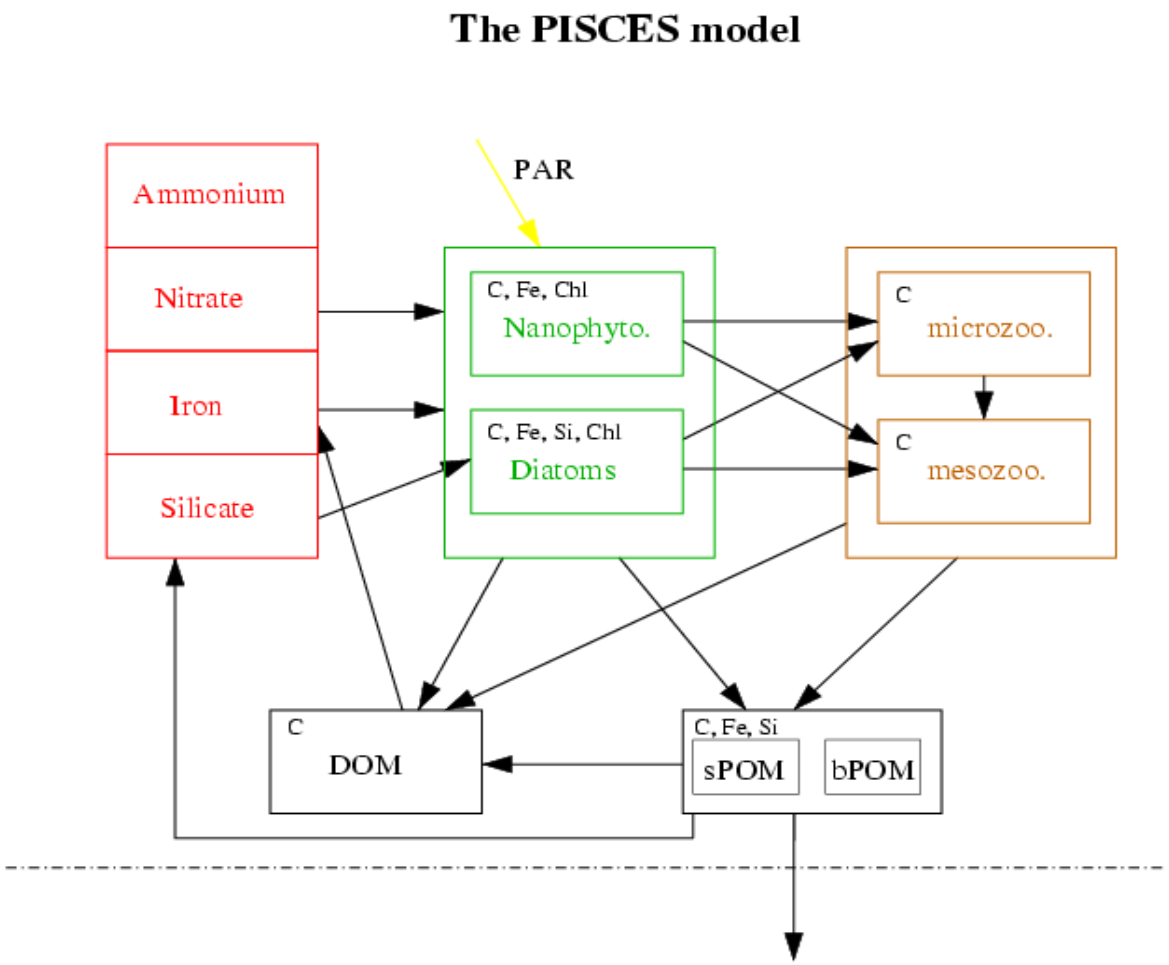

Figure 6: Architecture of PISCES (Aumont and Bopp, 2006)

Atmospheric dust deposition, rivers and sediment mobilization are the three different sources of nutrients and these are explicitly modeled. The model of Tegen and Fung (1995), assuming constant values for the iron content and solubility (Jickells and Spokes, 2001; Moore et al., 2004), simulate climatological monthly maps of dust deposition from which iron deposition from the atmosphere has been estimated. River discharge of carbon is taken from the Global Erosion Model (GEM) of Ludwig et al (1996). Fe, N, P and Si supplies are derived from the

same model output by taking constant Fe/P/N/Si/C river ratios. Hence there is no seasonal variation in supply of nutrients by rivers (Koné et al., 2009). The parameterization of nitrogen-fixation in PISCES is done using implicit formulation. It is based on the assumptions that nitrogen fixation requires temperatures above 20°C and iron and is restricted to areas with insufficient ammonium and nitrate. Further details about PISCES can be found in the supplementary materials of Aumont and Bopp (2006).

The physical model was initialized from rest using the World Ocean Atlas 2001 (Boyer et al., 2005) January climatology temperature and salinity fields. The biogeochemical model was initialized from outputs of simulation delineated by Aumont and Bopp (2006).

The surface boundary conditions of the physical model are driven by daily wind stress and wind speed from ER40 reanalysis (Uppala et al., 2005). Daily 2m air temperature from the National Centers for Environmental Prediction-National Center for Atmospheric Research (NCEP-NCAR) reanalysis (Kalnay et al., 1996); monthly climatologies of cloudiness (Berliand and Strokina, 1980) and relative humidity (Trenberth et al., 1989) were also applied. Using semi-empirical or bulk formulae, longwave radiation and surface heat fluxes as well as evaporation are computed (Goose, 1997).

Sea surface salinity (SSS) is maintained by taking freshwater fluxes from rain and river runoffs into consideration. Precipitation from the Climate Prediction Center Merged Analysis of Precipitation (CMAP; Xie and Arkin, 1997) and monthly values of river discharge (UNESCO, 1996) are applied. SSS is nudged towards monthly mean climatological values from the World Ocean Atlas (Boyer et al., 2005) to prevent artificial model drift.

The RUN58-01 is spun up for a 7-year period (1992-1998). An interannual simulation is then performed over 1958 to 2001with a temporal resolution of five days. It has a zonal resolution of 2° with a meridional resolution of 0.5° at the equator and larger at higher altitudes. Koné et

al., (2009) used the same model to study the controls (physical and biogeochemical) of phytoplankton seasonal cycle in Indian Ocean and showed that the model is able to replicate the seasonal cycle quite well when compared to SeaWiFS, including the onset of blooms there. The main processes which influence biological production in the Indian Ocean can therefore be said to be adequately resolved by the model.

Compared to the RUN58-01, the RUN58-07 has a horizontal resolution of 2°, increasing to approximately 1° over the Southern Ocean. They both have a temporal resolution of 5 days with 73 times-steps per year. In terms of parameterization, the representation of light limitation in the evolution of PISCES model used in this run has been modified compared to the one described in Aumont and Bopp (2006) and RUN58-01.The formulation of Geider et al. (1998) on which the influence the light limitation has on growth of nano-phytoplankton in PISCES is modified in this run by removing the nutrient co-limitation term and the dependence on temperature, in accordance to the findings of Li et al. (2010).

It can however be observed from the 'Results' section that there is an issue regarding the bathymetry of the RUN58-01 in coastal areas, hence the white cells. This is due to an error when the original outputs were interpolated but it did not affect the values of the variables in the remaining cells.

3.2 Observed Datasets

Remotely-sensed data provide the only observations of basin-wide biological variability (Wiggert et al., 2006). SeaWiFS was launched on 1st August 1997 and have provided ocean chlorophyll data from September 1997 to December 2010 for research in biogeochemical processes.

Monthly SeaWiFS Chlorophyll-a data were acquired from the Ocean Colour Website (http://oceancolor.gsfc.nasa.gov/) for the period September 1997 to December 2010. These are image representations of binned data products with a resolution of 9km. The data are in Hierarchical Data Format (HDF) and were used to create images using MATLAB. Chl-a concentration (mg/m^3) data will be used to validate the biogeochemical part of the coupled model.

Altimeters have been providing scientists with precise and accurate remote sensing data of sea level since October 1992 for the study of ocean dynamics. Satellite altimetry measures the time taken by an emitted radar pulse to travel from the satellite to the surface and back to the satellite receiver. Some processing involving the precise location of the satellite is then performed and this yields data on sea-surface heights. These data have been proved to be accurate to the order of 4 cm (Fu and Cheney, 1995).

In this study, altimeter data will be used to investigate how well the physical part of the model represents the region. Merged data of Absolute Dynamic Topography (MADT) and Mean Sea Level Anomaly (MSLA) were obtained from AVISO (Archiving, Validation and Interpretation of Satellite Oceanographic) website (http://www.aviso.oceanobs.com/en/). The data are in Network Common Data Form (NetCDF) format and images were created from these using Matlab.

The MADT is a gridded product (1/3° by 1/3°) of sea surface heights above geoid and is derived from Ssalto/Duacs Multimission altimeters (taken from Jason-1 and 2, TOPEX/Poseidon (T/P), Envisat, GEOSAT Follow-on (GFO, ERS-1 and 2, and Geosat satellites). The data period is from October 1992 to July 2012.

The MSLA is a gridded product of sea surface heights computed with respect to a seven-year mean. The data was taken from Envisat with the association Jason-1, T/P and GFO. The period is from October 1992 to July 2012.

El Niño Southern Oscillation (ENSO) and Indian Ocean Dipole (IOD) are the two main large scale climate modes investigated in this study. The ENSO index used is Niño 3.4 (5°S-5°N; 170°W-120°W) and was extracted from the Climate Prediction Center of National Oceanic and Atmospheric Administration (NOAA). These are monthly sea surface temperature anomalies in the Niño 3.4 region from 1950-present and are based on the Extended Reconstructed Sea Surface Temperature (ERSST) v3b data.

The IOD index was acquired from the KNMI Climate Explorer website (http://climexp.knmi.nl) which collects climate data and provides analysis tools. The Dipole Mode Index (DMI) is the difference between the SSTA in the western (50°E-70°E, 10°S-10°N) and eastern (90°E-110°E, 10°S-0°N) Indian Ocean (Saji et al., 1999). The data are monthly from March 1958 to August 2008 and was from HadISST1 (Hadley Centre's sea ice and sea surface temperature data set).

Data for the Mixed Layer Depth (MLD) was acquired from the Ifremer/Los Mixed Layer Depth Climatology website (http://www.ifremer.fr/cerweb/deboyer/mld/home.php). The MLD is estimated from a fixed threshold on temperature profiles obtained from ARGO floats, World Ocean Database 2009 (WOD09), World Ocean Circulation experiment (WOCE), Research Moored Array for African-Asian-Australian Monsoon Analysis and Prediction (RAMA) and Tropical Atmosphere Ocean Project (TAOP). The criterion used is as follows: "MLD_DT02 = depth where ($\theta = \theta 10m \pm 0.2$ °C)". The data has a regular 2°C × 2°C grid and are monthly data from 1969 to 2009 (Keerthi et al., 2012)

Nutrient concentration data (Nitrate and Silicate) were acquired from the World Ocean Atlas 2005 (WOA05) which are analysed (1° grid) climatological data of in situ measurements at standard depths for different time scales (monthly, seasonally and annually). Associated statistical fields of observed oceanographic profile data interpolated to standard depth levels on both 1° and 5° grids are also included.

4 METHODOLOGY

In this study, the depth of the 20°C isotherm (D20) has been chosen as a proxy for the thermocline. 20°C was chosen to remain consistent with previous studies (Vinayachandran et al., 2002; Hermes and Reason, 2008). The depth of the 20°C isotherm was estimated by finding the level at which the temperature is closest to the 20°C criterion. The concentration of chlorophyll-a (Chl-a) was calculated as the sum of chlorophyll in the two phytoplankton size classes namely diatoms and nano-phytoplankton. During this study, the surface chlorophyll was mostly taken into consideration and denoted by SChl-a (units: mg m^{-3}). SChl was obtained by averaging the chlorophyll-a concentration over the two upper layers of the model (i.e. 20 m depth) (Currie et al., 2013) and eventually used for comparison with remotely-sensed data (SeaWiFS).

The mean seasonal cycle over a specific time interval was subtracted from the monthly time series of all the physical and biogeochemical variables to obtain their specific de-seasoned anomalies.

It should be noted that initial analysis was carried out using the RUN58-07 but it eventually became apparent that it was necessary to do the analysis on both runs (RUN58-01 and RUN58-07) as the RUN58-07 showed high over-estimation of SChl-a in the Indian Ocean when compared on the same time period as the RUN58-01 and remotely-sensed data (SeaWiFS) (Figure 30 in Appendix).

El Niño Southern Oscillation (ENSO) and Indian Ocean Dipole (IOD) were used as large scale climate modes to study their influence on the physical and biogeochemical variables. Their specific standard indices were used to represent their interannual signal. ENSO is characterised by the sea surface temperature (SST) anomalies over the Niño 3.4 region (120°W-170°W, 5°N-5°S) in the Pacific Ocean whereas the IOD is characterised by the dipole mode index (DMI;

Saji et al., 1999) calculated as the difference in SST anomalies between the western (50°E-70°E, 10°S-10°N) and eastern (90°E-110°E, 10°S-0°N) equatorial Indian Ocean. Indices for both climate events were created from the coupled physical-biogeochemical model to be compared with indices created from observational data. However, ENSO and IOD indices have a strong correlation of approximately 0.53 for September-November between them and this makes it difficult to isolate any signal associated with only one of these climate modes (Yamagata et al., 2004). Therefore, pure positive (negative) Indian Ocean Dipole and positive (negative) El Niño Southern Oscillation years are taken into consideration to study the variability of the 20°C thermocline depth and the SChl-a in the SCTR. A positive (negative) pure IOD is identified as an event when El Niño (La Niña) does not co-occur. The same applied for a positive (negative) pure ENSO which do not co-occur with a positive (negative) IOD. These pure years of IOD and ENSO were obtained from Yamagata et al. (2004) and are summarised in the table below.

Table 1: Years of pure positive (negative) IOD and ENSO

	Years of positive El Niño	Years of negative El Niño	Years of positive IOD	Years of negative IOD
1	1965	1967	1961	1960
2	1969	1971	1967	1989
3	1976	1973	1977	1992
4	1986	1975	1994	1996
5	1991	1988		

In total, 5 pure positive (negative) ENSO and 4 pure positive (negative) IOD were identified over a time period of 1960-2007 as shown in Table 1.

For this study, the whole Seychelles-Chagos Thermocline Ridge (SCTR) region was divided into 3 sub-regions, namely sub-region 1 (5°S-12°N, 55°E-65°E), sub-region 2 (5°S-12°N, 65°E-75°E) and sub-region 3 (5°S-12°N, 75°E-90°E). This was done since the SCTR has a large spatial distribution (55°E-90°E) and during extreme climate events such as IOD and ENSO, the eastern part of the SCTR exhibits completely different physical and biological mechanisms compared to the western part. Figure 7 below shows how the SChl-a anomalies vary from one sub-region to another during the strong 1997-1998 ENSO/IOD.

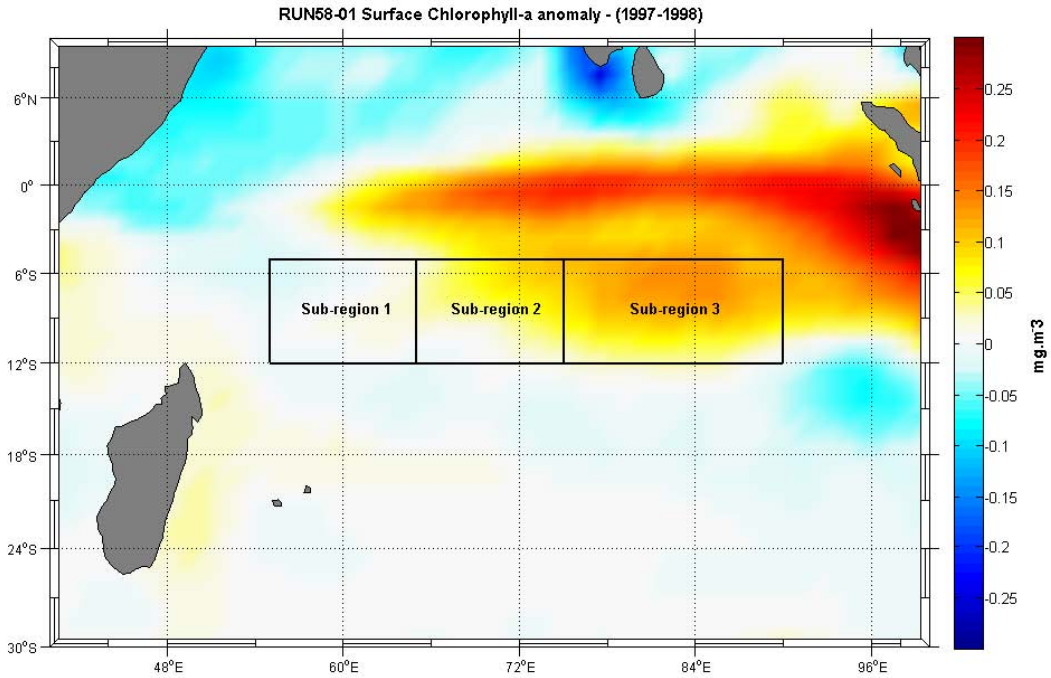

Figure 7 : SChl-a anomalies (mg-Chl/m^3) from the RUN58_01 model in the southern tropical Indian Ocean over a time frame of 2 years (1997-1998). The 3 sub-regions superimposed are super-imposed on the figure. The anomaly was calculated over a 1990-2001 climatology.

It can be observed that a positive SChl-a anomaly arises in sub-region 3, a slight positive anomaly in sub-region 2 whereas sub-region 1 exhibits a minor negative anomaly. This shows how the biogeochemical variable is contrasting in the SCTR region. It has a strong variability and this is why it has been split into three distinct sub-regions.

The comparison between RUN58-01 and RUN58-07 will also be investigated in this study. However, only the physical (SSH, D20 and MLD) and biogeochemical variable (SChl-a) used in this study will be taken into consideration.

5 MODEL VALIDATION

5.1 Physical Model

In the tropics, the thermocline depth oscillations are generally reflected in the SSH variations and they are often a mirror-image of each other. Hence, SSH has been used as a proxy for thermocline depth in previous studies (Susanto et al., 2007; Polo et al., 2007; Grodsky et al., 2007).

In this study, remotely-sensed SSH data from AVISO were used to see how well the physical variables, namely SSH and thermocline depth (D20), of the two runs (RUN58-01 and RUN58-07) are resolved. The seasonal cycle of sea surface height anomalies (SSHA) was constructed from altimetry data and then compared to the seasonal cycle of SSHA of the two different runs (Figure 8). The cycles were calculated using monthly climatology over a time period of 9 years (1993-2001) for both the two models and altimetry data.

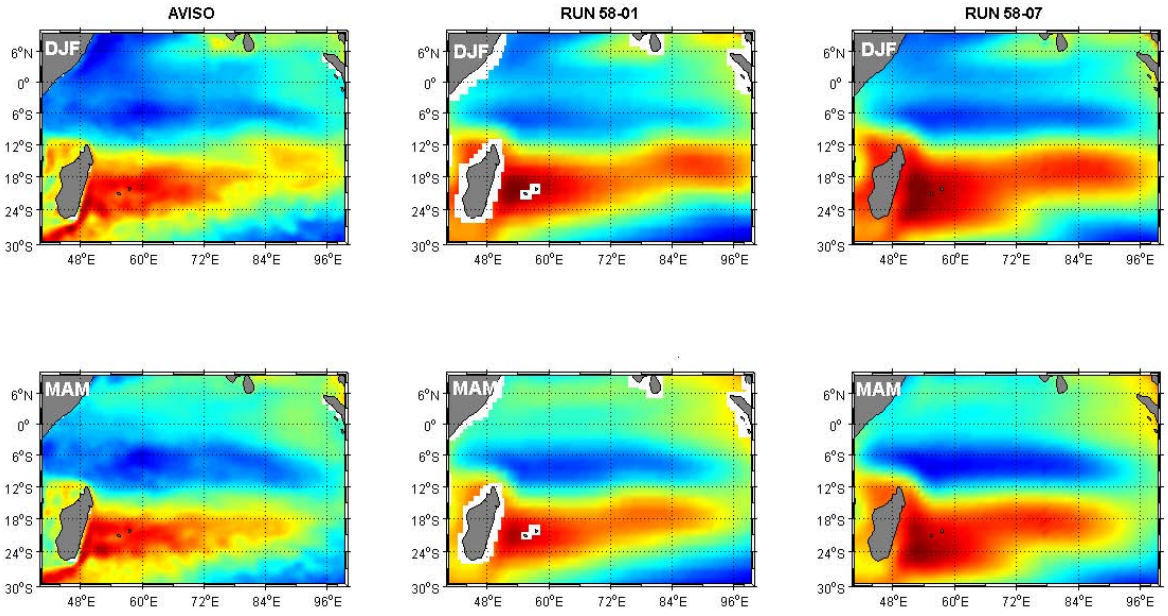

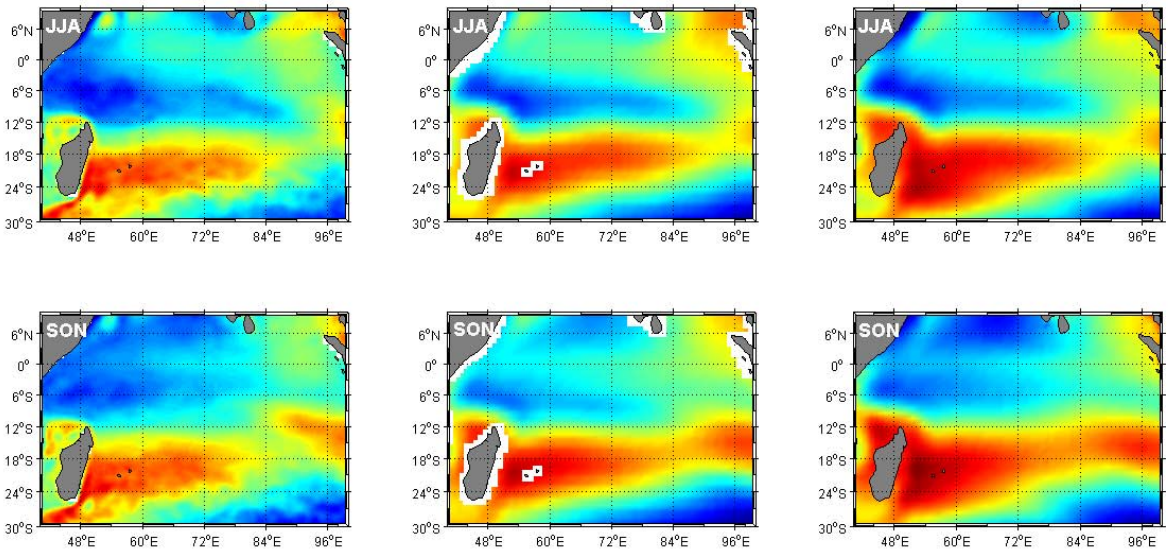

Figure 8: Seasonal cycle of Sea Surface Height (SSH) Anomaly (cm) from Altimetry data (Left Panels), RUN58-01 (Middle Panels) and RUN58-07 (Left Panels) from 1993 to 2001.

A slight under-estimation of the SSH can be observed in the north-western part of the Indian Ocean (6°S-6°N, 40°E-60°E) in the two runs, with the RUN58-01 exhibiting a greater under-estimation compared to the RUN58-07. In the north-eastern part of the Mozambique Channel, an over-estimation of the SSH can be observed in the two runs. It is interesting to note that the runs do not pick up the East Madagascar Current (EMC) also. Overall, the two runs shows agreement with the remotely-sensed data although as expected, the features are smoother in the model due to the 1/3° resolution altimetry data compared to the 1/2° resolution for RUN58-01 and 2° resolution for RUN58-07. In the two runs, the negative SSH anomaly identified by Donguy and Meyers (1995) can be observed between the latitudes 5°S-9°S.

The time series of SSHA in the specific region of SCTR (5°S-12°S, 55°E-90°E) was also constructed for the two runs and altimetry data from January 1993 to December 2001. The anomalies were calculated with respect to the 1993-2001 climatology for all sets of data.

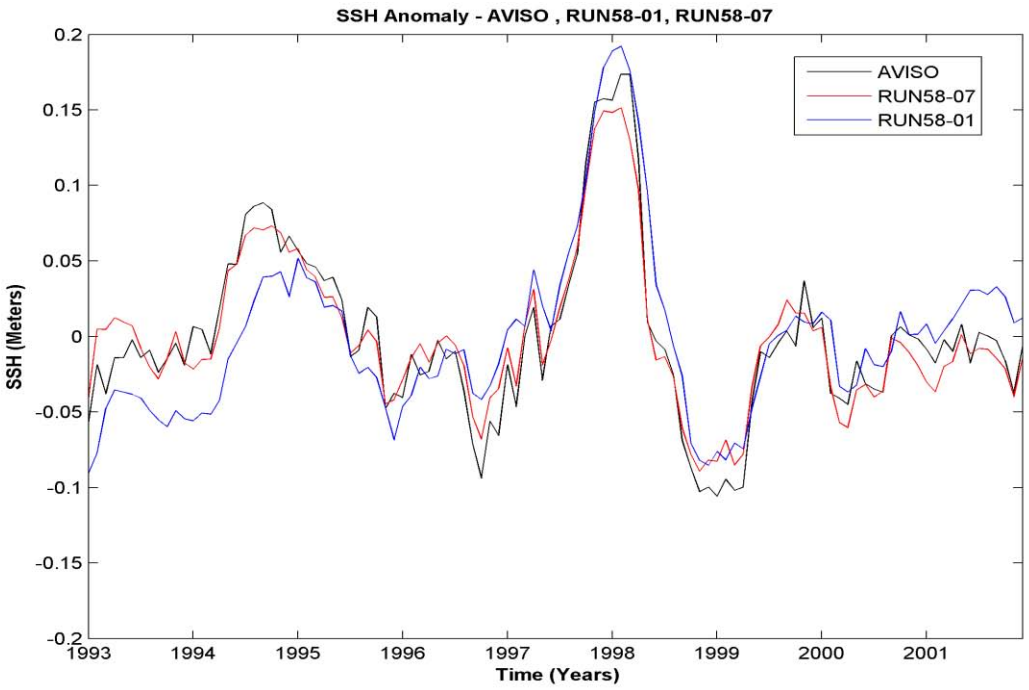

Figure 9: Time series of de-seasoned anomalies of SSH of remotely-sensed data (black), RUN58-07 (red) and RUN58-01 (blue) over the whole SCTR region (5°S-12°S, 55°E-90°E) from January 1993 to December 2001.

The SSHA from RUN58-01 exhibits an under-estimation during the first 3 years and an over-estimation from mid-1996 to the end of 2001 compared to AVISO data. However, they have a correlation coefficient of 0.8470 at the 99% significance level.

RUN58-07 shows a slight under-estimation during the last 2 years but in general, the time series of altimetry SSHA agree with the SSHA of RUN58-07 with a high correlation coefficient of 0.9715 at the 99% significance level.

The time series of the 20°C isotherm depth (D20) anomaly from the two runs was superimposed on Figure 10, with an inverted y-axis, to be compared with the SSHA from AVISO.

The depth of the 20°C isotherm for RUN58-01 correlates well with the SSHA from AVISO with a negative correlation coefficient of -0.8969 at 99% significance level. The RUN58-07

seems to correlate better with AVISO data with a high negative correlation of -0.9547 at 99% significance level.

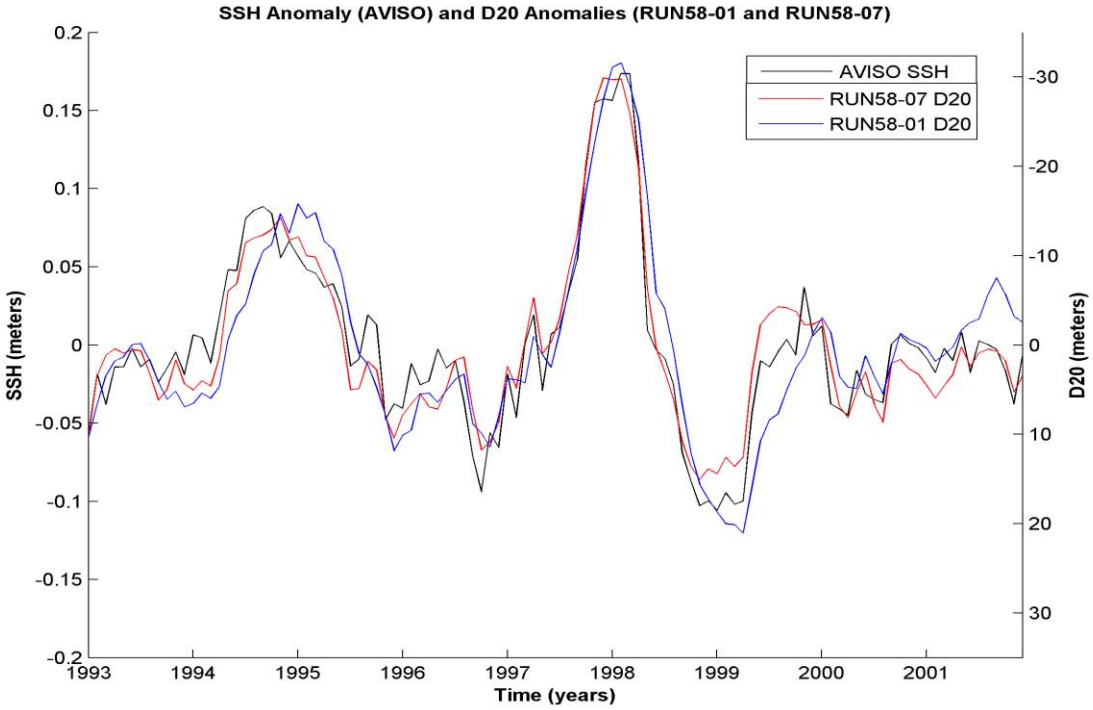

Figure 10: Time series of SSH anomaly of remotely-sensed data (black) with the depth of the 20°C isotherm from RUN58-07 (red) and RUN58-01 (blue) superimposed over the figure with an inverted y-axis. These were calculated over the whole SCTR region (5°S-12°S, 55°E-90°E) from January 1993 to December 2001.

This agrees with the study on the relationship between sea level and stratification in the tropics by Carton et al. (1996) where they suggest that an increase in sea level by 1-2 cm is reflected in a deepening of the thermocline by 2-4 m. The deepening of the thermocline during the 1997-1998 ENSO/IOD can be observed in the figure.

Based on the similarity of the dominant features of SSHA (Figure 8), the strong positive correlation of SSHA between the runs and observations (Figure 9); and the strong negative correlation between SSHA of AVISO and depth of 20°C thermocline from the runs (Figure

10), the coupled model seems to capture the main features and variability of the SCTR reasonably well.

5.2 Biogeochemical Model

Figure 11 shows the mean seasonal variability of SChl-a concentration in observations and the two runs over the same time frame (1998-2001). It can be observed from the figure that the chlorophyll patterns from the two runs are much smoother and that they generally overestimate the chlorophyll in the tropical/subtropical Indian Ocean in austral winter and spring.

From December to February (DJF), elevated SChl-a concentration are observed in the north-western part of the Arabian Sea whereas oligotrophic conditions prevail in the south-eastern part of the Arabian Sea and Southern Hemisphere. These features are comparatively well reproduced in both runs although the spatial distribution is overestimated to some extent in the Arabian Sea and off Somalia. However, in the Bay of Bengal, RUN58-07 overestimates both the intensity and the spatial distribution of SChl-a. RUN58-01 exhibits high phytoplankton blooms around Sri Lanka and this is not the case in observations and Run 58-07.

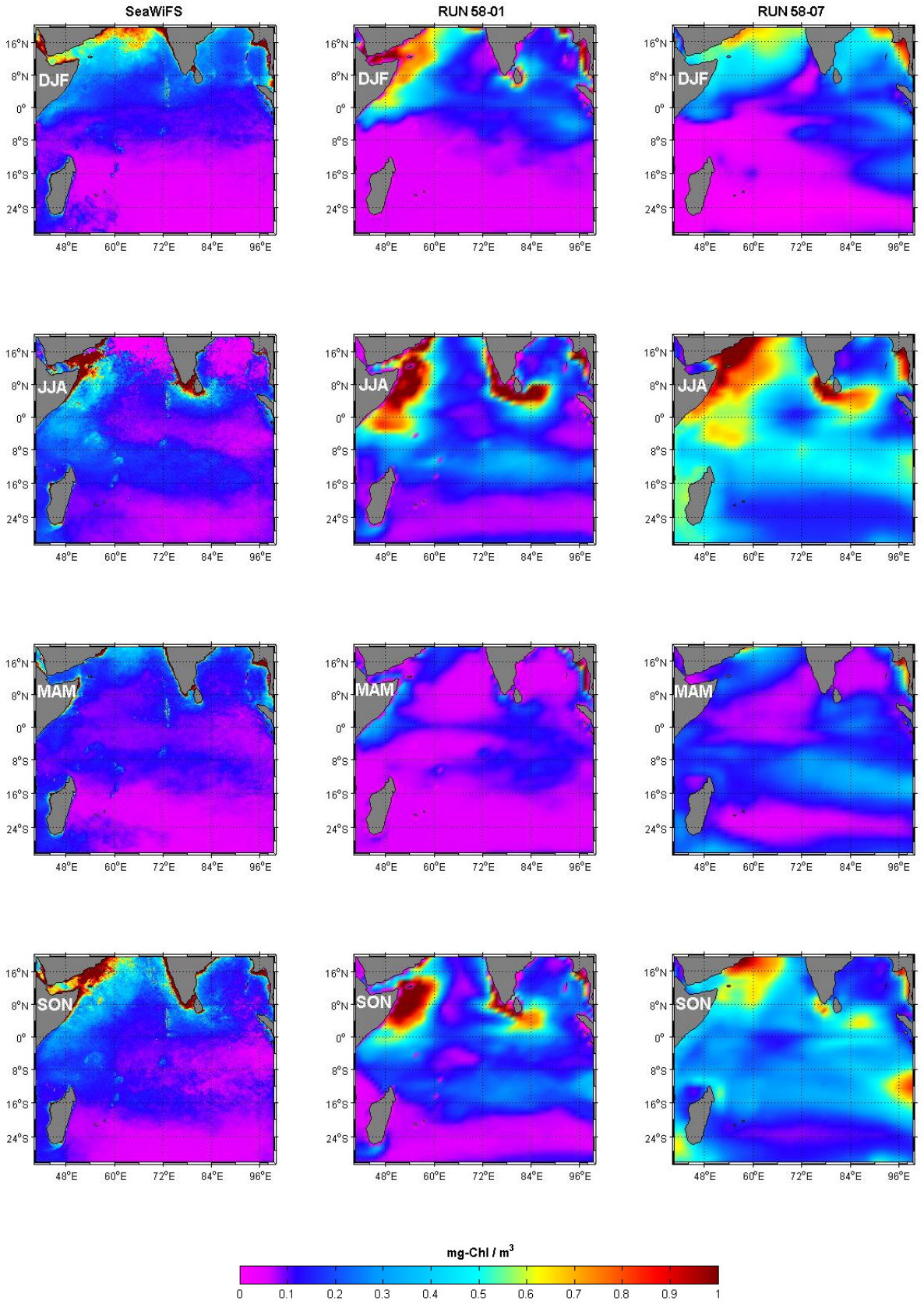

Figure 11: Seasonal evolution of surface Chlorophyll-a (mg-Chl /m^3) pattern from SeaWiFS (Left Panels), the RUN58-01 (Middle Panels) and the RUN58-07 (Right Panels). The seasonal cycle was calculated over the 1998-2001 for the SeaWiFS as well as the two models.

Relative to DJF, a decrease in chlorophyll for the two runs and observations can be observed in most regions of the Indian Ocean basin from March to May (MAM). These oligotropic conditions are likely due to less wind stirring, increased stratification and reduced Ekman pumping. However, a high chlorophyll signature can be seen in RUN58-07 in the southeastern tropical Indian Ocean which is not the case in SeaWiFS data.

During the southwest monsoon and the intermonsoon seasons (JJA and SON respectively), the runs simulate higher magnitudes of chlorophyll in the eastern part and open ocean of the Indian Ocean compared to observations, particularly RUN58-07. Along the coasts of Somalia and the Arabian Peninsula, the southern tip of India and Sri Lanka, the runs seem to overestimate the spatial distribution of phytoplankton blooms. Although the spatial distribution and magnitude of SChl-a concentration are over-estimated in both runs, they do capture the major features of the observations. Nonetheless, RUN58-01 shows better overall agreement with SeaWiFS data compared to the RUN58-07, which largely overestimates the SChl-a content in austral winter and spring.

The monthly climatology of SChl-a concentration was computed from the two runs and observations in each of the 3 sub-regions of the SCTR over the same time interval (1998-2001). Observations reveal that Chl-a has an annual cycle in all 3 sub-regions, with a peak in concentration in June-August, although the cycle is weaker in the eastern sub-region 3 (Figure 12).

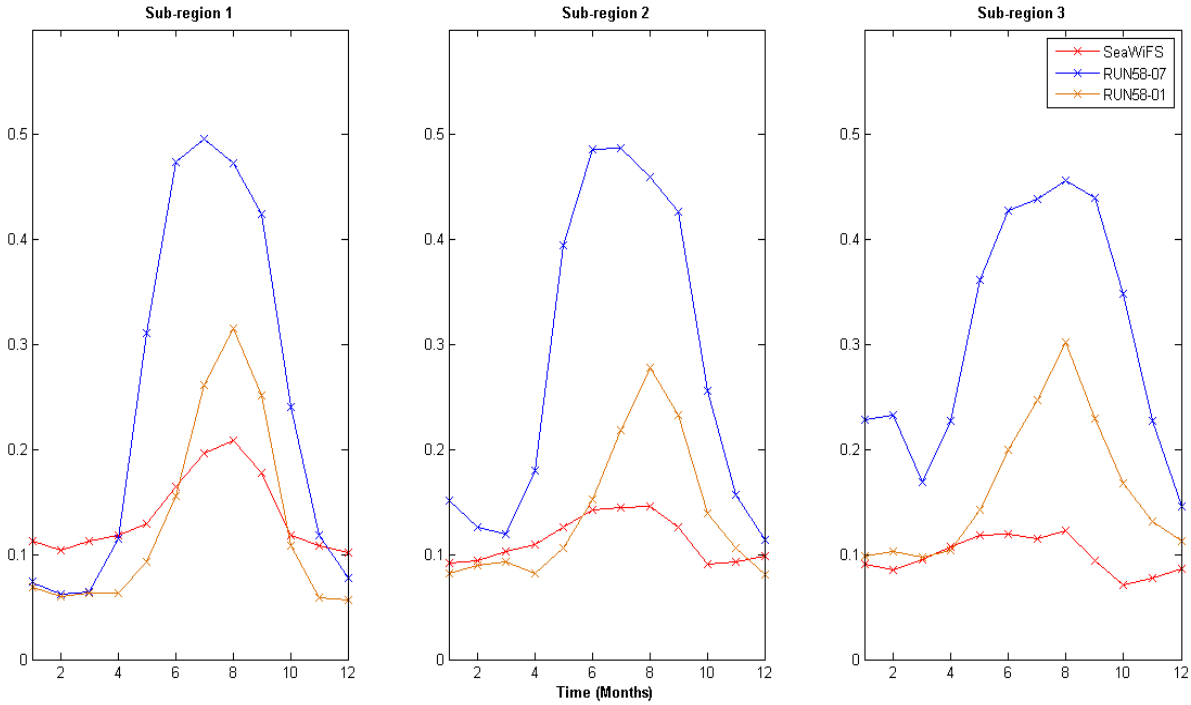

Figure 12: Monthly Climatology of SeaWiFS (red), RUN58-01 (Orange) and RUN58-07 (Blue) surface Chl-a (mg-Chl/m^3) over sub-regions of the SCTR. The climatology for all of them was calculated over a period of 1998-2001.

In the western part of the SCTR, RUN58-01 under-estimates the SChl-a from October to June and over-estimates the concentration from July to September. RUN58-07 shows an under-estimation in surface concentration from December to April but a large over-estimation from May to November. In the central part of the SCTR, RUN58-01 over-estimates the surface blooms from June to November whereas RUN58-07 exhibits an over-estimation throughout the year. However, in the eastern part, both runs display an over-estimation throughout the year with a higher estimation in RUN58-07.

RUN58-01seems to reproduce a better seasonal cycle of SChl-a and is more closely related to observations than the RUN58-07.

The SChl-a content is obtained from the addition of chlorophyll from diatoms and nano-phytoplankton. Hence, in Figure 13, the concentrations of the two variables were investigated separately to understand their variability and their relationship with the over-estimation in both runs.

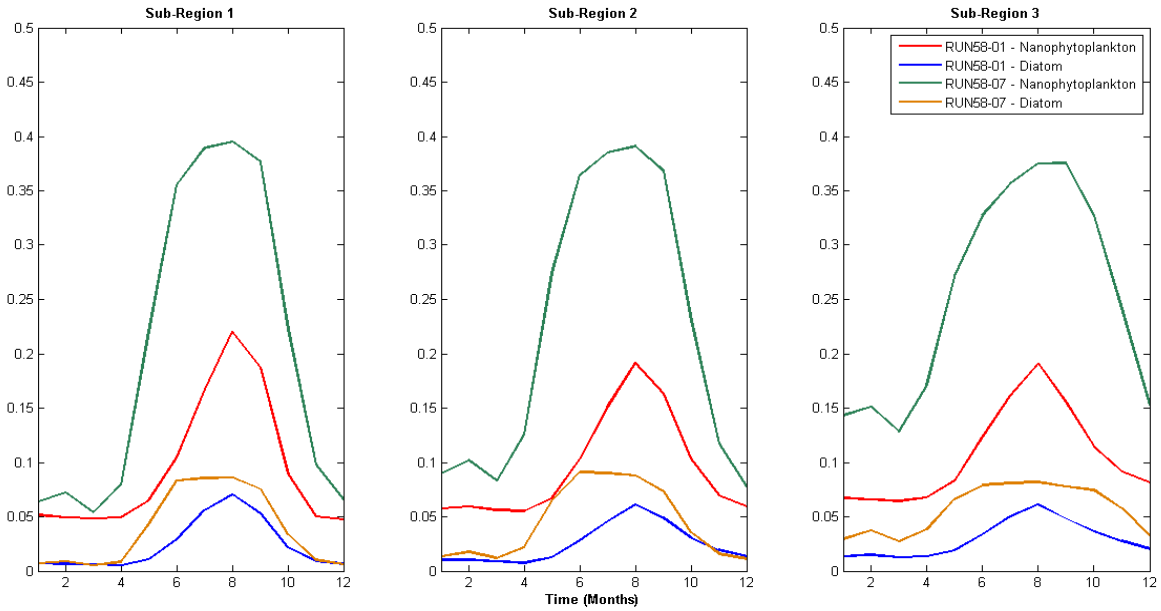

Figure 13: Monthly Climatology of surface Chl-a concentration (mg-Chl/m^3) from Diatoms and Nano-phytoplankton of the 2 runs (RUN58-01 and RUN58-07) over a time period of 1990 to 2001.

Comparing the monthly climatology of both runs shows that the seasonal cycle of nano-phytoplankton from RUN58-07 is relatively excessive compared to RUN58-01. However, the seasonal cycles of diatoms from both runs are quite similar with a slight higher concentration in RUN58-07 and they have the same seasonality as observations (SeaWiFS; Figure 12).

Chlorophyll maxima are sometimes not detected by ocean colour sensors since they are found deeper than the bottom of the euphotic zone and not at or near the surface. Hence, investigating the vertical distribution of SChl-a in the model is important. Seasonal vertical sections of chlorophyll-a are shown in Figure 14 and Figure 15 for RUN58-01 and RUN58-07 respectively. These were calculated over a period of 12 years (1990-2001).

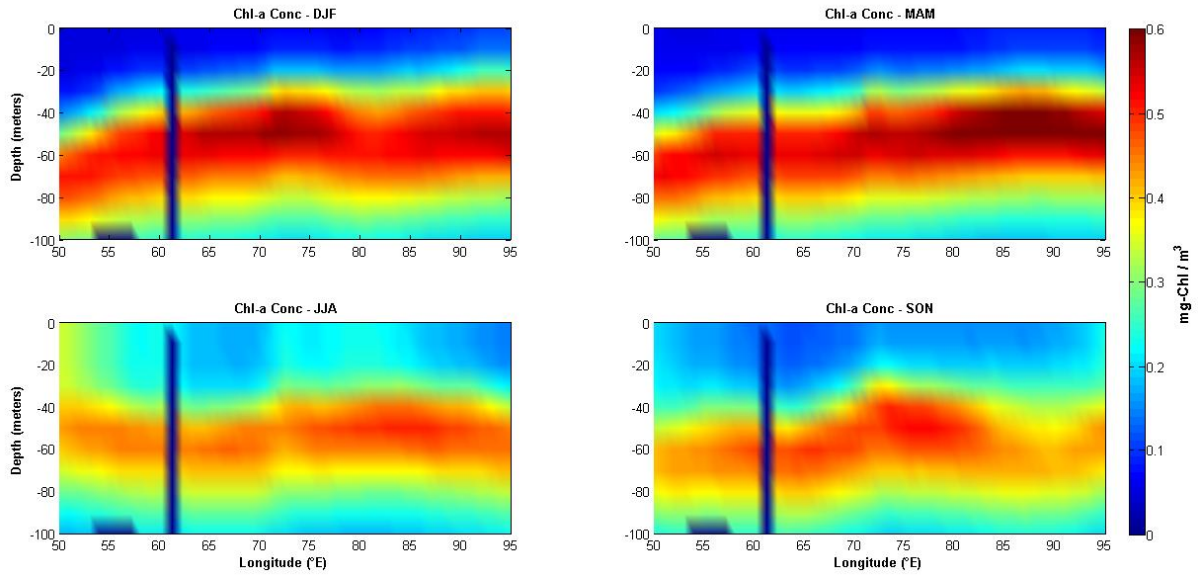

Figure 14: Vertical section of the model RUN58-01 chlorophyll-a concentration averaged over the latitudes (5°S-12°N) from Longitudes 50°E to 95°E over 12 years (1990-2001).

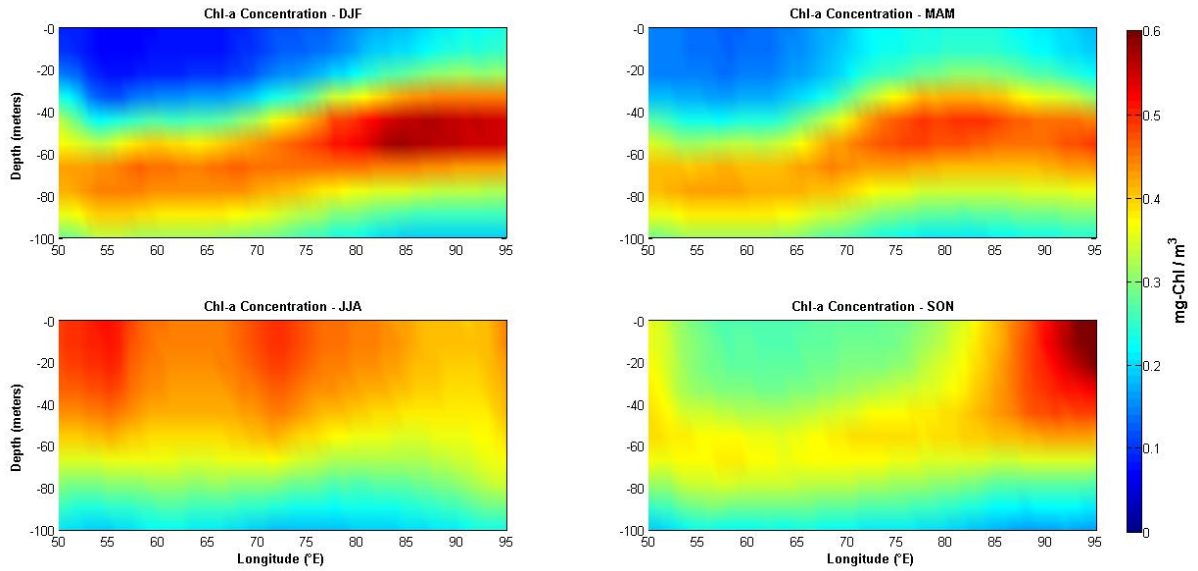

Figure 15: Vertical section of the model RUN58-07 chlorophyll-a concentration averaged over the latitudes 5°S-12°N from Longitudes 50°E to 95°E over 12 years (1990-2001).

In general, it can be observed that in austral summer and fall, the DCM is more intense in RUN58-01 compared to the RUN58-07. However, in austral winter and spring, the DCM remains in a depth range of 40-80 meters in RUN58-01 with some phytoplankton cells drifting near the surface compared to austral summer and fall. In RUN58-07, the bloom reaches the

surface and is more pronounced and widespread during these specific months compared to RUN58-01.

In austral summer, surface water in the specified region (50°E-95°E) is oligotrophic as seen in DJF of Figures 14 and 15. Deep chlorophyll maxima (DCM) (approximately 0.5 mg/m^3 for RUN58-07 and approximately 0.6 mg/m^3 for RUN 58-01) can be observed as from 40m to 80m deep in the eastern part of the Indian Ocean. In the western and central part, high chlorophyll content can be observed from 50m to 80m deep. In austral winter, a less intense DCM is present in RUN58-01 at a depth of approximately 40m to 80m. Surface concentration increases to approximately 0.25 mg/m^3 in western and eastern part of the SCTR. However, in RUN58-07, no deep chlorophyll maximum is present. High concentration of Chl-a can be observed from the surface down to 60m deep with higher surface concentration in the western and central part compared to the eastern part. From September to November, the surface concentration decreases in RUN58-01. In RUN58-07, the surface concentrations also decreases in the western and central part with higher concentration located at around 50-70m deep. However, in the eastern part, a patch of high concentration can be found from the surface up to 50m deep.

The monthly climatology of the mixed layer depth (MLD) from the two runs was calculated for a period of 32 years, from 1970-2001, in order to compare with that from de Boyer Montégut et al. (2004), which is based on observations. The mixed layer depth was plotted for the 3 sub regions of the SCTR. (Figure 16).

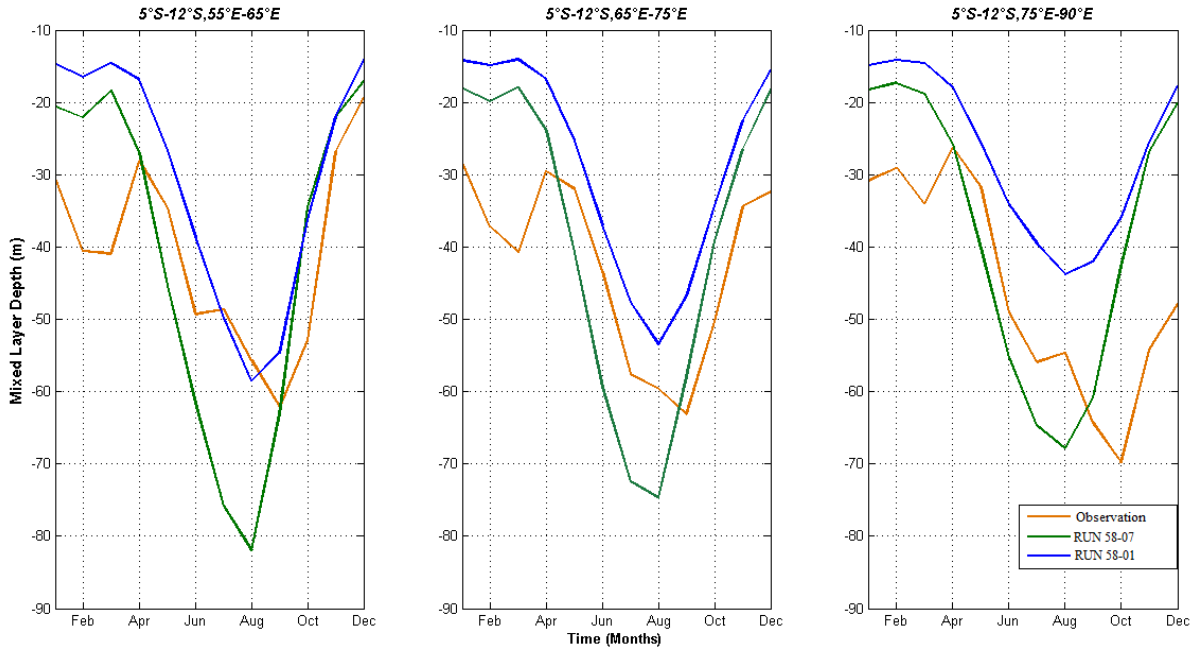

Figure 16: Monthly climatology of the mixed layer depth (MLD) from observation (orange), RUN58-01 (blue) and RUN58-07 (green). These were calculated over a time period of 38 years (1970-2007) for observations and 32 years (1970-2001) for both runs.

In the western part of the SCTR, RUN58-01 under-estimates the MLD from January to June but reproduces the MLD quite well till the end of the year. However, RUN58-07 under-estimates the MLD during the first 4 months but then, it exhibits an over-estimation until September and remains quite close to observations until December. In the central part, RUN58-01 under-estimates the MLD throughout the year but is still very close to observations from May to October. The MLD from RUN58-07 was under-estimated in the first 4 months and over-estimated from May to September. In the eastern part, RUN58-01 highly under-estimates the MLD by approximately 15m throughout the year whereas RUN58-07 under-estimates the MLD only from September to April. The MLD from RUN58-01 seems to correlate well with the observations in the western and central part of the SCTR whereas in the eastern part, the RUN58-07 reproduced the MLD closest to the observations although the deepest thermocline is observed in August whereas it occurs in October in observations. However, neither of the

two runs captured the deepening of the MLD from Jan to March followed by the shallowing from March to April in the whole SCTR region.

The deeper mixed layer depth from the RUN58-07 in sub-regions 1 and 2 cannot explain the extent of the high SChl-a concentration compared to observations. The MLD in sub-region 3 is at roughly the same depth as in observations but the Chl-a content is very high compared to observations.

The monthly climatology of the vertical distribution (0-100m deep) of nitrate concentration of the World Ocean Atlas 2005 (WOA05) and the RUN58-07 was compared for sub-regions 1, 2 and 3 in Figure 17. The nutricline depth (estimated here as the nitrate 2.4mmol m^{-3} isopleth, Resplandy et al., 2009) was superimposed on the figures. It should be noted that the nutricline is calculated by taking the depth of the value of nitrate concentration which is the closest or is equal to 2.4 mmol m^{-3}. However, it should also be noted that the months of May and October are derived from coarse resolution observations (70 data points averaged between 0 and 100m), whereas the other months are derived from an average of 230 data points. Hence, the amplitude of nutricline is exaggerated to some extent (Resplandy et al., 2009).

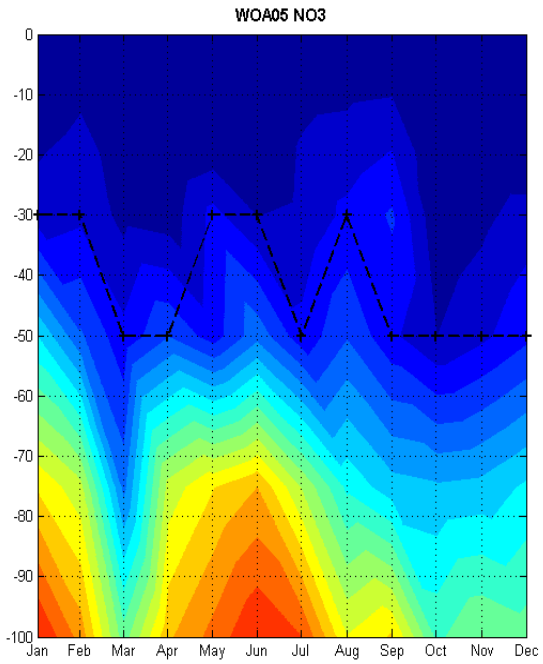
WOA05 NO3
0
-10
-20
-30
-40
-50
-60
-70
-80
-90
-100
Jan Feb Mar Apr May Jun Jul Aug Sep Oct Nov Dec

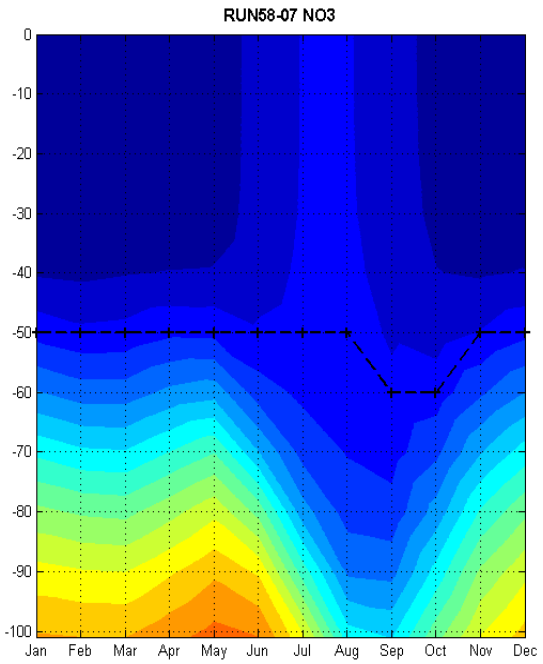
RUN58-07 NO3
0
-10
-20
-30
-40
-50
-60
-70
-80
-90
-100
Jan Feb Mar Apr May Jun Jul Aug Sep Oct Nov Dec

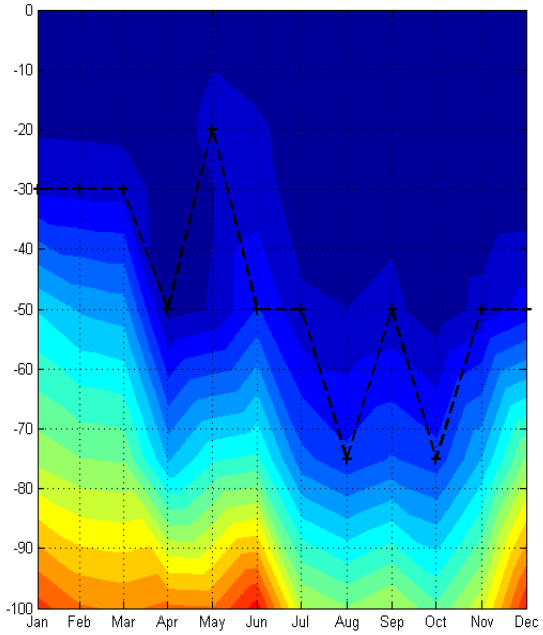
0
-10
-20
-30
-40
-50
-60
-70
-80
-90
-100
Jan Feb Mar Apr May Jun Jul Aug Sep Oct Nov Dec

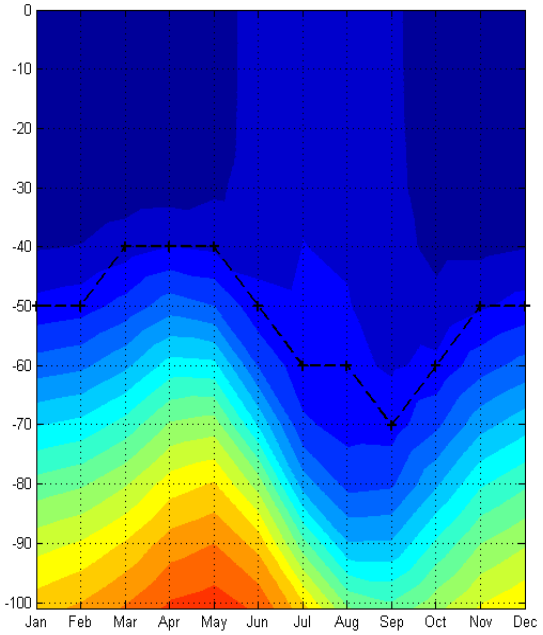
0
-10
-20
-30
-40
-50
-60
-70
-80
-90
-100
Jan Feb Mar Apr May Jun Jul Aug Sep Oct Nov Dec

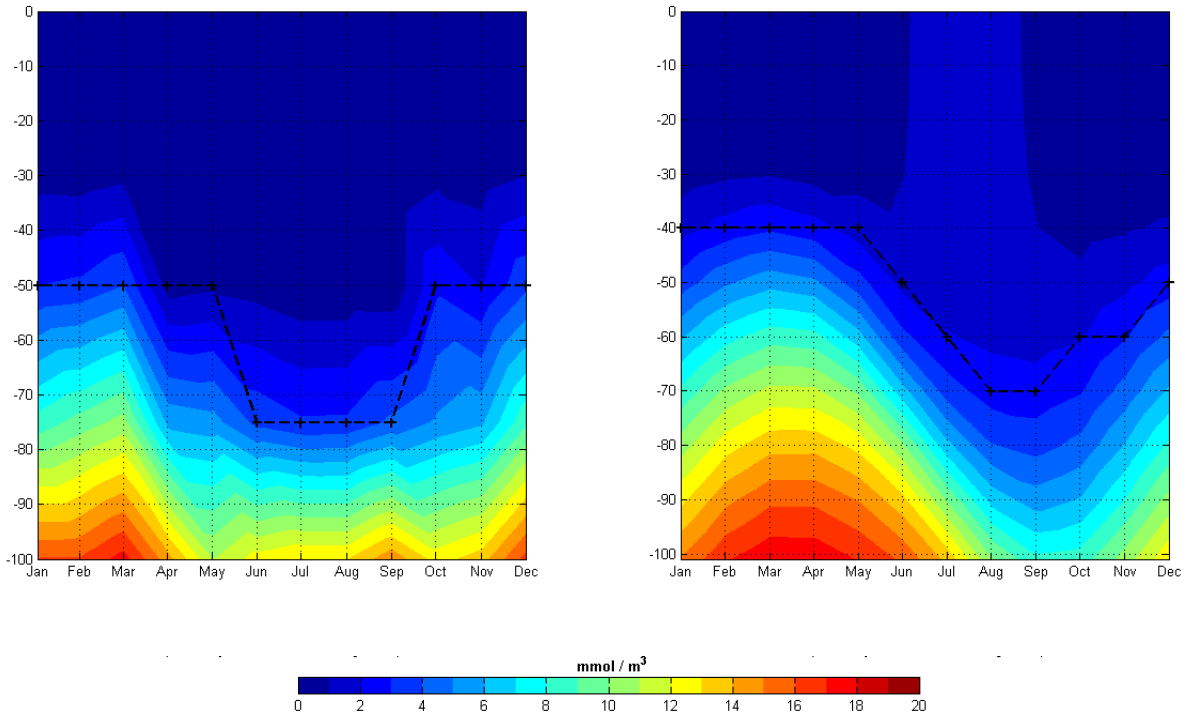

Figure 17: Monthly climatology of vertical distribution of nitrate concentration (mmol/m^3) from WOA05 (left) and the RUN58-07 (right) over the western (First row), central (Second row) and eastern (Third row) sub-regions of SCTR. The depth of the nutricline (2.4mmol/m3 isopleth) was superimposed on the figure. The monthly climatology was calculated over a time frame of 16 years for the RUN58-07 model (1990-2005) and 80 years (1925-2004) for nitrate from WOA05).

The model seems to correctly reproduce the nitrate concentration with a decrease in nitrate concentration as from June but it did not pick up the drastic decrease in March. However, it appears that the model under-estimates the upwelling to some degree in April-June. The nutricline depth is deeper in the model compared to observations. The amount of nutrients (nitrate) in the upper-layer of the ocean is hence under-estimated by the model and this should have been followed by a decrease in phytoplankton and not an increase as is observed in the RUN58-07 outputs of SChl-a concentration as shown in Figure 11. The resulting nutricline in the model is constant throughout the year except in September and October. This may be due to the coarse resolution of the model (2°).

In the central sub-region, the model shows the same cycle compared to the western sub-region with an increase in nitrate from January to May and a decrease as from May to August-

September where it reaches its lowest nitrate concentration. In the observations, there is a decrease in nitrate concentration from January to April and a slight increase from April to June which is due to upwelling during this time of the year. As from June, the concentration decreases till October and a slight increase is observed by the end of the year. Relative to observations, the overall nutricline remains deeper in the model and this is not reflected by a lower concentration of SChl-a compared to observations.

In the eastern sub-region, the model exhibits high nitrate concentration from January to May in the first 100m. The nutricline depth is shallower in the model throughout the year and this may explain the higher concentration in this region compared to the other sub-regions.

However, in all the sub-regions of the SCTR, it can be observed that from June to October, there is a column of high nitrate concentration up to the surface in the model. This water column is bringing more nutrients to the surface and it may be playing a role in the high over-estimation of SChl-a content of RUN58-07 during these months.

The seasonal cycles of the vertical distribution of nitrate concentration averaged over the latitudes 5°S to 12°S from WOA05 and the RUN58-07 are compared in Figure 18. It can be observed that the model seems to correctly resolve the seasonal cycle of the nitrate concentration with higher concentration in the upper 100m in austral summer and fall compared to austral winter and spring, although the magnitude of nitrate concentration is over-estimated to some extent in austral fall.

In austral summer, observations show that higher nitrate concentration is present at a shallower depth compared to the model especially from longitudes 60°E to 85°E. The maximum concentration however is found in the 60-100m depth range. From March to May, nitrate

concentration decreases in observations with the DCM located at a depth of 90m whereas in the model, higher concentration of nitrate occurs and at a shallower depth (60- 100 m).

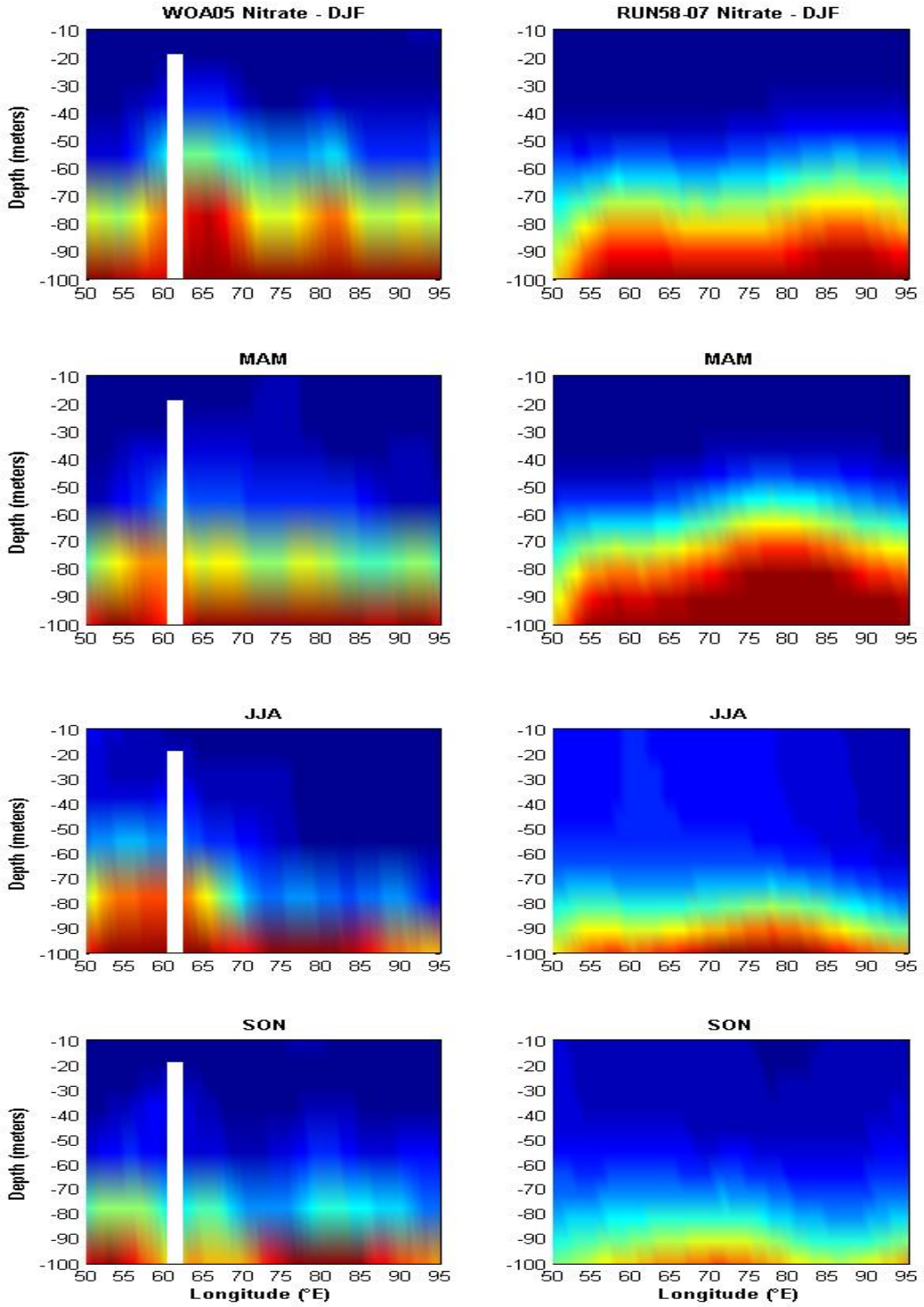

Figure 18: Seasonal evolution of the vertical distribution of nitrate concentration (mmol/m^3) from longitudes 50°E to 95°E and averaged over the latitudes (5°S-12°N) from the RUN58-07 (1990-2005) and WOA05 (1925-2004).

In austral winter and spring, the intense signature near the 60-100m depth range disappears in the model with the maximum located near 100m deep whereas a high concentration is still present in observations in the 70-100m depth range for austral winter and 80-100m depth range for austral spring.. However, it can be observed that the nitrate concentration along the water column and near the surface in the model is greater compared to austral summer and fall. Wind stirring and induced upwelling may be responsible for bringing the nutrients in shallow water. However, these were not compared with nitrate concentration from RUN58-01 since the nutrient outputs from the run were not available.

RUN58-07 is overestimating the intensity of SChl-a in the subtropical Indian Ocean more than the RUN58-01and this overestimation is mainly driven by the Chl-a content in nano-phytoplankton. Comparing nitrate concentration and the mixed layer depth from their respective observations indicate that they are playing a minor role in the over-estimation but they do not completely explain the high Chl-a content. However, the spatial distribution of SChl-a in the model seems to be respected. This over-estimation may be the result of the difference in the parameterization controlling the growth rate of nano-phytoplankton between the two runs.

This section has shown that the physical part (SSH and D20) of both RUN58-01 and RUN58-07 correlates well with observation, although RUN58-07 seems to reproduce better the SSH and D20. However, it has been found that in austral winter and spring, both RUN58-01 and RUN58-07 exhibit an over-estimation in surface chlorophyll-a concentration in the Indian Ocean and the studied region compared to observations. Nonetheless, although the magnitude and spatial distribution of the phytoplankton blooms are over-estimated to some extent, RUN58-01 shows better agreement with SeaWiFS compared to RUN58-07. Analysis of the

MLD and the nitrate concentration of RUN58-07 do not completely explain the high over-estimation in this specific run although it has been shown that the nano-phytoplankton component is responsible for this over-estimation.

Hence, SeaWiFS data and both runs will be used to assess the annual cycle of surface chlorophyll-a in the SCTR region which is one of the main aims of this study. Regarding the interannual variability related to pure IOD and ENSO, RUN58-01 will be used to investigate the physical variables (SST and D20) as well as the biogeochemical variable (SChl-a) in the SCTR.

6 Results

6.1 Annual cycle of surface chlorophyll-a

Upwelling plays an important role in the concentration of surface chlorophyll-a by influencing the amount of nutrients which are brought into the euphotic zone, hence providing all the necessary conditions for phytoplankton blooms. Therefore it is important to understand the annual cycle of the 20°C isotherm in the SCTR region.

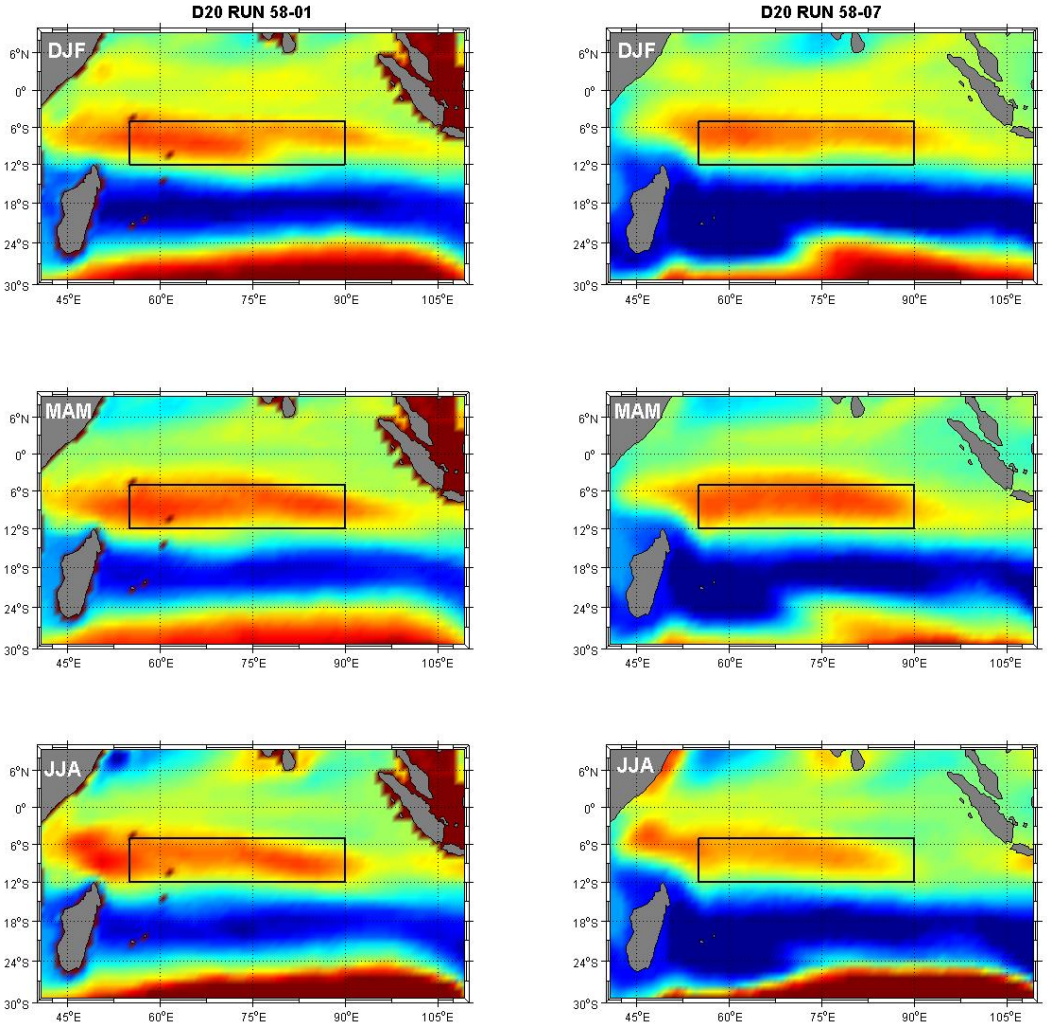

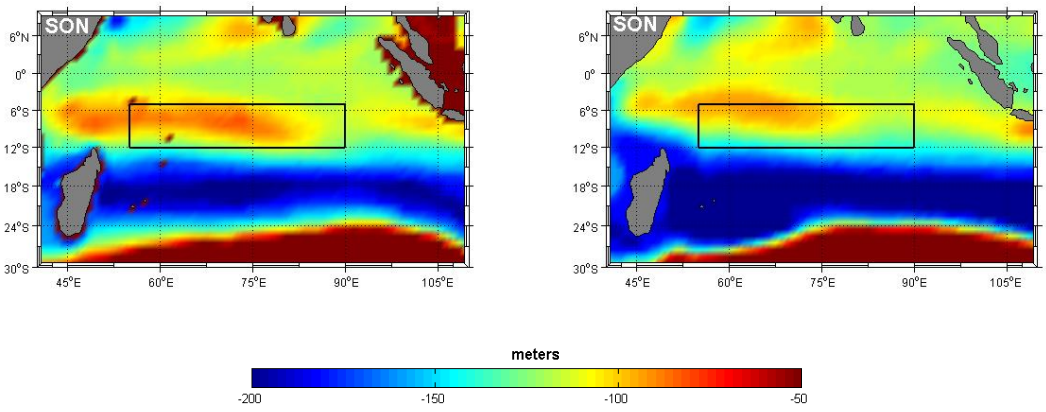

Figure 19: Seasonal variability of the 20°C isotherm (D20; meters) in the Indian Ocean from RUN58-01 (Left panels) and RUN58-07 (Right Panels) over a time period of 12 years (1990-2001).

The seasonal variability of the 20°C isotherm depth of the two runs is shown in Figure 19. Upwelling is present throughout the year in the SCTR region. In austral summer and fall, it extends between 55°E to 90°E and 5°S to 12°S in RUN58-07. However in RUN58-01, it extends further west up to approximately 45°E and further east up to approximately 95°E. In JJA, the peak upwelling region shifts westward to latitudes 3°S-7°S and longitudes 45°E-55°E. However, a weaker region is found from 5°S-12°S and 55°E-90°E. During austral spring, the upwelling region is weaken and it is concentrated between latitudes 3°S-8°S and longitudes 45°E-75°E. It can be observed that the D20 from RUN58-01 seems to be shallower compared to RUN58-07 in austral summer, winter and spring.

The details are however better resolved in RUN58-01 which has a 1/2° resolution unlike the 2° resolution of RUN58-07. Nonetheless, the upwelling regions compare well with the study done by Hermes and Reason (2008) in which a 1/3° resolution model was used.

The annual cycle of surface chlorophyll-a concentration was investigated using SeaWiFS data and both RUN58-01 and RUN58-07 as shown in the next figure.

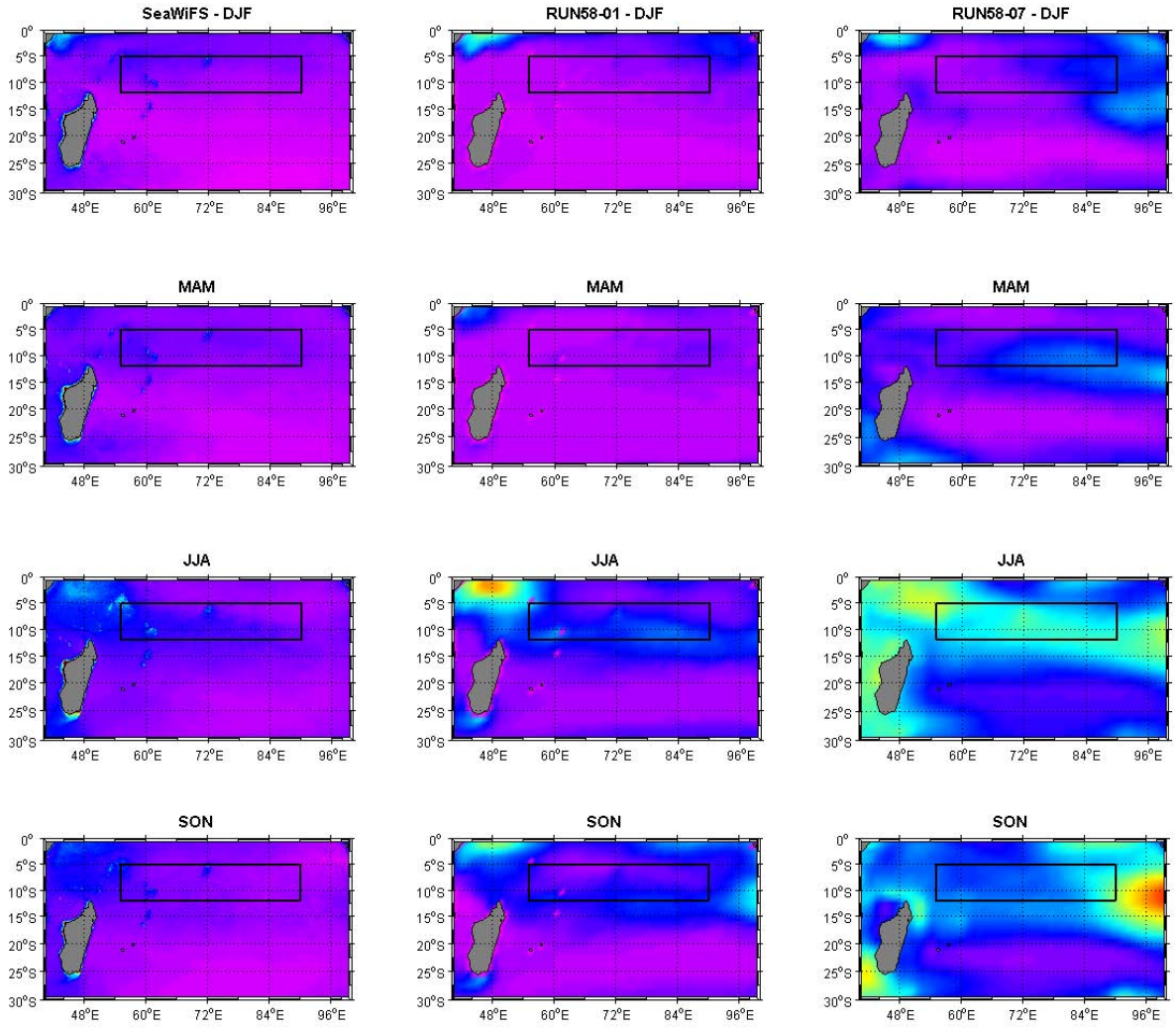

Figure 20: Average Seasonal Cycle of Chlorophyll-a concentration from SeaWiFS (Left Panels), RUN58-01 (Middle Panels) and RUN58-07 (Right Panels) over the southern tropical Indian Ocean with the SCTR (5°S-12°S, 55°E-90°E) region shown in the box. The average seasonal cycle is calculated over the 1998-2001 periods for SeaWiFS and the two runs.

The results of SChl-a pattern in remotely-sensed data show that in austral summer, the SCTR is quite an oligotrophic region with some patches of SChl-a in the north-western part of the region and around the Saya de Malha Bank (SMB) (60°E-10°S) and the Chagos Archipelago Islands (CA) (71.5°E-6°S). However, neither RUN58-01 nor RUN58-07 captured those

patches of SChl-a. They do reproduce the oligotrophic conditions although a minor higher SChl-a is observed in the eastern part of the SCTR in both runs, with the RUN58-07 expressing higher magnitude than the RUN58-01. Overall, the northern part of the SCTR exhibits higher SChl-a concentration compared to the lower part.

In MAM, the SCTR region is less oligotrophic compared to in DJF. SeaWiFS data show a slight increase in SChl-a concentration. The patches around the SMB and CM Islands can still be observed. However, the spatial distribution of SChl-a seems to be more widespread in the whole SCTR region compared to DJF where it was more concentrated in the northern part. RUN58-01 appears to reproduce the chlorophyll concentration quite well in the eastern part of the SCTR, whereas in the western part, the concentration is lower compared to SeaWiFS. It does, nevertheless, capture the SChl-a patch around SMB and CA but in lower magnitude. RUN58-07 however exhibits a higher SChl-a concentration compared to SeaWiFS and RUN58-01 in the whole region.

In austral winter, the study region exhibits high biological productivity with higher SChl-a concentration in all the sub-regions of the SCTR. Around the CA and SMB, higher concentration of chlorophyll is observed compared to austral summer and fall. However, the north-eastern part of the SCTR seems oligotrophic with low SChl-a concentration whereas the north-western part is highly productive. RUN58-01 seems to capture the spatial pattern of SChl-a blooms although the magnitude is to some extent over-estimated. Low and high SChl-a concentration is observed in the north-eastern part and north-western part of the SCTR respectively. The run also captures the high Chl-a content around the island (60E-10S). Compared to SeaWiFS, the RUN58-07 seems to capture the spatial pattern of SCl-a with a higher and lower chlorophyll content in the north-western and north-eastern part of the region

respectively although the magnitude is highly over-estimated. It does not capture the high concentration around the SMB and CA and this may be due to its coarse resolution (2°).

In SON, the biological productivity in the SCTR region decreases compared to austral winter. High chlorophyll-a content can be seen around the islands and in the north-western part of the region whereas in the eastern part, low productivity prevails. The SChl-a concentration from RUN58-01 does exhibit a decrease in the concentration although the magnitude and the spatial distribution are over-estimated to some extent. RUN58-07, however, displays a high concentration in the whole SCTR region with a peak in concentration in the eastern part. The spatial extent and magnitude is overly-estimated in this run.

It can be observed that in austral summer and fall, although the 20°C isotherm is shallow, and hence upwelling is implied, this is not reflected by phytoplankton blooms near the surface. This shows an insignificant or weak relationship between SChl-a and D20 in this region. Other factors beyond the shallowing of the nutricline are influencing the surface chlorophyll-a concentration.

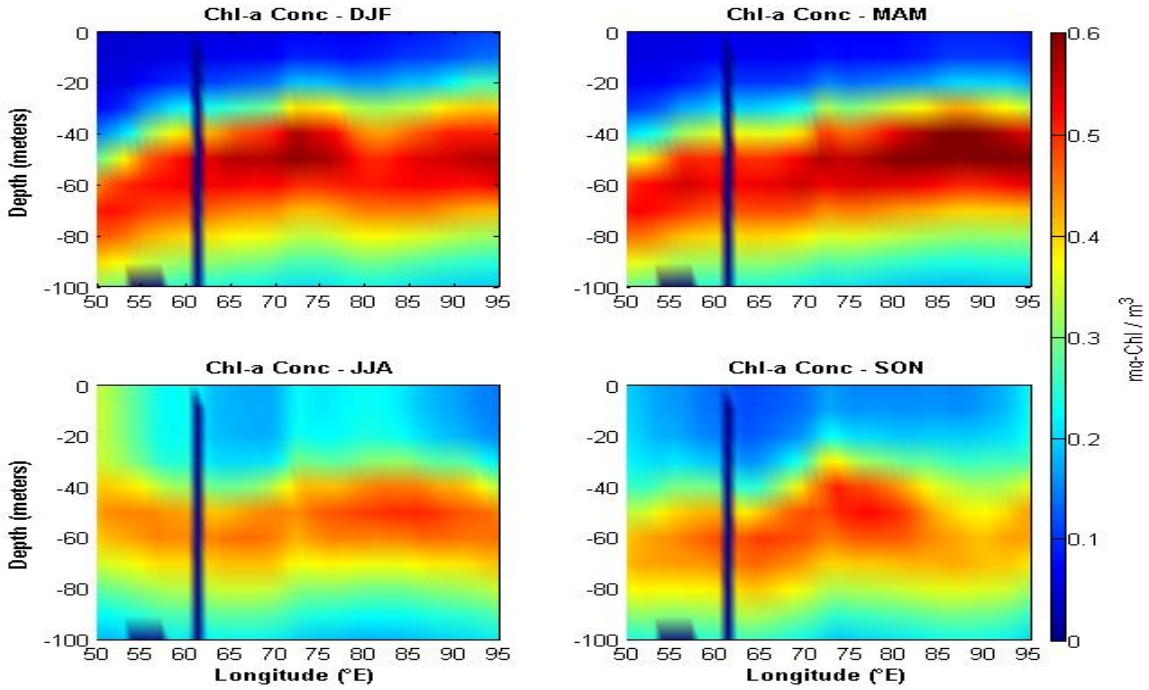

Figure 21: Vertical section of chlorophyll-a concentration from RUN58-01averaged over the latitudes (5°S-12°N) from Longitudes 50°E to 95°E over 12 years (1990-2001)

From Figure 21, we can observe the deep chlorophyll maximum (DCM) in the region. The SCTR is known as a DCM region (George et al., 2012). In austral summer and fall, the DCM seems to be concentrated between 30m and 80m in the whole SCTR region. The surface concentration is low during these periods. However, in austral winter and spring, the surface chlorophyll-a concentration increases whereas the sub-surface Chl-a decreases. Nevertheless, the sub-surface remains more concentrated in phytoplankton than the surface layers. Vertical mixing seems to occur since the phytoplankton is more spread in the region from June to November.

6.2 Interannual variability in the SCTR

Emphasis will now be put on the interannual variability of the sea surface temperatre (SST) and depth of 20°C isotherm and surface chlorophyll-a concentration using RUN58-01. Pure positive (negative) Indian Ocean Dipole and positive (negative) El Niño Southern Oscillation will be taken into consideration to investigate the influence of these climate modes on the variability of the above-mentioned variables.

6.2.1 Physical Response

Figure 22 and 23 represents the Nino 3.4 Index and the Dipole Mode Index (DMI) from 1960 to 2007, constructed from the OGCM (RUN58-01) used in this study. These indices were compared with indices created from observations.

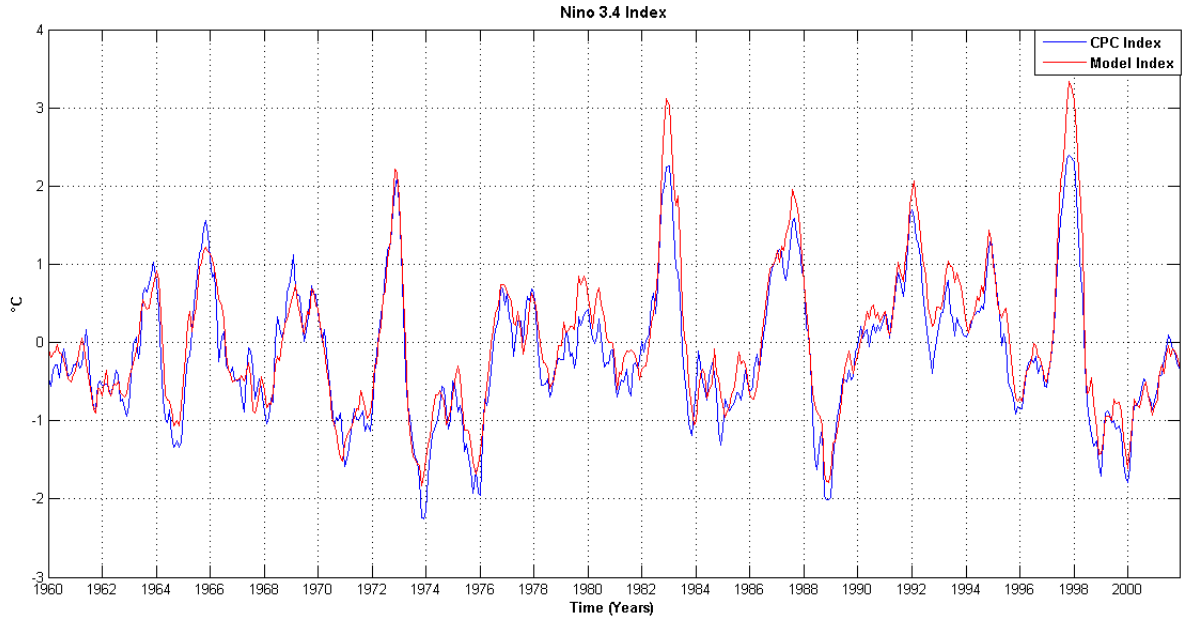

Figure 22: Index of Nino 3.4 from the model and observational data from 1960 to 2001.

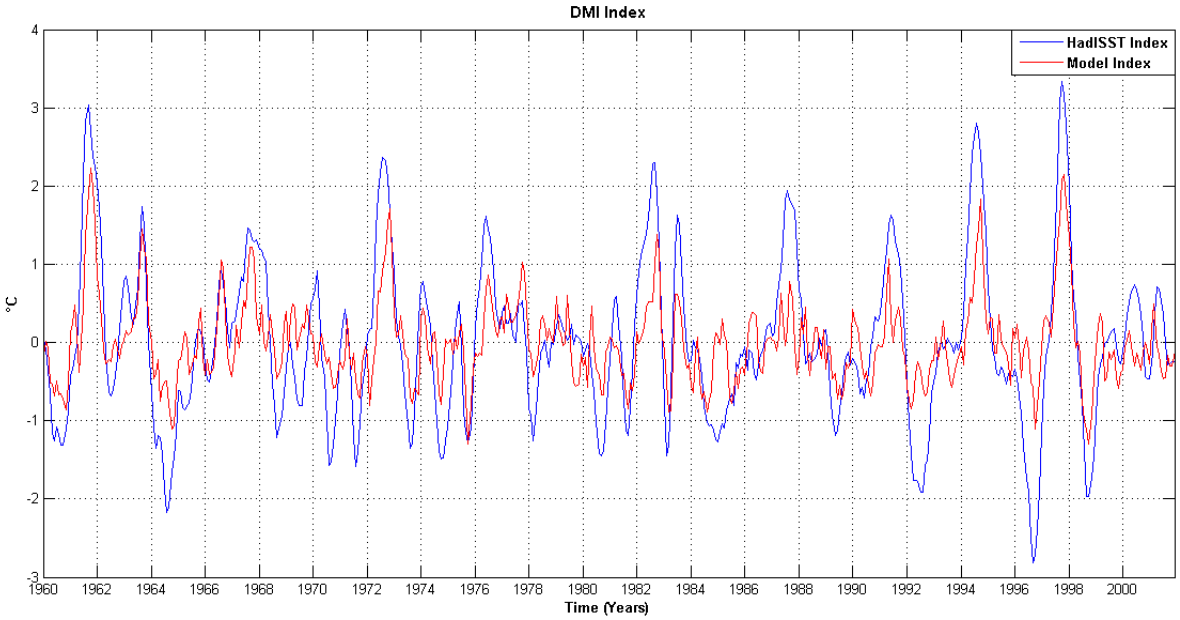

Figure 23: Index of Indian Ocean Dipole from the model and observational data from 1960 to 2001.

The Nino 3.4 index and the DMI from RUN58-01 show good agreement with observations with a correlation coefficient of 0.9540 for Nino 3.4 and a correlation coefficient of 0.7621 for DMI, both at 99% significance level.

In total, 5 pure positive (negative) ENSO and 4 pure positive (negative) IOD were identified over a time period of 1960-2007 as shown in table 1 in the Methodology section. Composites of the variables in these specific years (0) and the next year (+1) were then performed.

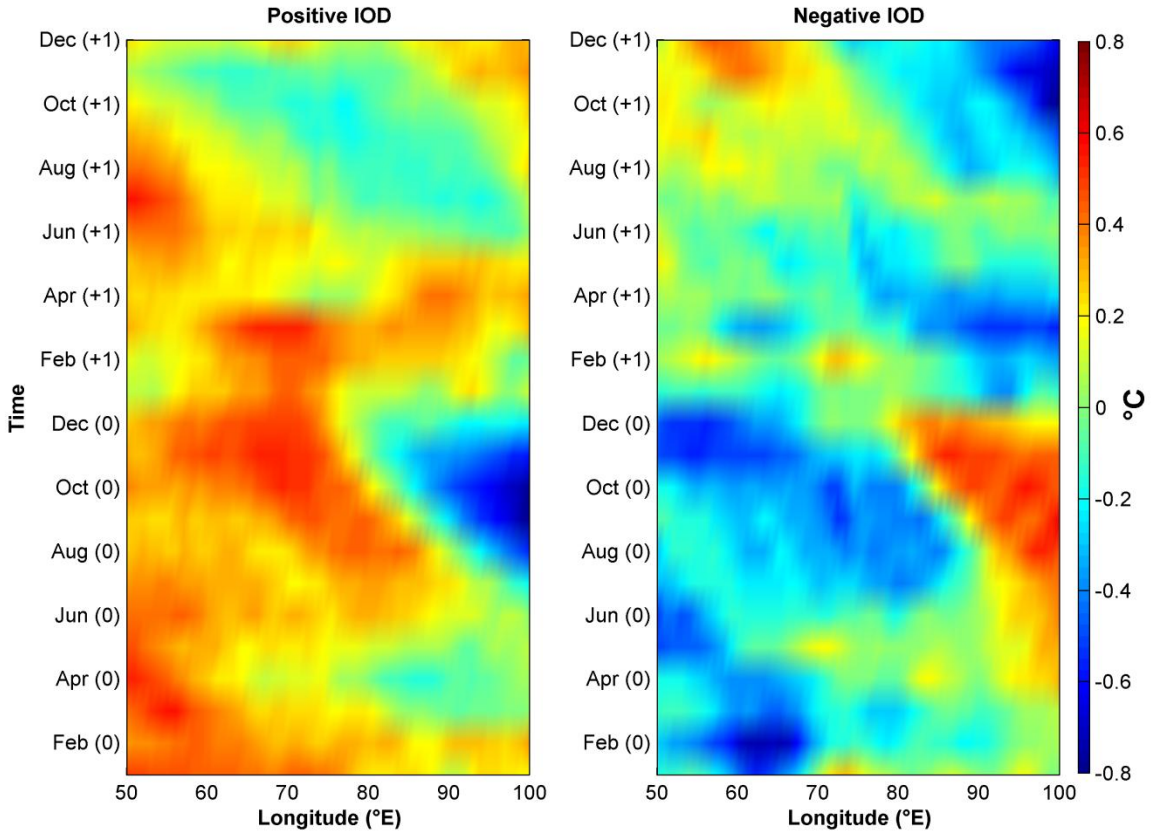

Figure 24: Time-Longitudinal diagrams of the model composite SST anomalies averaged over the latitudes 5°S-12°S for pure positive IOD (1961, 1967, 1977 and 1994) and pure negative IOD (1960, 1989, 1992 and 1996).

In Figure 24, the dipole mode can be clearly seen in the SST anomalies of the IOD composites. During pure positive IOD, a negative SST anomaly starts in the eastern tropical Indian Ocean in austral winter. At the same time, a positive SST anomaly develops in the western tropical Indian Ocean. The positive and negative SST anomalies reach their peak in intensity and expand westwards in October and then dissipate by the end of the same year.

During pure negative IOD, the opposite occurs. Positive and negative SST anomaly develop in the eastern and western part of the Indian Ocean respectively and the anomaly dissipates by the end of the year.

These time-longitudinal figures in both pure positive IOD and pure negative IOD have also been plotted for individual years constituting the composites (Figure 31 in Appendix) and it

can be observed that the spatial patterns of SST anomalies in the study area are more or less the same during all the events.

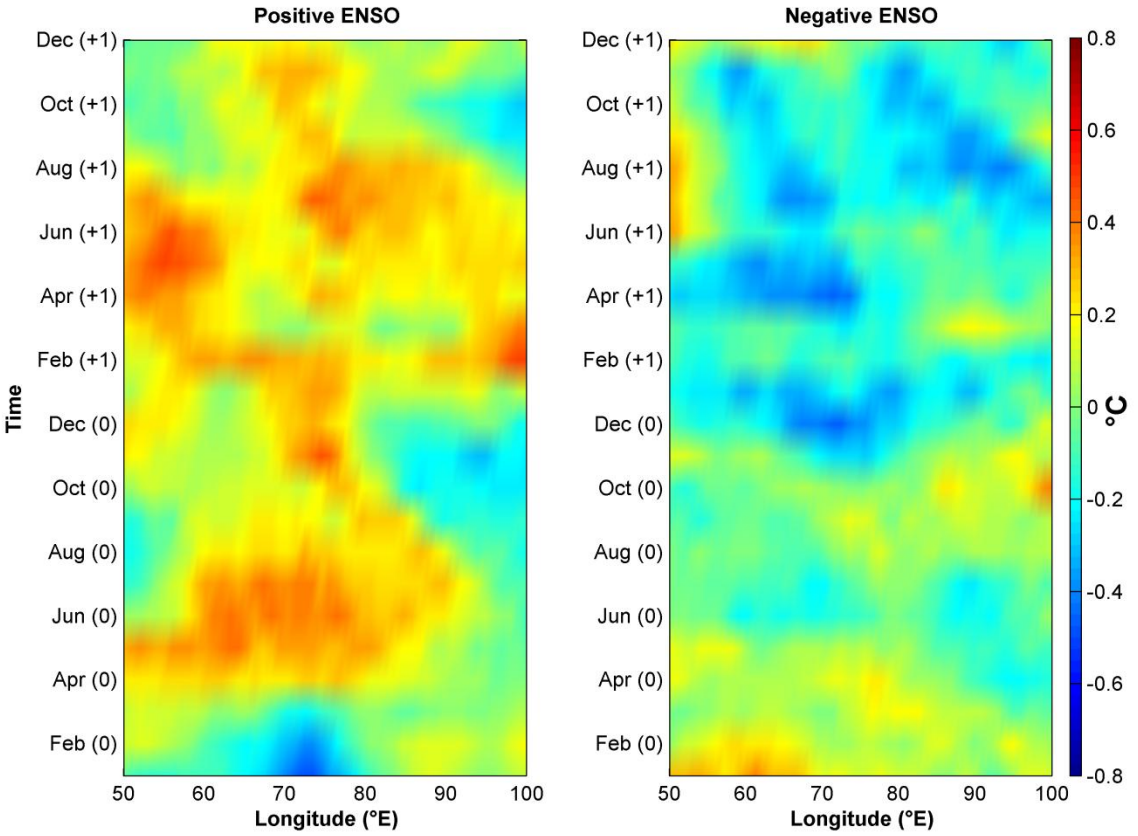

Figure 25: Time-Longitudinal diagrams of composite SST anomalies averaged over the latitudes 5°S-12°S for pure positive ENSO (1965, 1969, 1976, 1986 and 1991) and pure negative ENSO (1967, 1971, 1973, 1975 and 1988).

During pure positive ENSO, a positive SST anomaly develops in the western and central Indian Ocean, after ENSO develops in the Pacific Ocean. This positive anomaly lasts till the end of the next year with some intensification at times (Feb (+1) and July (+1)). At the same time, a slight negative SST anomaly develops in the eastern Indian Ocean and lasts for only 3 months. During a pure negative ENSO, slight positive SST anomalies develop in the region during the same year and last for two months. However, during the year following the negative ENSO, a slight negative SST anomaly can be observed in the entire region.

SST anomalies of the different years constituting the composites of the pure positive and negative ENSO (as observed in Figure 32 in Appendix) are however very erratically distributed, with mostly positive anomalies in SCTR region during positive ENSO years; and positive anomalies during the 1967 La Niña but a negative anomaly during 1973 La Niña. The results may have been dominated by these strong events.

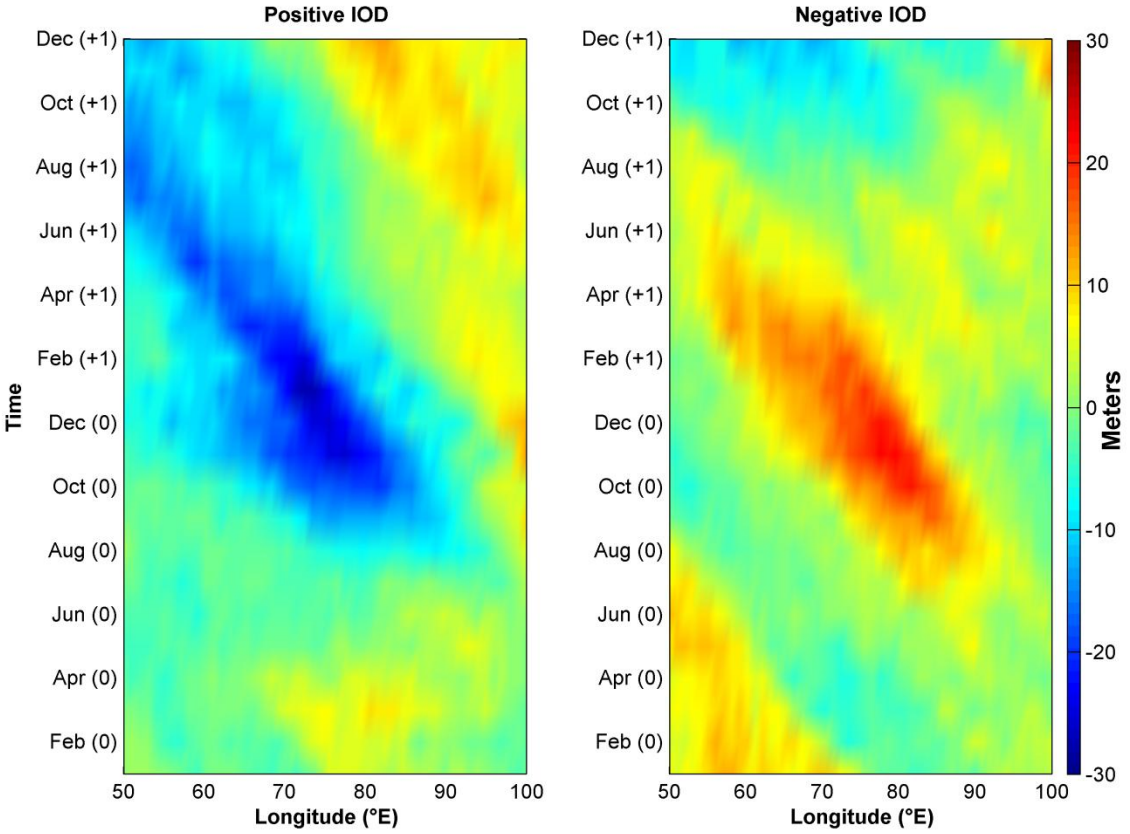

Figure 26: Time-Longitudinal diagrams of composite depth of 20°C isotherm anomalies averaged over the latitudes 5°S-12°S for pure positive IOD (1961, 1967, 1977 and 1994) and pure negative IOD (1960, 1989, 1992 and 1996).

The time-longitudinal diagram of composites of pure IOD revealed that the variability of the depth of 20°C isotherm in the tropical Indian Ocean (TIO) is largely influenced by the IOD. During a pure positive IOD, which starts in May-June, the thermocline depth slightly shoals in the eastern part of the Indian Ocean whereas in the central part and eastern part of the SCTR,

it starts to deepen as from August. This shoaling and deepening is maximum during the climax of IOD (October-November) and it gradually shifts westward. The dynamical reason for this westward thermocline movement is related to the planetary Rossby waves which propagate at a speed of approximately 0.184 ms^{-1} which was calculated from the figure. However, it is slower than the theoretical phase speed of free Rossby waves which varies between approximately 0.26ms^{-1} and 0.23ms^{-1} from latitudes 7.5°S and 10.5°S in the Indian Ocean (Gnanaseelan and Vaid, 2010). Even after the IOD recedes at the end of the year, the deepening persists throughout the whole next year in the western part. In December of the next year, the SCTR is characterised by a deepening of the thermocline in sub-region 1 and a shoaling in sub-region 3.

During a pure negative IOD, the spatial pattern of the anomalies has the opposite sign to that during the positive IOD. A shoaling in the thermocline is observed in sub-region 3 of the SCTR as soon as the negative IOD starts (May-June) and this shoaling shift westward to reach its maximum during the climax of the negative IOD (October-November). This westward movement is due to Rossby waves (Rao and Behera, 2005; Yu et al., 2005) and its speed is approximately 0.171 ms^{-1}, still slower than its theoretical phase speed. The thermocline then starts to deepen as from December to finally reach its mean position in April of next year.

However, compared to the pure positive IOD, the magnitude of the anomalies during the pure negative IOD are weaker and only a minor negative anomaly is observed in the eastern tropical Indian Ocean.

When considering each specific years which form the composites of the pure positive and negative IOD (Figure 33 in Appendix), it is observed that during all the events, the D20 anomalies are the same in the study region. that is negative and positive during positive and negative IOD respectively. These give confidence in the results.

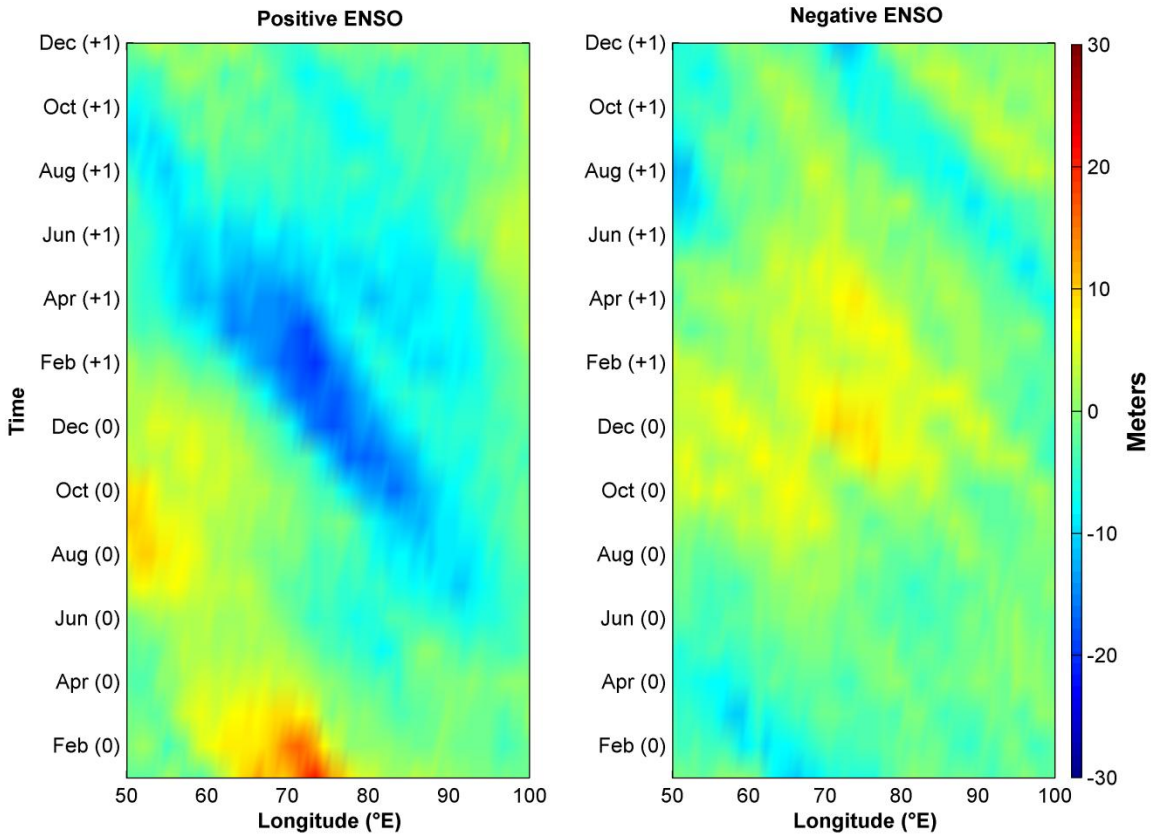

Figure 27: Time-Longitudinal diagrams of composite depth of 20°C isotherm anomalies averaged over the latitudes 5°S-12°S for pure positive ENSO (1965, 1969, 1976, 1986 and 1991) and pure negative ENSO (1967, 1971, 1973, 1975 and 1988).

During pure positive ENSO, a slight negative anomaly of the thermocline depth starts to develop in the eastern part of the SCTR after ENSO starts in the Pacific Ocean. This negative anomaly shifts westward at a speed of 0.18 ms^{-1} due to Rossby waves, replacing the slight positive anomaly in the western part. The signature recedes in April of the next year at the same time as ENSO.

However, throughout pure negative ENSO, the thermocline shoals in the whole SCTR with a maximum shoaling in the sub-region 2 during December when ENSO is at its most intense point. This signature starts to recede the next year and ends in June.

Figure 34 in Appendix investigates all the events of positive ENSO and negative ENSO. It is observed that negative D20 anomalies occur in the study region during positive ENSO.

However during negative ENSO, one event (1967) is characterized by strong negative anomalies in the study region whereas during the other events, slight positive anomalies occur. This strong negative anomaly might have influenced the composite of the negative ENSO years.

6.2.2 Biological Response

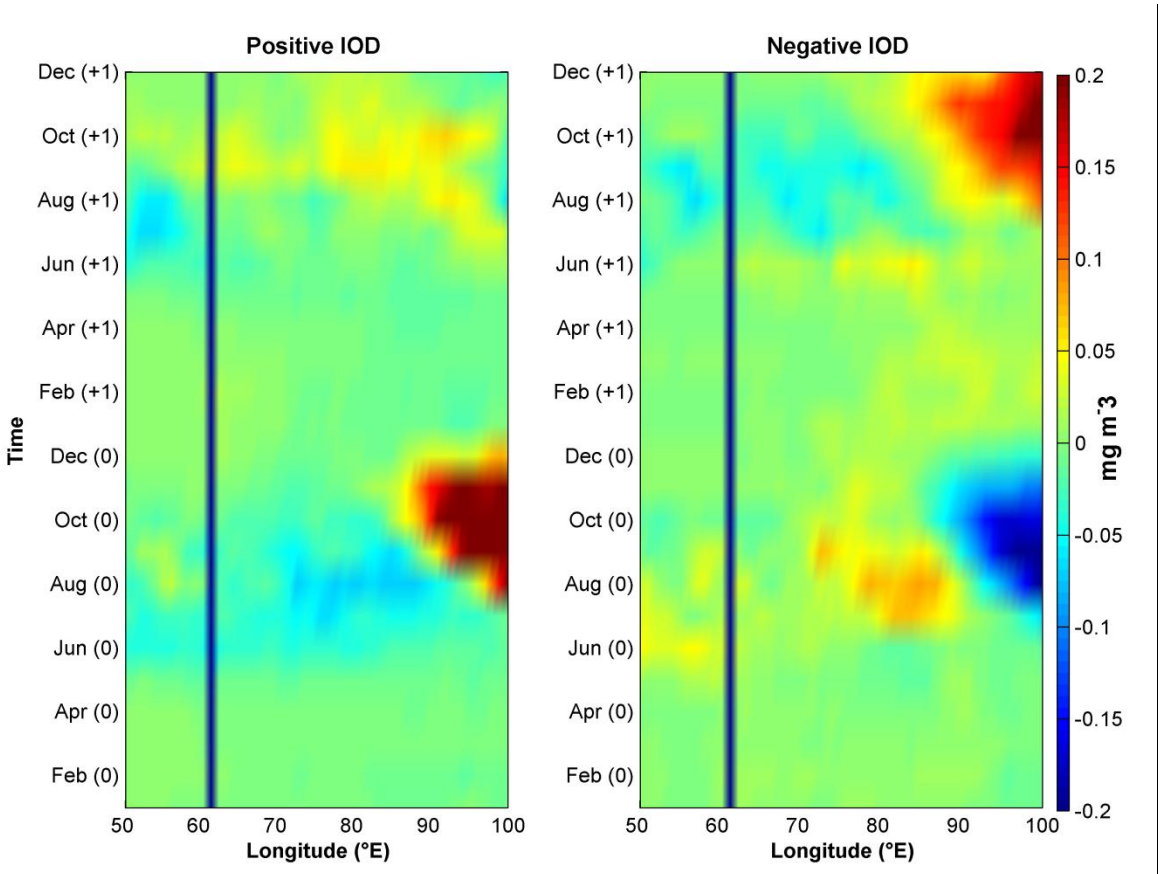

Figure 28: Time-Longitudinal diagrams of composite surface chlorophyll-a concentration anomalies averaged over the latitudes 5°S-12°S for pure positive IOD (1961, 1967, 1977 and 1994) and pure negative IOD (1960, 1989, 1992 and 1996).

During pure positive IOD, a slight negative anomaly of SChl-a is detected along the section 50°E-95°E in June and it lasts for approximately 2 months. A positive SChl-a anomaly can be

seen to develop along the section 90°E-100°, as observed in Currie et al. (2013). It persists for approximately five months (August-December)

On the contrary, a negative signature of SChl-a starts instantaneously in the eastern part of TIO during a pure negative IOD. It reaches its maximum westward extend and magnitude in October (Climax of IOD) and disappears by January of the next year.

Investigating the individual years used to create the composites of SChl-a during positive and negative IOD (Figure 35 in Appendix) have shown that the signature observed in the study region is similar during all the events and this gives confidence in the results.

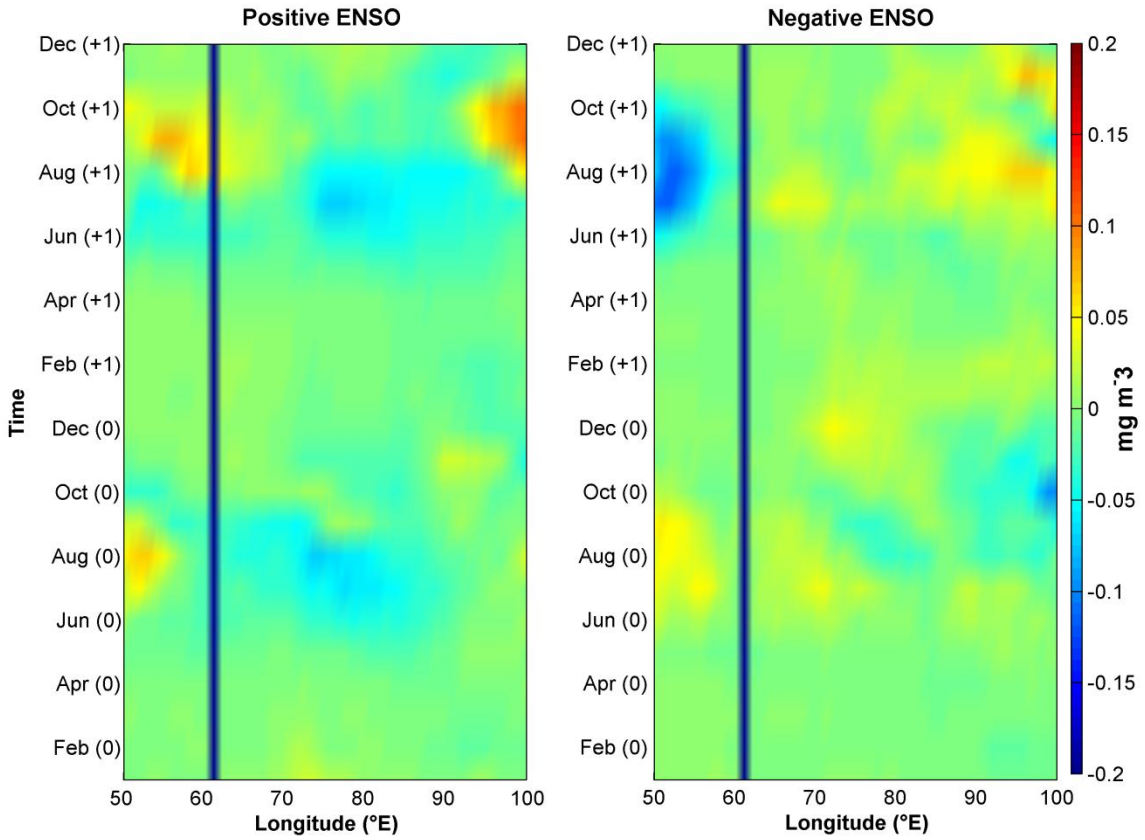

Figure 29: Time-Longitudinal diagrams of composite surface chlorophyll-a concentration anomalies averaged over the latitudes 5°S-12°S for pure positive ENSO (1965, 1969, 1976, 1986 and 1991) and pure negative ENSO (1967, 1971, 1973, 1975 and 1988).

During pure positive ENSO, a weak negative deviation from the mean of SChl-a is detected as from June in the central and in the eastern part of the SCTR, the negative signature disappears at the end of August. A minor negative anomaly is identified in August during pure negative ENSO from 80°E to 100°E and it persists for approximately 1 month in the eastern part of the SCTR and till December in the eastern part of the Indian Ocean.

Figure 36 in Appendix show that SChl-a during pure positive and negative ENSO does not exhibit a clear signature in its anomalies, with varying positive to negative anomaly in the study region. Hence, the composite of the positive and negative ENSO years demonstrate no important and clear signature in SChl-a anomalies.

7 DISCUSSION

Regarding the biogeochemical aspect of the two different runs of NEMO-PISCES, RUN58-01 has shown overall and better agreement with SeaWiFS compared to the RUN58-07, although the magnitude and spatial distribution are over-estimated to some degree. It has been shown in Figure 13 that the chlorophyll-a content in nano-phytoplankton is playing a major role in the over-estimation and the seasonal cycle of the total chlorophyll-a in RUN58-07 since its nutrient co-limitation term and dependence on temperature have been removed from the Geider et al. (1998) formulation. However, assessing the causes of the differences between the two runs and observations is not an easy task. The dependence on aeolien iron supply, specific to the Indian Ocean (Wiggert and Murtugudde, 2007), and the signal to noise ration of satellite-derived chlorophyll (Ballabrera-Poy et al., 2003) have not been addressed in this study.

Considering the physical component of the two runs, both correlates well with observations with RUN58-07 (0.9715 and -0.9547 correlation coefficients with SSH and D20 respectively) showing a higher correlation with observations compared to RUN58-01 (0.847 and -0.8969 correlation coefficients with SSH and D20 respectively). However, RUN58-01 has been used for the interannual variability of the physical variables in the SCTR since it is better to compared the physical and biogeochemical aspects of the same run rather than another run.

7.1 Annual cycle of surface chlorophyll-a

The SCTR region is quite oligotrophic during austral summer, with low concentration of phytoplankton cells at the surface. The mixed layer depth and the deep nutricline are responsible for the low nutrient environment (Resplandy et al., 2009). The mixed layer depth during this period remains shallower than the nutricline. Therefore, the concentration of

nutrients in the euphotic zone is reduced and the concentration of SChl-a is low. Nevertheless, deeper waters have enough nutrients to favour phytoplankton blooms, hence the presence of a deep chlorophyll maximum (George et al., 2012) in the model SCTR region, as can be observed in Figure 21. This is in agreement with Resplandy et al. (2009) who detailed the low concentration of surface chlorophyll-a during austral summer.

During March-April-May, the SCTR region favours more surface phytoplankton cells compared to austral summer and this is seen in the slight increase in SChl-a concentration in the study region. During this period, the south-easterlies start to increase and shift northward (Hermes and Reason, 2008) and this will cause an increase in vertical mixing, favouring upwelling and consequently bringing more nutrients to the surface and generating more photosynthesis at the surface.

An annual peak of surface chlorophyll-a concentration occurs during austral winter as shown by SeaWiFS and model data. Wind driven upwelling also reaches its annual peak during this period, hence initiating this winter bloom (Wiggert et al., 2006). Strong winter winds prevail over the entire SCTR region causing the mixed layer depth to deepen. Positive Ekman pumping will enhance the effect of wind-driven mixing and cause upwelling of deep nutrient-rich water to the surface (Resplandy et al., 2009). This entrainment of nutrients in the MLD allows photosynthesis to take place, hence increasing the surface chlorophyll-a concentration. Entrainment of phytoplankton cells from the DCM also occur as the subsurface phytoplankton concentration decreases when surface concentration increases (Figure 21). This is in agreement with the study of Resplandy et al. (2009) who showed that due to the combination of high concentration of phytoplankton cells at the surface and decreased incoming shortwave radiation (SW), photosynthetically active radiation (PAR) decreases since light cannot penetrate in deep waters. Hence, an increase in SChl-a production is compensated with a decrease in sub-surface Chl-a production.

During the boreal fall intermonsoon, the monsoon winds start to relax and the SCTR-phytoplankton blooms dissipate with the water column re-stratification and nutrient depletion (Wiggert et al., 2006; Resplandy et al., 2009).

The results showed that SChl-a in the SCTR peaks during austral winter (June to August), both in SeaWiFS and the coupled models, hence revealing an annual cycle in chlorophyll-a, in agreement with Resplandy et al. (2009).

It is observed that the area south of the Seychelles-Chagos Thermocline Ridge (SCTR) is SChl-a depleted throughout the year. This is because it is characterised by low-nutrient waters and deep thermocline (Longhurst, 2006) associated with the subtropical gyre system (George et al., 2012). Studying the physical and biochemical aspects of the Mascarene Plateau (delineated by Seychelles in the north (5°S,56°E) and Mauritius in the south (20°S, 57°E)), New et al. (2005) showed that the South Equatorial Current (SEC) is responsible for the higher SChl-a concentration north of the subtropical gyre compared to the south. The SEC forms the northern boundary of the subtropical gyre system and it acts as a sharp border between the northern nutrient-rich waters and the southern nutrient-poor waters. It delivers high nutrient concentration to the surface layers in the northern part. This is because on the northern side of the SEC, density surfaces are uplifted and the water masses have high nutrient concentration (on density levels).

The western part of the SCTR and the Saya de Malha Bank (SMB) (60°E-10°S) as well as the Mascarene Islands exhibit high phytoplankton blooms all year long (Figure 20). New et al. (2005) suggested that the SEC tends to divert around the banks rather that flowing over them. Hence, the ecosystem is presumably trapped, explaining the high surface chlorophyll-a concentration around the SMB and the Mascarene Islands throughout the year.

7.2 Interannual variability - Physical Response

During IOD and ENSO, southeasterlies off Sumatra and Java intensify and this leads to a cooling of SST in the eastern Indian Ocean as shown in Figure 24 (Left; June to December) and Figure 25 (Left; June-November). This intense wind regime increases evaporation from the surface, coastal upwelling and vertical mixing (Shinoda et al., 2004), causing the negative SST anomaly and suppressing atmospheric convection there. At the same time, the sea level anomaly becomes negative in this region and this results in the shoaling of the thermocline (Saji et al., 1999). The strong southeasterlies are known to weaken after October and this results in a decrease in coastal upwelling (Murtugudde et al., 2000) and surface evaporation as well as an increase in solar radiation, due to the suppressed convective clouds. This forcing causes the SST anomalies to shift from negative to positive in the eastern Indian Ocean as seen in Figure 24 (Left, January to June) and Figure 25 (Left; January to July) (Tokinaga and Tanimoto, 2004). In the western Indian Ocean, warming of SST occurs as a result of the strong southeasterlies regime and its effect in the eastern IO. Due to the shifting of the trade winds, convergence is increased in the western part, leading to a reduced wind speed and evaporation. Hence, this will cause a warming up of SST in the western IO. At the same time, thermocline depth will deepen due to a reduced eastward transport (Saji et al., 1999).

During pure positive IODs, significant negative D20 anomalies (deepening) occur in the model SCTR region whereas positive D20 anomalies (shoaling) occur in the eastern subtropical Indian Ocean. On the contrary, positive D20 anomalies are observed in the model SCTR during pure negative IODs with no or minor deepening in the eastern Indian Ocean. These results agree with the work done by Tozuka et al. (2010). Easterly wind anomalies develop along the equator during positive IOD, exciting an upwelling favourable equatorially trapped Kelvin waves. The Kelvin waves radiate into the eastern ocean and on reaching the eastern edge; shoal

the thermocline in the eastern equatorial Indian Ocean by generating coastal upwelling (Vinayachandran et al., 2002). An upwelling Rossby wave is reflected offshore (westward) causing the shoaling of the thermocline to move westward (from longitude 100°E to 80°E – Figure 33 Left). Currie et al. (2013) showed that this upwelling Rossby waves occur on both sides of the equator. However, a deeper than normal thermocline depth is observed in the central and western SCTR region. This negative anomaly (deepening) is influenced by an off-equatorial convergence which is due to the large-scale Ekman pumping velocities in the eastern equatorial Indian Ocean. It spreads westward as symmetrical Rossby waves signals (Currie et al., 2013). The deepening of the thermocline in the western IO has a larger amplitude than the shoaling in the eastern IO since it interacts with the normally-shallow SCTR (Hermes and Reason, 2008; Yokoi et al., 2008). However, by August of the next year, the deepening starts to weaken in the SCTR due to the reduction of the negative Ekman pumping velocity (w_e) and the transition to positive w_e in the eastern part of the Indian Ocean (Trenary and Han, 2012).

Pure negative IOD are related to anomalous Ekman pumping velocity (w_e) in the eastern Indian Ocean and this forced the arrival of upwelling Rossby wave in austral winter, as suggested by Tozuka et al. (2010). On the eastern boundary of the Indian Ocean, equatorial westerlies generate equatorial Ekman convergence and an eastward-propagating downwelling Kelvin wave whereas anomalous southward alongshore winds cause coastal downwelling. Positive Ekman pumping velocity anomalies will arise in the eastern tropical Indian Ocean due to these anomalous winds, causing the 20°C isotherm to shoal (positive anomaly). In December (0), the negative IOD reaches its climax with the positive w_e also reaching its peak (Trenary and Han, 2012). The upwelling Rossby waves continue to propagate westward, attaining its maximum amplitude in December (0) in the SCTR region, causing the maximum shoaling in this particular month. As from January (+1), the planetary waves propagate at a weakened amplitude while the positive w_e weaken in the eastern tropical Indian Ocean.

During positive ENSO, the thermocline deepens in the SCTR region. This deepening is due to the downwelling Rossby waves which propagate westward from the south-eastern Indian Ocean (Perigaud and Delecluse, 1993; Masumoto and Meyers, 1998; Chambers et al., 1999). This deepening is however not as intense as it is during positive IOD events since ENSO is known to affect the thermocline depth mostly south of 10°S (Rao and Behera, 2005; Yu et al., 2005; Xie et al., 2002).

It should be noted that, in the model, the spatial pattern of D20 and SST anomalies are quite similar during IOD years and this suggests that the IOD-linked surface temperature anomaly is influenced by the variability of thermocline depth. A deepening of the 20°C isotherm is associated with a positive SST anomaly as the deep cold water cannot influence the temperature of the surface layers. Similarly, a shallow thermocline corresponds to negative SST anomalies as cold water is brought towards the ocean surface (Rao and Behera, 2005). This is in agreement with previous studies (Murtugudde et al., 2000; Xie et al., 2002; Tozuka et al., 2010) where it has been shown that the IOD-SST relationship is greatly dominated by wind-driven changes of the thermocline depth.

However, no conformity is to be noted between the D20 and SST anomalies during ENSO years. In response to Pacific SST anomalies, the adjustments of the ascending and descending branches of the Walker circulation (Reason et al., 2000; Venzke et al., 2000) force changes in surface winds (Klein et al., 1999; Du et al., 2009) and cloud cover. These influence the surface heat fluxes which drive the ENSO-related SST anomalies, hence no relationship between ENSO-linked surface temperature and thermocline depth. Nevertheless, in the eastern part of the Indian Ocean, ENSO forcing does shoal the thermocline in austral summer but due to the monsoon related wind reversal in the Northern Hemisphere, the upwelling winds that lift the cold waters to the ocean surface (thus influencing the SST signal) are hindered at this time of the year (Xie et al., 2002, Schott et al., 2009).

It is shown in this study that the variability of the SCTR is mainly influenced by the Indian Ocean Dipole. During IOD, wind anomalies develop at the equator and these produce strong Ekman pumping in the central and eastern Indian Ocean, south of the equator. Hence, the thermocline deepens between 5°S and 12°S. Due to planetary wave dynamics, this deepening propagates westward (Masumoto and Meyers, 1998; Webster et al., 1999) and hence influences the SCTR. Similar processes occur during ENSO but it is located farther south and hence, does not greatly influence the SCTR (Rao and Behera, 2005; Yu et al., 2005; Currie et al., 2013).

Schott et al. (2009) gave a more detailed explanation by showing that the off-equatorial anticyclonic wind regimes are better formed and that the equatorial easterlies are stronger during IOD compared to ENSO years. The ocean's response reflects these differences since the IOD-forced Rossby waves will be confined north of 10°S, hence largely influencing the SCTR compared to ENSO-forced Rossby waves which might influence the SCTR south of 10°S (Xie et al., 2002).

7.3 Interannual variability – Biological Response

During a pure positive IOD, the typical spatial distribution of surface chlorophyll-a in the Indian Ocean is entirely disrupted (Levy et al., 2007; Wiggert et al., 2009, Currie et al., 2013). The maximum variability in the bloom observed is in the eastern Indian Ocean and in the eastern part of the SCTR (sub-region 3) with a positive anomaly of surface chlorophyll-a whereas for all the other years, anomalies are usually negative in this specific region (Jayakumar and Gnanaseelan, 2012). According to Wiggert et al. (2009), these anomalies of chlorophyll-a are due to the wind regime anomalies that can impact upwelling and intensity of vertical mixing; as well as the distribution of planetary waves (Rossby waves) which in turn have an effect on the thermocline depth.

The south-easterly wind anomalies along the coast of Sumatra and Java during the positive IOD are upwelling favourable, hence shoaling the thermocline depth (as seen in Figure 26) and driving coastal surface nutrient enrichment. This D20 shoaling and nutrient enrichment is due to the offshore Ekman transport by surface wind stress or upward vertical velocity at the bottom of Ekman layer (Ekman pumping velocity; Pedlosky, 1998) by wind stress curl (Jayakumar and Gnanaseelan, 2012). Nagura and McPhaden (2008) stated that in austral summer, the Wyrtki Jet (Wyrtki, 1973), which usually operates to keep the thermocline and nutricline deep in the eastern tropical Indian Ocean, is restrained by the anomalous equatorial easterlies present throughout pure positive IOD. This forcing explains the prominent biological enhancement (phytoplankton blooms) and physical influence (20°C isotherm) during the IOD manifestation in the eastern Indian Ocean. As from January, the blooms dissipate and this may develop due to the onset of onshore winds (Wiggert et al., 2009).

In the central and western part of the SCTR, a slight negative anomaly of SChl-a is observed during the early stage of IOD (June-August). This signature then dissipates and SChl-a reaches its mean concentration. This is because the SCTR is an offshore region, hence exhibiting weak variability in SChl-a. The deep thermocline during a positive IOD seems to have no effect on the SChl-a anomaly in the region. A possible explanation may be that the central and western part of the SCTR is known as a deep chlorophyll maximum (DCM) region (Resplandy et al., 2009) and hence an anomaly in phytoplankton cells will not be detected at the surface.

The contrary occurs during pure negative IOD with a negative anomaly in the eastern Indian Ocean and the eastern SCTR region (sub-region 3). However, this negative anomaly started a month earlier than the positive anomaly during positive IOD. No upwelling favourable winds are present off the coasts of Sumatra and Java. However, coastal downwelling occurs due to the anomalous southward alongshore winds, deepening the nutrient-rich waters (deep

nutricline). Hence, surface waters will be depleted of phytoplankton cells, reducing the SChl-a concentration in this region.

When considering pure positive and negative ENSO, no significant features are observed in surface chlorophyll-a anomaly in the studied region. The minor negative anomaly in the SCTR starting in May may be due to the minor negative anomaly (deepening) of the 20°C isotherm observed in the SCTR at the same time, which deepened the nutricline, hence limiting the essential nutrients for phytoplankton blooms. The positive anomaly (shoaling) of the 20°C isotherm in the SCTR during pure negative ENSO does not reflect in phytoplankton blooms at the surface. This is in agreement with the study done by Currie et al. (2013) which showed that ENSO has no significant influence on the surface chlorophyll-a in this specific region of the Indian Ocean. The DCM in the region may leave no signature at the surface and ENSO is known to influence the Indian Ocean's response south of 10°S (Rao and Behera, 2005; Yu et al., 2005; Xie et al., 2002).

8 CONCLUSION

The Seychelles-Chagos Thermocline Ridge (SCTR), the main area of this study, has a strong interannual variability of thermocline depth (Masumoto and Meyers, 1998) and intra-seasonal variability of chlorophyll-a (Jayakumar and Gnanaseelan, 2012). The main aims of the study were to investigate the annual cycle of surface chlorophyll-a in the SCTR region, as well as the variability of the thermocline depth and surface chlorophyll-a in relation to IOD and ENSO events.

The short record of remotely-sensed data of surface chlorophyll-a (SeaWiFS) makes it difficult to confidently study the impacts of the large scale climate modes (IOD and ENSO) on the biological aspect of the ocean and its annual cycle. However, the use of coupled physical-biogeochemical general circulation models (NEMO-PISCES) with a 44-year hindcast(RUN58-01) and a 50-year hindcast (RUN58-07) has enabled the investigation of the variations associated with IOD and ENSO in the Indian Ocean, more specifically in the SCTR and throughout the upper layers. Thus, physical, biogeochemical and remotely-sensed data sets have allowed the characterisation of the surface and subsurface variability of oceanic physical and biological responses in the study region.

Best coverage data of surface chlorophyll-a available provided by SeaWiFS and coupled bio-physical models showed that the SCTR region exhibits an annual cycle in surface chlorophyll-a concentration, with a peak during austral winter (June-August). Due to the strong winter south-easterlies on the region during this period, wind-driven mixing and upwelling is enhanced, bringing nutrient-rich waters near the surface, causing entrainment to the surface and production of phytoplankton cells. In austral summer, the mixed layer depth is usually shallower than the nutricline and strong winds do not prevail over the region, hence hindering surface phytoplankton blooms. With an increase in south-easterlies over the region in austral

fall, wind-driven vertical mixing will increase, positively influencing the SChl-a content. The wind regimes over the SCTR region start to subside during austral spring causing nutrient depletion and less surface phytoplankton blooms.

The seasonal vertical distribution of chlorophyll-a across the SCTR showed that when surface blooms are triggered, subsurface production decreases. Light and nutrient limitations play a major role in this reduction in subsurface, showing that phytoplankton growth at the surface and subsurface is in a phase reversal.

The physical part of both RUN58-01 and RUN58-07 shows good agreement with observational data but when considering the biogeochemical part, RUN58-01 shows better agreement with SeaWiFS compared to the Run58-07 which over-estimates the surface chlorophyll-a content in austral winter and spring. This over-estimation was dominated by the chlorophyll-a content in nano-phytoplankton. The nutrient co-limitation and the dependence on temperature terms of the formulation of Geider et al. (1998) were removed in RUN58-07. The influence of light limitation on the growth rate of nano-phytoplankton depends on this modified version of the formulation and hence, nano-phytoplankton was produced in higher concentration in the model.

Results of the study showed that thermocline variations of the SCTR are mostly influenced by the Indian Ocean Dipole (IOD) whereas El Niño Southern Oscillation (ENSO) has a weaker and less-extensive influence on the variations. Equatorial easterlies and anticyclonic wind regimes are stronger during IOD in comparison to ENSO and hence, planetary Rossby waves are confined north of 10°S, largely influencing the SCTR region. During ENSO, these planetary waves influence the SCTR south of 10°S (Xie et al., 2002; Schott et al., 2009). Hence, the subsurface variability of the Indian Ocean can be attributed to a prevailing IOD influence.

The IOD is mainly responsible for the disruption of the variability of surface chlorophyll-a in the SCTR. The western part of the SCTR (sub-region 1), which is known to be more productive and hence have more phytoplankton cells, is more oligotrophic than the eastern part (sub-region 3) where phytoplankton blooms occur during positive IOD. The upwelling favourable south-easterly winds which prevail along the coast of Java and Sumatra during positive IOD events are accountable for these phytoplankton blooms since they bring nutrient-rich waters to the euphotic zone where all the conditions are met for high phytoplankton production. The opposing situation occurs during negative IOD events with downwelling favourable southward alongshore winds, deepening the nutricline. However, ENSO does not have a consequential impact on the surface chlorophyll-a in the SCTR region and this is because ENSO mainly influences the SCTR south of 10°S.

The outcomes of this study are useful in understanding the variability of the physical and biogeochemical oceanic responses during IOD and ENSO events and to better comprehend the forcing which drive the interannual variation of the surface chlorophyll-a concentration in the SCTR region.

Chlorophyll-a response has been shown to vary according to different large scale climate modes (ENSO and IOD). As phytoplankton constitutes the foundation of aquatic food webs in open-ocean environments, they are the primary producers and heterotrophs depends on them. Anomalies in their concentration attributed to climate modes will hence have great impact on the ecology of all trophic levels. An example of this would be the eastward migration of the tuna fishery in synchronicity with an anomaly of phytoplankton growth and thermocline that occur during the 1997/1998 IOD (Marsac and Le Blanc, 1999; Menard et al., 2007). Understanding the climate-related impacts on the phytoplankton growth is instrumental in the catch of purse seine fleets in the Indian Ocean. Hence, the utilization and conservation of fish stocks of tuna and tuna-like species can be optimised.

8.1 Recommendation and future works

Higher resolution coupled physical-biogeochemical models with longer-term datasets and higher accuracy can be used to improve this study. More emphasis should be put on the difference in wind regimes in the Indian Ocean between the Indian Ocean Dipole (IOD) and the El Niño Southern Oscillation (ENSO) of the specific coupled model since these are the main drivers for upwelling. Integrated chlorophyll-a concentration variability can also be investigated during positive and negative IOD and ENSO events as the SCTR is a region of deep chlorophyll maximum (DCM) which is usually found in the depth range 50-80m.

The region around the Saya de Malha Bank and the Chagos Archipelago is always high in phytoplankton productivity as can be observed by the high concentration of surface chlorophyll-a concentration. Previous studies have given some arguments to why phytoplankton blooms always occur in these regions. However, no tangible study has been done to investigate these high SChl-a content.

The next step from this study is to correlate the results presented here with datasets of catch per unit effort (CPUE) of purse seine fleets from the Indian Ocean Tuna Commission (IOTC) to investigate the migration of tuna and tuna-like species during large scale climate modes especially during IOD when the eastern part of the SCTR is more productive than the western part.

Through the Sustained Indian Ocean Biogeochemistry and Ecosystem Research (SIBER) (Hood et al., 2010), higher resolution and longer-term datasets of physical-biogeochemical-biological models are being made available and these coupled ecosystem models can be used to better understand and predict the physical, biogeochemical and biological variability; as well as the impacts of climate modes on the Indian Ocean. Their feedback on the ecosystem of the ocean would hence be more accessible.

9 APPENDIX

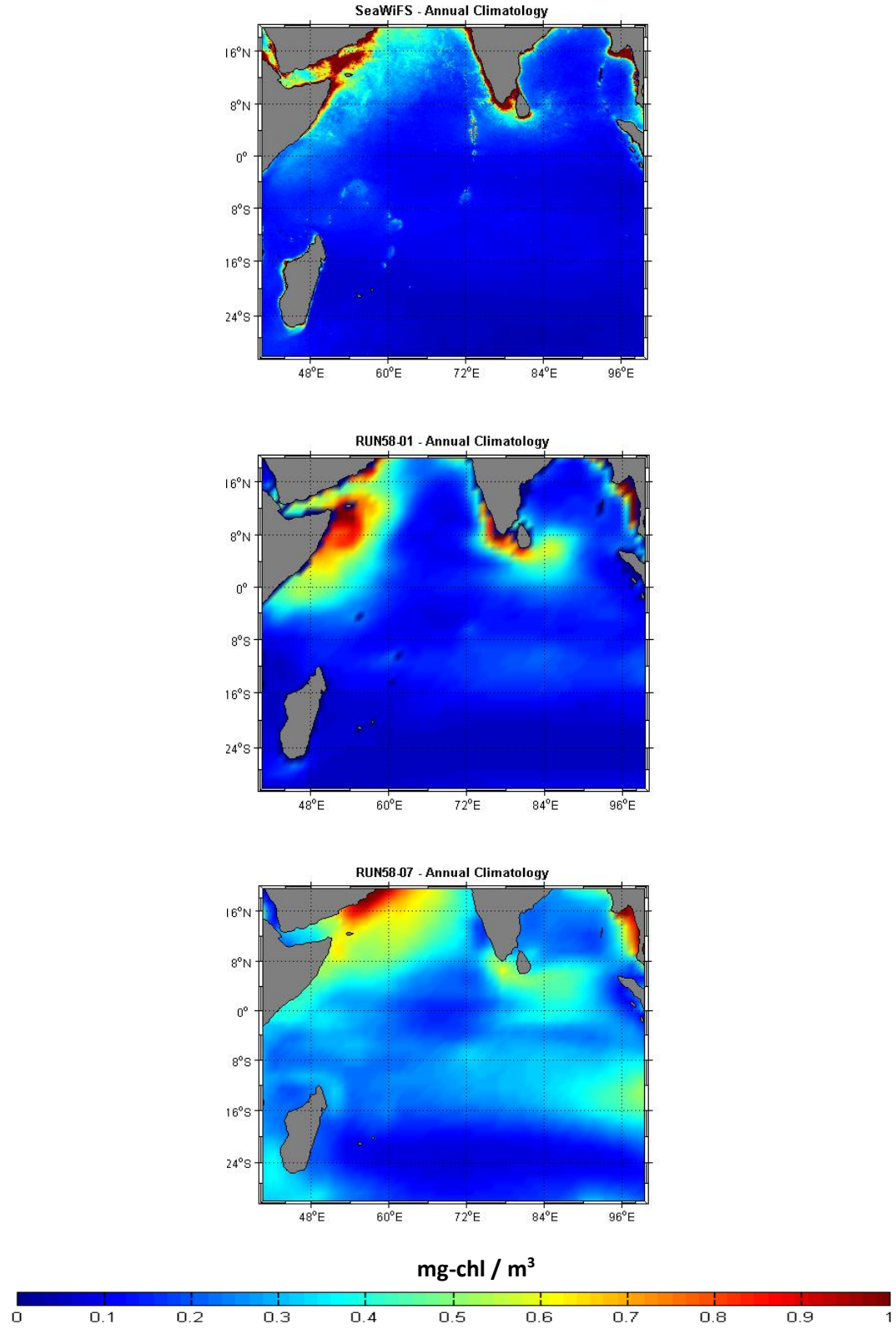

Figure 30: Annual Climatology of surface chlorophyll-a concentration (mg-Chl/m^3) from SeaWiFS (first row), RUN58-01 (second row) and RUN58-07 (third row). Tee climatology was calculated over a time period of 4 years (1998-2001).

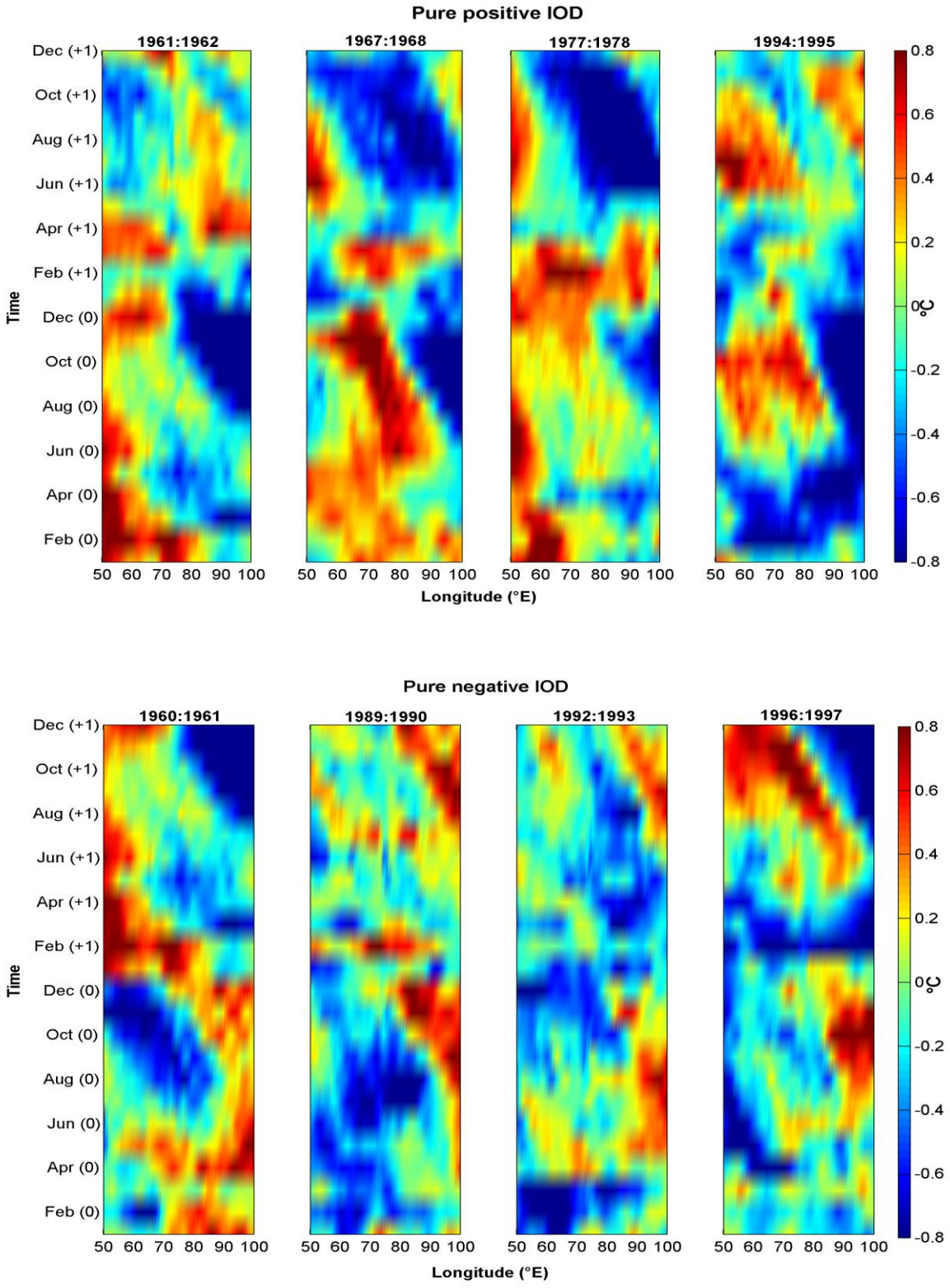

Figure 31: Time-Longitudinal diagrams of composite SST anomalies averaged over the latitudes 5°S-12°S for specific pure positive IOD years (1961, 1967, 1977 and 1994; first row) and pure negative IOD years (1960, 1989, 1992 and 1996; second row).

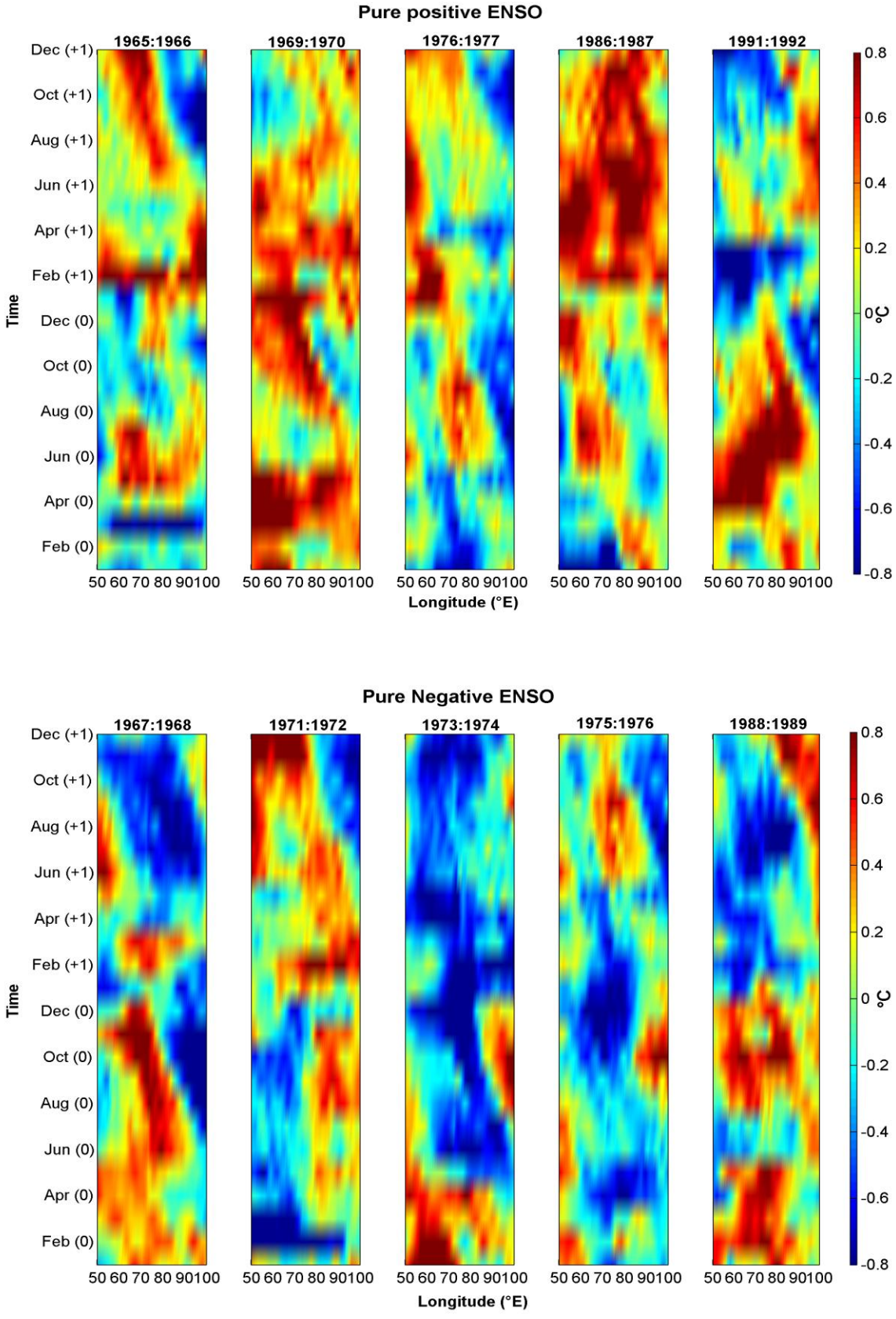

Figure 32: Time-Longitudinal diagrams of composite SST anomalies averaged over the latitudes 5°S-12°S for specific pure positive ENSO years (1965, 1969, 1976, 1986 and 1991; first row) and pure negative ENSO (1967, 1971, 1973, 1975 and 1988; second row).

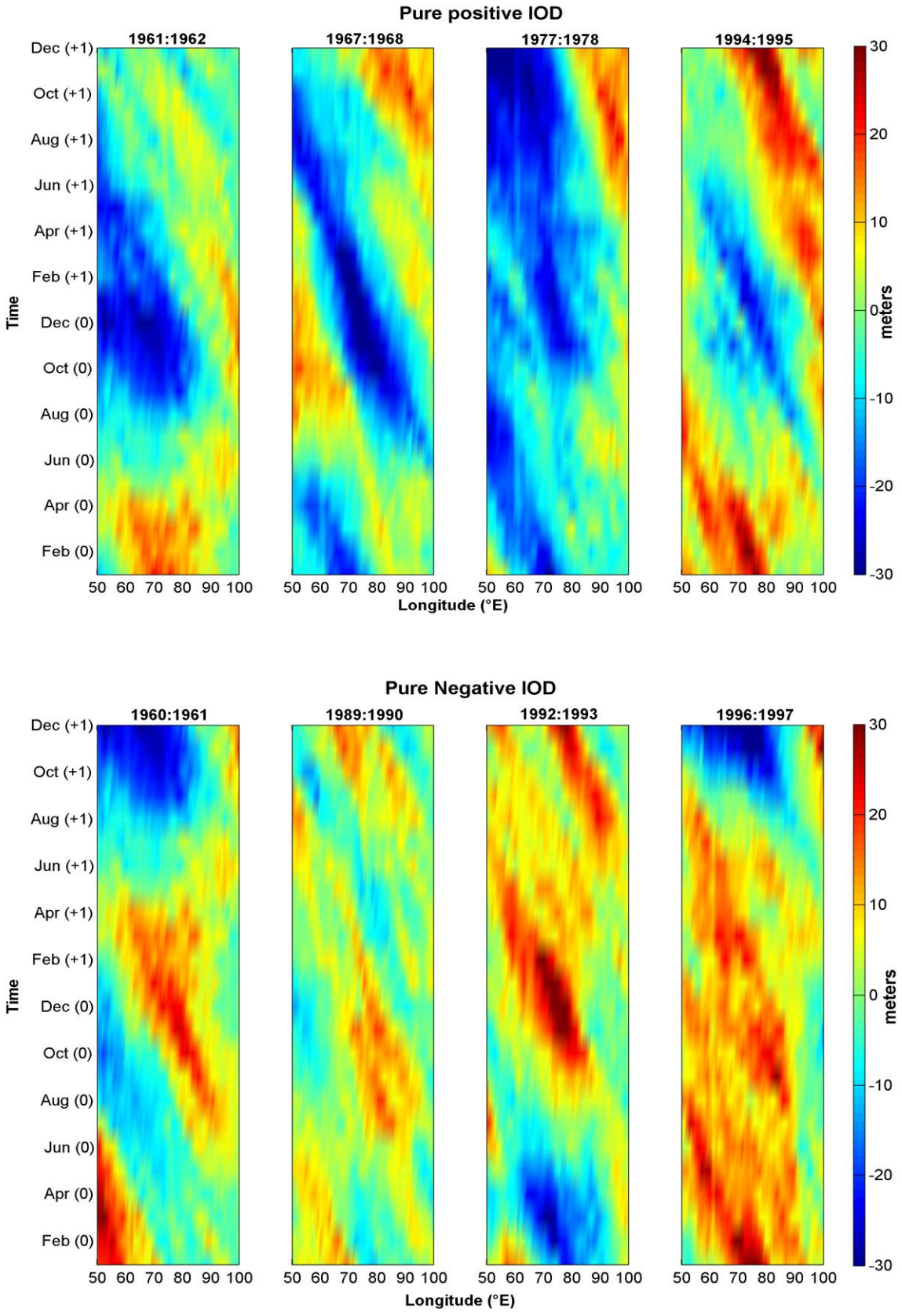

Figure 33: Time-Longitudinal diagrams of composite depth of 20°C isotherm anomalies averaged over the latitudes 5°S-12°S for specific pure positive IOD years (1961, 1967, 1977 and 1994; first row) and pure negative IOD years (1960, 1989, 1992 and 1996; second row).

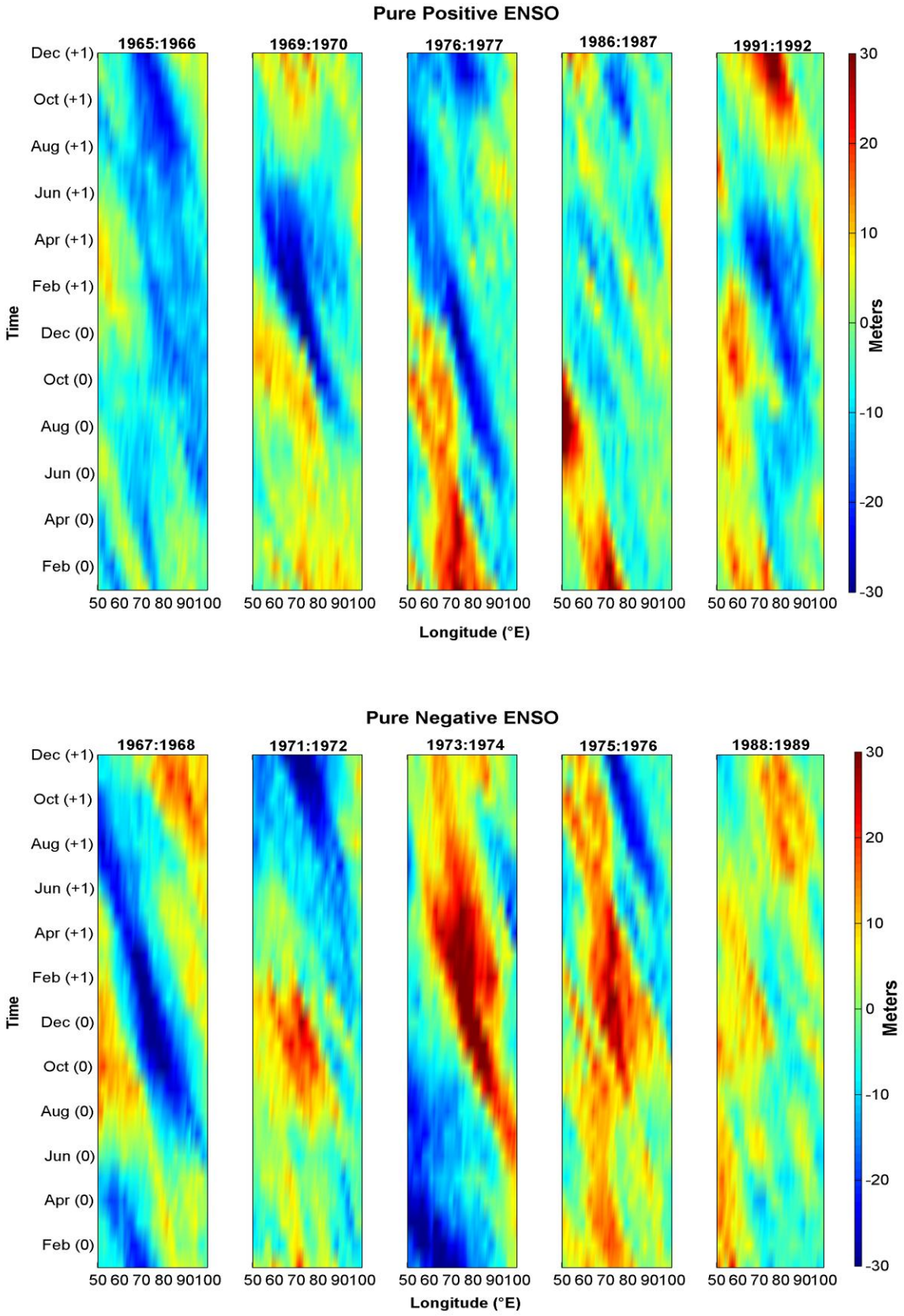

Figure 34: Time-Longitudinal diagrams of composite depth of 20°C isotherm anomalies averaged over the latitudes 5°S-12°S for specific pure positive ENSO years (1965, 1969, 1976, 1986 and 1991; first row) and pure negative ENSO (1967, 1971, 1973, 1975 and 1988; second row).

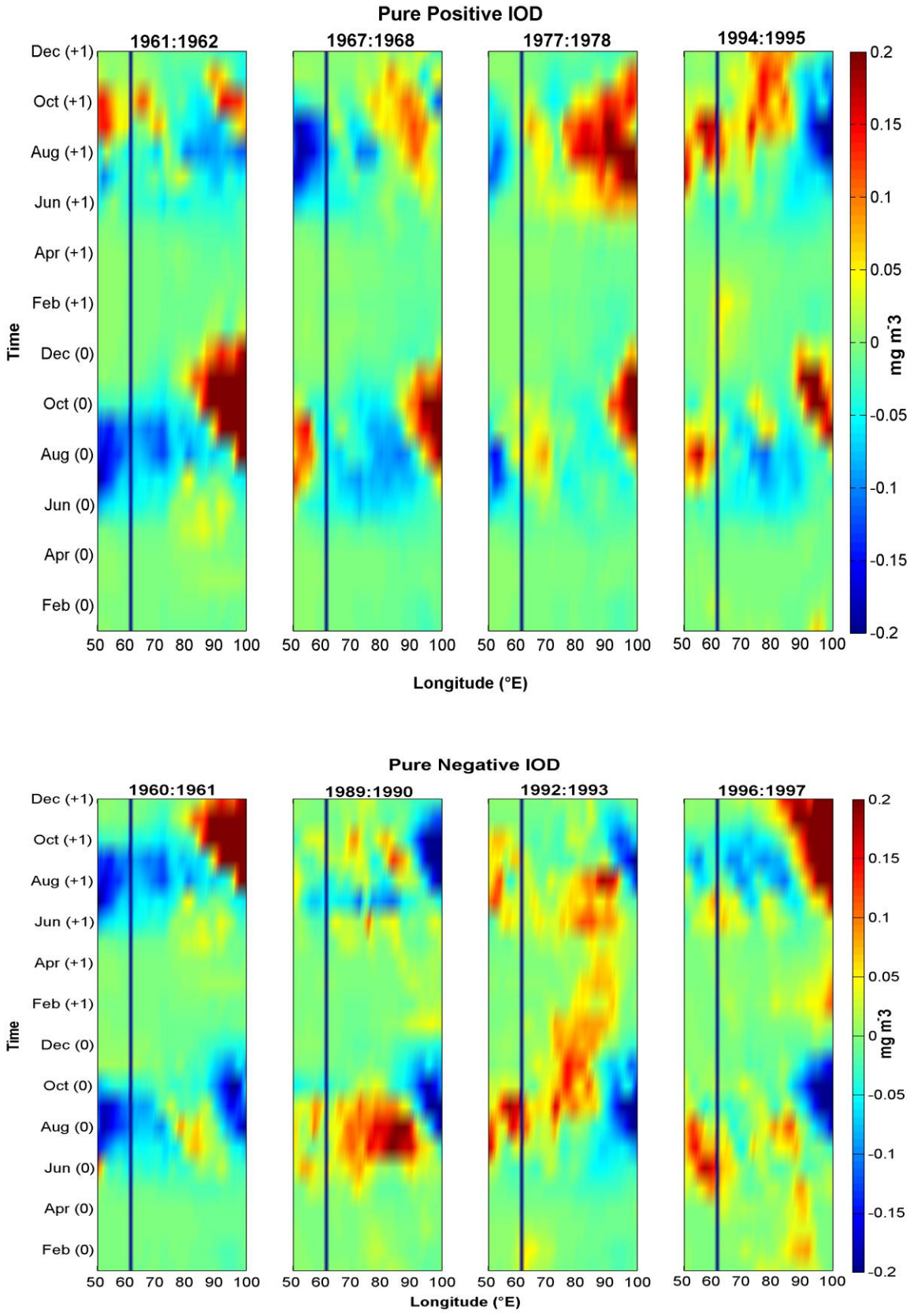

Figure 35: Time-Longitudinal diagrams of composite SChl-a anomalies averaged over the latitudes 5°S-12°S for specific pure positive IOD years (1961, 1967, 1977 and 1994; first row) and pure negative IOD years (1960, 1989, 1992 and 1996; second row)

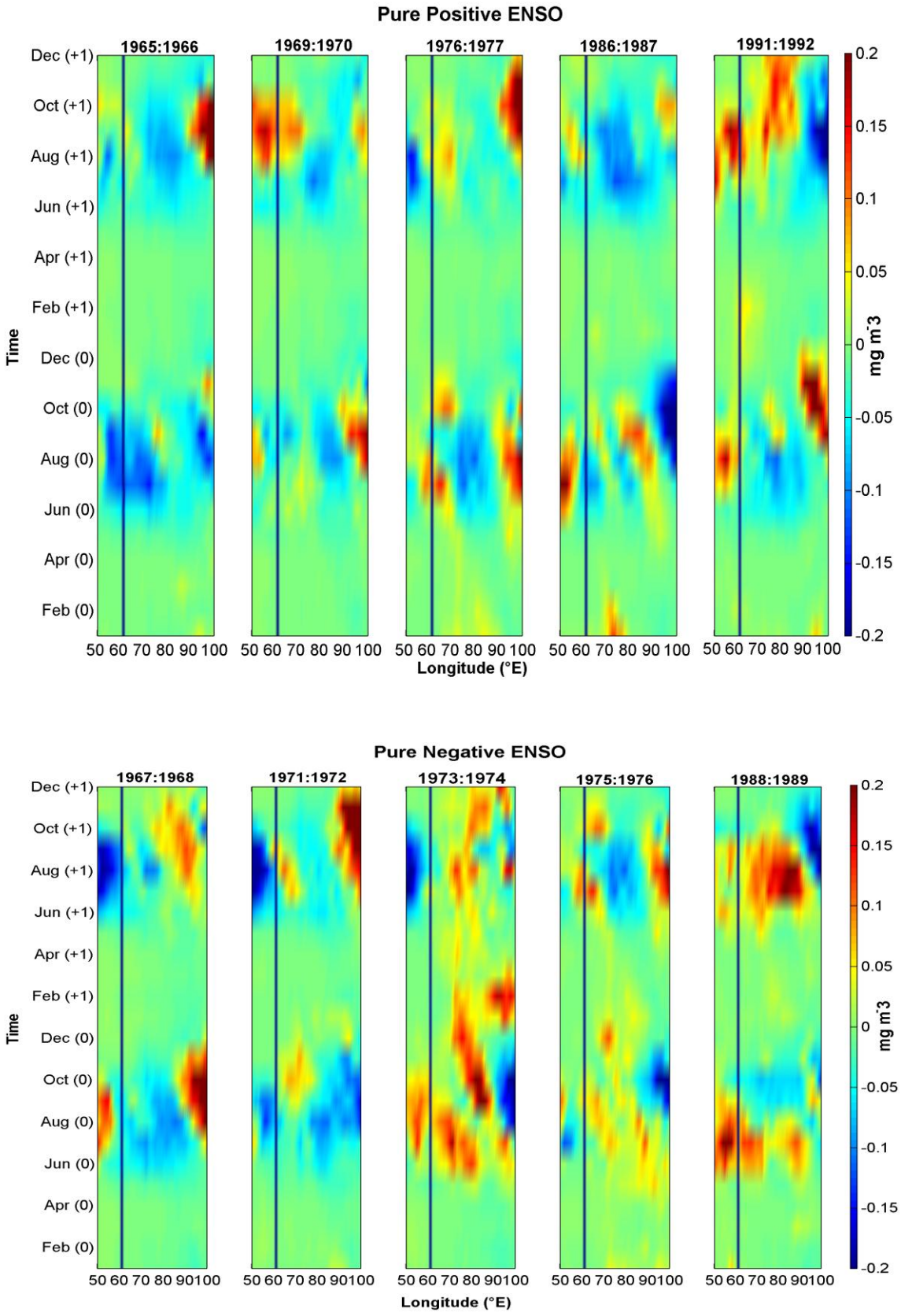

Figure 36: Time-Longitudinal diagrams of composite SChl-a anomalies averaged over the latitudes 5°S-12°S for specific pure positive ENSO years (1965, 1969, 1976, 1986 and 1991; first row) and pure negative ENSO (1967, 1971, 1973, 1975 and 1988; second row)

10 References

Alexander, M. A., Bladé, I., Newman, M., Lanzante, J.R., Lau, N.G., and Scott, J.D.: The Atmospheric Bridge: The Influence of ENSO Teleconnections on Air-Sea Interaction over the Global Oceans, Journal of Climate, 15, 2205-2231, 2002.

Annamalai, H., Lie, P., and Xie, S.-P.: Southwest Indian Ocean SST Variability: Its Local Effect and Remote Influence on Asian Monsoons, Journal of Climate, 18, 4150-4167, 2005.

Aumont, O. and Bopp, L.: Globalizing results from ocean in situ iron fertilization studies. Global Biogeochemical Cycles 20, GB2017, doi:10.1029/2005GB002591, 2006.

Aumont, O., Bopp, L., and Schulz, M.: What does temporal variability in aeolian dust deposition contribute to sea-surface iron and chlorophyll distributions?, Geophysical Research Letters, 35, L07607, doi:10.1029/2007GL031131, 2008.

Aumont, O., Maier-Reimer, E., Blain, S., and Monfray, P.: An ecosystem model of the global ocean including Fe, Si, P colimitations, Global Biogeochemical Cycles, 17, 1060, doi:10.1029/2001GB001745, 2003.

Berliand, M. E. and Strokina T. G.: Global Distribution of the Total Amount of Clouds, 71 pp., Hydrometeorological Publishing House, 1980.

Birkett, C., Murtugudde, R., Allan, T.: Indian Ocean climate event brings floods to East Africas's lakes and the Sudd March, Geophysical Research Letters, 29, 1031-1034, 1999.

Black, E., Silingo, J., and Sperber, K.R.: An Observational Study of the Relationship between Excessively Strong Short Rains in Coastal East Africa and Indian Ocean SST, Monthly Weather Review, 131, 74-94, 2003.

Blanke, B. and Delecluse, P.: Variability of the Tropical Atlantic Ocean Simulated by a General Circulation Model with Two Different Mixed-Layer Physics, Journal of Physical Oceanography, 23, 1363-1388., 1993

Boyer, T., Levitus, S., Garcia, H., Locarnini, R. A., Stephens, C., and Antonov, J.: Objective Analyses of Annual, Seasonal and Monthly Temperature and Salinity for the World Ocean on a 0.25° Grid, International Journal of Climatology, 25, 931-945, doi: 10.1002/joc.1173, 2005.

Busalacchi, A. J. and Picaut, J.: Seasonal variability from a model of the Tropical Atlantic Ocean, Journal of Physical Oceanography, 13, 1564-1588, 1983.

Chambers, D. P. and Taply, B.D.: Anomalous warming in the Indian Ocean coincident with El Niño, Journal of Geophysical Research, 104, 3035-3047,1999.

Chen, Y. and Gao, X.: Comparison of Two Methods for Phytoplankton Chlorophyll-a Concentration Measurement, Journal of Lake Science, 12, 185-188, 2000.

Cravatte, S., Madec, G., Izumo, T., Menkes, C., and Bozec, A.: Progress in the 3-D circulation of the eastern equatorial Pacific in a climate ocean model, Ocean Modelling, 17, 28-48, doi:10.1016/j.ocemod.2006.11.003, 2006.

Currie, J. C., Lengaigne, M., Vialard, J., Kaplan, D. M., Aumont, O., Naqvi, S. W. A., and Maury, O.: Indian ocean Dipole and El Niño/Southern Oscillation impacts on regional chlorophyll anomalies in the Indian Ocean, Biogeosciences, 10, 1-22, doi:10.5194/bg-10-1-2013, 2013.

de Boyer Montégut, C., Madec, G., Fisher, S. A., Lazar, A., and Iudicone, D.: Mixed layer depth over the global ocean: An examination of profile data and a profile-based climatology, Journal of Geophysical Research, 19, C12003, doi:10.1029/2004JC002378, 2004.

de Boyer Montégut, C., Vialard, J., Shenoi, S. S. C., Shankar, D., Durand, F., Ethé, C., and Madec, G.: Simulated Seasonal and Interannual Variability of the Mixed Layer Heat Budget in the Northern Indian Ocean, Journal of Climate, 20, 3249-3268, DOI: 10.1175/JCLI4148.1, 2007.

Drbohlav, H. K. L., Gualdi, S., and Navarra, A.: A Diagnostic of the Indian Ocean Dipole Mode in El Niño and Non-El Niño Years, Journal of Climate, 2005.

Du, Y., Xie, S.-P, Huang, G., and Hu, K.-M: Role of air-sea interaction in the long persistence of El Niño-induced North Indian Ocean warming, Journal of Climate, 22, 2023-2038, 2009.

Du, Y., Xie, S.-P., Huang, G., and Hu, K.-M.: Role of air-sea interaction in the long persistence of El Niño-induced North Indian Ocean warming, Journal of Climate, 22, 2023-2038, 2009.

Duvel, J. P. and Vialard, J.: Indo-Pacific Sea Surface Temperature Perturbations Associated with Intraseasonal Oscillations of Tropical Convection, Journal of Climate, 20, 3056-3082, doi: 10.1175/JCLI4144.1, 2007.

Enfield, D. B. and Mayer, D. A.: Tropical Atlantic sea surface temperature variability and its relation to El Niño-Southern Oscillation, Journal of Geophysical Research, 12, 929-945, 1997.

Falkowski, P. G., Barber, R. T., and Smetacek, V.: Biogeochemical controls and feedbacks on ocean primary production, Science, 281, 200–206, doi:10.1126/science.281.5374.200, 1998.

Falkowski, P. G. and Raven, J.A.: Aquatic Photosynthesis, Blackwell Science, Malden, MA, 1997.

Feng, M. and Meyers, G.: Interannual variability in the tropical Indian Ocean: a two-year time-scale of Indian Ocean Dipole, Deep-Sea Research, Part II, 50, 2263-2284, doi:10.1016/S0967-0645(03)00056-0, 2003.

Fichefet, T. and Maqueda, M. A. M.: Sensitivity of a global sea ice model to the treatment of ice thermodynamics and dynamics, Journal of Geophysical Research, 102, 12609-12646, 1997.

Fiedler, P. C.: The annual cycle and biological effects of the Costa Rica Dome, Deep-Sea Research, Part I, 49, 321-338, 2002.

Fu, L.-M. and Cheney, R. E.: Application of Satellite Altimetry to Ocean Circulation Studies: 1987-1994, Reviews of Geophysics, 33, 212-223, 1995.

Geider, R. J., MacIntyre, H. L., and Kana, M. T.: A dynamic regulatory model of phytoplanktonic acclimation to light, nutrients, and temperature, Limnology and Oceanography, 43, 679-694, 1998.

George, J. V., Nuncio, M., Chacko, R., Anilkumar, N., Noronha, S. B., Patil, S. M., Pavithran, S., Alappattu, D. P., Krishnan, K. P., and Achuthankutty, C. T.: Role of physical processes in chlorophyll distribution in the western tropical Indian Ocean, Journal of Marine Systems, 113–114, 1–12, 2013.

Glebushko, K.: The El Niño phenomenon: from understanding to predicting. Discovery guide, 2004.

Gnanaseelan, C. and Vaid, B. H.: Interannual variability in the Biannual Rossby waves in the tropical Indian Ocean and its relation to Indian Ocean Dipole and El Niño forcing, Ocean Dynamics, 60, 27-40, doi: 10.1007/s10236-009-0236-z, 2010.

Goddard, L. and Graham, N. E.: Importance of the Indian Ocean for simulating rainfall anomalies over eastern and southern Africa, Journal of Geophysical Research, 104, 19099-19116, 1999.

Goose, H.: Modelling the large-scale behaviour of the coupled ocean-sea-ice system, Ph.D. thesis, Univeristé Catholique de Louvain, Louvain-La-Neuve, Belgium, 1997.

Hermes, J. C. and Reason, C. J. C: Annual cycle of the South Indian Ocean (Seychelles-Chagos) thermocline ridge in a regional ocean model, Journal of Geophysical Research, 113, C04035, doi:10.1029/2007JC004363, 2008.

Hong, C.-C., Lu, M.-M., and Kanamitsu, M.: Temporal and spatial characteristics of positive and negative Indian Ocean dipole with and without ENSO, Journal of Geophysical Research, 113, D08107, doi:10.1029/2007JD009151, 2008.

Hong, L., Wang, C., Zhou, Y., Chen, M., Liu, H., Lin, Z., and Song, X.: The distribution of chlorophyll a in the tropical eastern Indian Ocean in austral summer, Acta Oceanologica Sinica, 31, 146-159, doi: 10.1007/s13131-012-0244-6, 2012.

Huang, B., Liu, Y., and Chen, J.: Temporal and spatial distribution of size-fractionized phytoplankton biomass in East China Sea and Huanghai Sea, Acta Oceanologica Sinica, 28, 156-164, 2006.

Izumo, T., de Boyer Montégut, C., Luo, J. –J., Behera, S. K., Masson, S., and Yamagata, T.: The Role of the Western Arabian Sea Upwelling in Indian Monsoon Rainfall Variability, Journal of Climate, 21, 5603-5623, doi: 10.1175/2008JCLI2158.1, 2008.

Izumo, T., Vialard, J., Lengaigne, M., de Boyer Montégut, C., Behera, S. K., Luo, J. –J., Cravatte, S., Masson, S., and Yamagata T.: Influence of the state of the Indian Ocean Dipole following year's El Niño, Nature Geoscience, 168-172, doi: 10.1038/NGEO760, 2010.

Jackett, D. R. and McDougall, T. J.: Minimal Adjustment of Hydrographic Profiles to Achieve Static Stability, Journal of Atmospheric and Oceanic Technology, 12, 381-389, 1995.

Jayajumar, A., Vialard, J., Lengaigne, M., Gnanaseelan, C., McCreary, JR., J. P., and Kumar, P. B.: Process controlling the surface temperature signature of the Madden-Julian Oscillation in the thermocline ridge of the Indian Ocean, Climate Dynamics, 37, 2217-2234, doi: 10.1007/s00382-010-0953-5, 2011.

Jayakumar, A. and Gnanaseelan, C.: Anomalous intraseasonal events in the thermocline ridge region of Southern Tropical Indian Ocean and their regional impacts, Journal of Geophysical Research, 117, C03021, doi:10.1029/2011JC007357, 2012.

Jickells, T. D. and Spokes, L. J.: Atmospheric iron inputs to the oceans, in Biogeochemistry of Fe in Seawater, edited by Turner D. R. and Hunter K. A., 85–121 pp., Wiley Interscience, New York, 2001.

Jin, F-F. and An, S-I.: Thermocline and Zonal Adventive Feedbacks within the Equatorial Ocean Recharge Oscillator Model for ENSO, Geophysical Research Letters, 26, 19, 2989-2992, 1999.

Jury, M. R., Pathack, B., and Parker, B.: Climatic determinants and statistical prediction of tropical cyclone days in the southwest Indian Ocean, Journal of Climate, 12, 1738-1746, 1999.

Kalnay, E., Kanamitsu, M., Kistler, R., Collins, W., Deaven, D., Gandin, L., Iredell, M., Saha, S., White, G., Woollen, J., Zhu, Y., Chelliah, M., Ebisuzaki, W., Higgins, W., Janowiak, J., Mo, K. C., Ropelewski, C., Wang, J., Leetmaa, A., Reynolds, R., Jenne, R., and Joseph, D.: The NCEP/NCAR 40-Year Reanalysis Project, Bulletin of the American Meteorological Society, 77, 437-471, 1996.

Kawamiya, M. and Oschlies, A.: Formation of a basin-scale surface chlorophyll pattern by Rossby waves, Geophysical Research Letters, 28, 4139-4142, 2001.

Keerth, M. G., Lengaigne, M., Vialard, J., de Boyer Montégut, C., and Muraleedharan, P. M.: Interannual variability of the Tropical Indian Ocean mixed layer depth, Climate Dynamics, 40, 743-759, doi: 10.1007/s00382-012-1295-2, 2012.

Klein, S. A., Soden, B. J., and Lau, N.-G.: Remote Sea Surface Temperature Variations during ENSO: Evidence for a Tropical Atmospheric Bridge, Journal of Climate, 12, 917-932, 1999.

Koné, V., Aumont, O., Lévy, M., and Resplandy, L.: Physical and Biogeochemical Controls of the Phytoplankton Seasonal Cycle in the Indian Ocean: A Modeling Study, in: Indian Ocean Biogeochemical Processes and Ecological Variability, vol. 185, edited by: J. D. Wiggert, R. R. Hood, S. Wajih, A. Naqvi, K. H. Brink, and S. L. Smith, p. 350, 2009.

Lau, N.-G. and Nath, M. J.: Impact of ENSO on the Variability of the Asian-Australian Monsoons as simulated in GCM Experiments, Journal of Climate, 13, 4287-4309, 2000.

Lengaigne, M. and Vecchi, G. A.: Contrasting the termination of moderate and extreme El Niño events in coupled general circulation models, Climate Dynamics, 35, 299-313, doi: 10.1007/s00382-009-0562-3, 2010.

Lengaigne, M., Boulanger, J.-P., Menkes, C., and Spencer, H.: Influence of the seasonal cycle on the termination of El Niño events in a coupled general circulation model, Journal of Climate, 19, 1850–1868, doi:10.1175/JCLI3706.1, 2006.

Lengaigne, M., Boulanger, J.-P., Menkes, C., Masson, S., Madec, G., and Delecluse, P.: Ocean response to the March 1997 Westerly Wind Event, Journal of Geophysical Research, 107, 8015, doi:10.1029/2001JC000841, 2002.

Lengaigne, M., Hausmann, U., Madec, G., Menkes, C., Vialard, J., and Molines, J.: Mechanisms controlling warm water volume interannual variations in the equatorial Pacific: diabatic versus adiabatic processes, Climate Dynamics, 38, 1031–1046, doi:10.1007/s00382-011-1051-z, 2012.

Lévy, M., Shankar, D., André, J.-M., Shenoi, S. S. C., Durand, F., and de Boyer Montégut, C.: Basin-wide seasona evolution of the Indian Ocean's phytoplankton blooms, Journal of Geophysical Research, 112, C12014, doi:10.1029/2007JC004090, 2007.

Li, T., Wang, B., Chang, C.-P., and Zhang, Y.: A Theory for the Indian Ocean Dipole-Zonal Mode, Journal of Atmospheric Sciences, 60, 2119-2135, 2003.

Li, T., Zhang, Y., Lu, E., and Wang, D.: Relative Role of Dynamics and Thermodynamics Processes in the Development of the Indian Ocean Dipole, Journal of the Atmospheric Sciences, 2002.

Longhurst, A.R.: Ecological Geography of the Sea, 2nd edition Academic Press, 560 pp., Amsterdam, 2006.

Ludwig, W., Probst, J.-L., and Kempe, S.: Predicting the oceanic input of organic carbon by continental erosion, Global Biogeochemical Cycles, 10, 23-41, 1996.

Marsac, F. and Le Blanc, J. L.: Oceanographic changes during the 1997–1998 El Niño in the Indian Ocean and their impact on the purse seine fishery, Indian Ocean Tuna Commission Proceedings, 2, 147–157, 1999.

Masumoto, Y. and Meyers, G.: Forced Rossby waves in the southern tropical Indian Ocean, Journal of Geophysical Research, 103, 27589-27602, 1998.

Masumoto, Y. and Yamagata, T.: Response of the Western Tropical Pacific to the Asian Winter Monsoon: The Generation of the Mindanao Dome, Journal of Physical Oceanography, 21, 1386-1398, 1991.

McCreary, JR., J. P., Kundu, P. K., and Molinari, R. L.: A numerical investigation of dynamics, thermodynamics and mixed-layer processes in the Indian Ocean, Progress in Oceanography, 31, 181-244, 1993.

McPhaden, M. J., Zebiak, S. E., and Glantz, M. H.: ENSO as an Integrating Concept in Earth Science, Science, 314, 1740–1745, doi:10.1126/science.1132588, 2006.

Ménard, F., Marsac, F., Bellier, E., and Cazelles, B.: Climatic oscillations and tuna catch rates in the Indian Ocean: a wavelet approach to time series analysis, Fisheries Oceanography, 16, 95–104, doi:10.1111/j.1365-2419.2006.00415.x, 2007.

Meyers, G., McIntosh, P., Pigot, L., and Pook, M.: The Years of El Niño, La Niña, and interactions with the tropical Indian Ocean, Journal of Climate, 20, 2872–2880, doi:10.1175/JCLI4152.1, 2007.

Monticelli, D., Ramos, J. A., and Quartly, G., D.: Effects of annual changes in primary productivity and ocean indices on the breeding performance of tropical roseate terns in the western Indian Ocean, Marine Ecology Progress Series, 351, 273-286, doi:10.3354/meps07119, 2007.

Moore, J. K., Doney, S. C., and Lindsay, K.: Upper ocean ecosystem dynamics and iron cycling in a global three-dimensional model, Global Biogeochemical Cycles, 18, GB4028, doi:10.1029/2004GB002220, 2004.

Murtugudde, R. and Busalacchi, A. J.: Interannual variability of the dynamics and thermodynamics of the tropical Indian Ocean, Journal of Climate, 12, 2300–2326, doi:10.1175/1520- 0442(1999)012<2300:IVOTDA>2.0.CO;2, 1999.

Murtugudde, R. G., McCreary, JR., J. P., and Busalacchi, A. J.: Oceanic processes associated with anomalous events in the Indian Ocean with relevance to 1997–1998, Journal of Geophysical Research, 105, 3295–3306, doi:10.1029/1999JC900294, 2000.

Nagura, M. and McPhaden, M. J.: The dynamics of zonal current variations in the central equatorial Indian Ocean, Geophysical Research Letters, 35, L23603, doi:10.1029/2008GL035961, 2008.

New, A. L., Stansfield, K., Smythe-Wright, D., Smeed, D. A., Evans, A. J., and Alderson, S. G.: Physical and biochemical aspects of the flow across the Mascarene Plateau in the Indian Ocean, Philosophical Transactions of the Royal Society, 363, 151-168, 2005.

Nidheesh, A. G., Lengaigne, M., Vialard, J., Unnikrishnan, A. S., and Dayan, H.: Decadal and long-term sea level variability in the tropical Indo-Pacific Ocean, Climate Dynamics, 41, 381–402, doi:10.1007/s00382-012-1463-4, 2013.

Nigam, S. and Shen, H.-S.: Structure of Oceanic and Atmospheric Low-Frequency Variability over the tropical Pacific and Indian Oceans. Part I: COADS observations, Journal of Climate, 6, 657-676, 1993.

Pan, H. Y. and Oort, A. H.: Global climate variations associated with sea surface temperature anomalies in the eastern equatorial Pacific Ocean for the 1958-1973 period, Monthly Weather Review, 111, 1244-1258, 1983.

Pedlosky, J: Ocean circulation theory. New York: Springer, 1998.

Perigaud, C. and Delecluse, P.: Interannual Sea Level Variations in the Tropical Indian Ocean from Geosat and Shallow Water Simulations, Journal of Physical Oceanography, 23, 1916-1934, 1992.

Prasad, T. G. and McClean, L.: Mechanisms for anomalous warming in the western Indian Ocean during pole mode events, Journal of Geophysical Research, 109, C02019, doi:10.1029/2003JC001872, 2004.

Qasim, S. Z.: Biological productivity of the Indian Ocean, Indian Journal of Marine Science, 6, 122-137, 1997.

Rao, S. A. and Behera, S. K.: Subsurface influence on SST in the tropical Indian Ocean: structure and interannual variability, Dynamics of Atmospheres and Oceans, 39, 103–135, doi:10.1016/j.dynatmoce.2004.10.014, 2005.

Rao, S. A., Behera, S. K., Masumoto, Y. and Yamagata, T.: Interannual subsurface variability in the tropical Indian Ocean with a special emphasis on the Indian Ocean Dipole, Deep-Sea Research, Part II, 49, 1549–1572, doi:10.1016/S0967-0645(01)00158-8, 2002.

Reason, C. J. C., Allan, R. J., Lindesay, J. A., and Ansell, T. J.: ENSO and climatic signals across the Indian Ocean Basin in the global context: Part I, interannual composite patterns, International Journal of Climatology, 20, 1285–1327, doi:10.1002/1097-0088(200009)20:11<1285::AID-JOC536>3.0.CO;2-R, 2000.

Resplandy, L., Vialard, J., Lévy, M., Aumont, O., and Dandonneau, Y.: Seasonal and intraseasonal biogeochemical variability in the thermocline ridge of the southern tropical Indian Ocean, Journal of Geophysical Research, 114, C07024, doi:10.1029/2008JC005246, 2009.

Roullet, G. and Madec, G.: Salt conservation, free surface, and varying levels: a new formation for ocean general circulation models, Journal of Geophysical Research, 105, 23927-23942, 2000.

Saji, N. H. and Yamagata, T.: Possible impacts of Indian Ocean Dipole mode events on global climate, 25, 151-169, 2003.

Saji, N. H., Goswami, B. N., Vinayachandran, P. N., and Yamagata, T.: A dipole mode in the tropical Indian Ocean, Nature, 401, 360–363, 1999.

Schott, F. A. and McCreary, JR., J. P.: The monsoon circulation of the Indian ocean, Progress in Oceanography, 51, 1-123, 2001.

Schott, F. A., Dengler, M., and Schoenefeldt, R.: The shallow overturning circulation of the Indian Ocean, Progress in Oceanography, 53, 57-103, 2002.

Schott, F. A., Xie, S.-P., and McCreary, JR., J. P.: Indian Ocean circulation and climate variability, Reviews of Geophysics, 47, RG1002, doi:10.1029/2007RG000245, 2009.

Shinoda, T., Hendon, H. H., and Alexander, M. A.: Surface and subsurface dipole variability in the Indian Ocean and its relation with ENSO, Deep-Sea Research, Part I, 51, 619-635, doi:10.1016/j.dsr.2004.01.005 2004.

Siedler, G., Church, J., and Gould, J.: Ocean Circulation and Climate: Observing and Modelling the Global Ocean, International Geophysics Series, 77, 136-139, 2001.

Siedler, G., Zangenberg, N., and Onken, R.: Seasonal Changes in the Tropica Atlantic Circulation: Observation and Simulation of the Guinea Dome, Journal of Geophysical Research, 97, 703-715, 1992.

Song, Q., Vecchi, G. A., and Rosati, A. J.: Indian Ocean variability in the GFDL coupled climate model, Journal of Climate, 20, 2895–2916, doi:10.1175/JCLI4159.1, 2007.

Sun, S., Lan, J., and Wang, Y.: Variations of SST and Thermocline Depth in the Tropical Indian Ocean During Indian Ocean Dipole Events, Journal of Ocean University of China, 2, 120-127, doi:10.1007/s11802-010-00129-2, 2010.

Susanto, R. D., Gordon, A. L., and Sprintall, J.: Observations and proxies of the surface layer Throughflow in Lombok Strait, Journal of Geophysical Research, 112, C03S92, doi:10.1029/2006JC003790, 2007.

Suzuki, T., Sakamoto, T. T., Nishimura, T., Okada, N., Emori, S., Oka, A., and Hasumi, H.: Seasonal cycle of the Mindanao Dome in the CCSR/NIES/FRCGC atmosphere-ocean coupled model, Geophysical Research Letters, 32, L17604, doi:10.1029/2005GL023666, 2005.

Takahashi, T., Broecker, W. S., and Langer, S.: Redfield Ration Based on Chemical Data from Isopycnal Surfaces, Journal of Geophysical Research, 90, 6907-6924, 1985.

Tegen, I. and Fung, I.: Contribution to the atmospheric mineral aerosol load from land surface modification, Journal of Geophysical Research, 100, 18707-18726, 1995.

Tokinaga, H. and Tanimoto, Y.: Seasonal transition of SST anomalies in the tropical Indian Ocean during El Niño and Indian Ocean Dipole years, Journal of Meteorological Society of Japan, 82, 1007-1018, 2004.

Tomczak, M. and Godfrey, J. S.: Regional Oceanography: An Introduction, 2nd improved edition, 390 pp., Daya Publication House, Delhi, India, 2003.

Tozuka, T., Kagimoto, T., Masumoto, Y., and Yamagata, T.: Simulated Multiscale Variations in the Western Tropical Pacific: The Mindanao Dome Revisited, Journal of Physical Oceanography, 32, 1338-1359, 2002.

Tozuka, T., Yokoi, T., and Yamagata, T.: A modeling study of interannual variations of the Seychelles Dome, Journal of Geophysics Resesearch, 115, 04005, doi:10.1029/2009JC005547, 2010.

Trenary, L. L. and Han, W.: Intraseasonal-to-Interannual Variability of South Indian Ocean Sea Level and Thermocline: Remote versus Local Forcing, Journal of Physical Oceanography, 42, 602-627, doi: 10.1175/JPO-D-11-084.1, 2012.

Trenberth, K. E., Olson, J. G., and Large, W. G.: A global ocean wind stress climatology based on ECMWF analyses, Climate and Global Dynamics Division, National Center for Atmospheric Research, Boulder, Colorado, 1989.

Trenberth, K. E.: The definition of El Niño, Bulletin of the American Meteorological Society, 78, 2771–2777, 1997.

Umatani, S. and Yamagata, T.: Response of the Eastern Tropical Pacific to Meridional Migration of the ITCZ: The Generation of the Costa Rica Dome, Journal of Physical Oceanography, 21, 346-363, 1991.

Ummenhofer, C. C., Gupta, A. S., and England, M. H.: Contributions of Indian Ocean Sea Surface Temperatures to Enhanced East African Rainfall, Journal of Climate, 22, 993-1013, doi: 10.1175/2008JCLI2493.1, 2009.

Uppala, S. M., KÅllberg, P. W., Simmons, A. J., Andrae, U., Bechtold, V. D. C., Fiorino, M., Gibson, J. K., Haseler, J., Hernandez, A., Kelly, G. A., Li, X., Onogi, K., Saarinen, S., Sokka, N., Allan, R., Andersson, E., Arpe, K., Balmaseda, M., Beljaars, A., van de Berg, L., Bidlot, J., Bormann, N., Caires, S., Chevallier, F., Dethof, A., Dragosavac, M., Fisher, M., Fuentes, M., Hagemann, S., Holm, E., Hoskins, B., Isaksen, L., Janssen, P., Jenne, R., Mc- Nally, A., Mahfouf, J.-F., Morcrette, J.-J., Rayner, N., Saunders, R., Simon, P., Sterl, A., Trenberth, K., Untch, A., Vasiljevic, D., Viterbo, P., and Woollen, J.: The ERA-40 re-analysis, Quarterly Journal of the Royal Meteorological Society, 131, 2961–3012, 2005.

Van Oldenborgh, G. J., Philip, S. Y., and Collins, M.: El Niño in a changing climate: a multi-model study, Ocean Science, 1, 85-95, 2005.

Vecchi, G. A. and Harrison, D. E.: Interannual Indian rainfall variability and Indian Ocean sea surface temperature anomalies, Earth's Climate: The Ocean-Atmosphere Interaction, Geophysical Monograh Series, 147, 247-260, 2004.

Venzke, S., Latif, M., and Villwock, A.: Coupled GCM ECHO-2. Part II: Indian Ocean response to ENSO, Journal of Climate, 13, 1371– 1383, 2000.

Vialard, J., Duvel, J. P., Mcphaden, M. J., Bouruet-Aubertot, P., Ward, B., Key, E., Bourras, D., Weller, R., Minnett, P., Weill, A., Cassou, C., Eymard, L., Fristedt, T., Basdevant, C., Dandonneau, Y., Duteil, O., Izumo, T., de Boyer Montégut, C., Masson, S., Marsac, F., Menkes, C., and Kennan, S.: Cirene: Air–Sea Interactions in the Seychelles–Chagos Thermocline Ridge Region, Bulletin of the American Meteorological Society, 90, 45–61, 2009.

Vinayachandran, P. N. and Saji, N. H.: Mechanisms of South Indian Ocean intraseasonal cooling, Geophysical Research Letters, 35, L23607, doi:10.1029/2008GL035733, 2008.

Vinayachandran, P. N. and Yamagata, T.: Monsoon Response of the Sea around Sri Lanka: Generation of Thermal Domes and Anticyclonic Vortices, Journal of Physical Oceanography, 28, 1946-1960, 1998.

Vinayachandran, P. N., Iizuka, S., and Yamagata, T.: Indian Ocean dipole mode events in an ocean general circulation model, Deep-Sea Research, Part II, 49, 1573–1596, doi:10.1016/S0967- 0645(01)00157-6, 2002.

Waconge, S. and Piton, B.: The near-surface circulation in the north-eastern corner of the South Atlantic Ocean, Deep-Sea Research, Part I, 39, 1273-1298, 1992.

Wallace, J. M., Rasmusson, E. M., Mitchell, T. P., Kousky, V. E., Sarachik, E. S., and von Storch, H.: On the structure and evolution of ENSO-related climate variability in the tropical Pacific: Lessons from TOGA, Journal of Geophysical Research, 103, 14241-14259, 1998.

Webster, P. J., Moore, A. M., Loschnigg, J. P., and Leben, R. R.: Coupled ocean-atmosphere dynamics in the Indian Ocean during 1997-98, Nature, 401, 356–60, doi:10.1038/43848, 1999.

Wiggert, J. D., Murtugudde, R. G., and Christian, J. R.: Annual ecosystem variability in the tropical Indian Ocean: Results of a coupled bio-physical ocean general circulation model, Deep-Sea Research, Part II, 53, 644–676, doi:10.1016/j.dsr2.2006.01.027, 2006.

Wiggert, J. D., Vialard, J., and Behrenfeld, M. J.: Basinwide modification of dynamical and biogeochemical processes by the positive phase of the Indian Ocean Dipole during the SeaWiFS era, in: Indian Ocean Biogeochemical Processes and Ecological Variability, vol. 185, edited by: J. D. Wiggert, R. R. Hood, S. Wajih, A. Naqvi, K. H. Brink, and S. L. Smith, p. 350, 2009.

Woodberry, K. E., Luther, M. E., and O'Brien, J. J.: The wind-driven seasonal circulation in the southern tropical Indian Ocean, Journal of Geophysical Research, 94, 17985-18002, 1989.
Wyrtki, K.: An equatorial jet in the Indian Ocean, Science, 181, 262–264, 1973.

Xie, P. and Arkin, P. A.: Global precipitation: A 17-year monthly analysis based on gauge observations, satellite estimates, and numerical model outputs, Bulletin of the American Meteorological Society, 78, 2539–2558, 1997.

Xie, S.-P.: A dynamic Ocean-Atmosphere Model of the Tropical Atlantic Decadal Variability, Journal of Climate, 12, 64-70, 1999.

Xie, S. P., Annamalai, H., Schott, F. A., and McCreary JR., J. P.: Structure and Mechanism of South Indian Ocean Climate Variability, Journal of Climate, 15, 864-878, 2002.

Xie, S. P., Hu, K., Hafner, J., Tokinaga, H., Du, Y., Huang, G., and Sampe, T.: Indian Ocean Capacitor Effect on Indo-Western Pacific Climate during the summer following El Niño, Journal of Climate, 22, 730-747, doi: 10.1175/2008JCLI2544.1, 2009.

Yamagata, T. and Iizuka, S.: Simulation of the tropical thermal domes in the Atlantic: A seasonal cycle, Journal of Physical Oceanography, 25, 2129-2139, 1995.

Yamagata, T., Behera, S. K., Luo, J. J., Masson, S., Jury, M. R., and Rao, S. A.: Coupled ocean-atmosphere variability in the tropical Indian Ocean, Geophysical Monograh Series, 147, 189–211, doi:10.1029/147GM12, 2004.

Yamagata, T., Behera, S. K., Rao, S. A., Guan, Z., Ashok, K., and Saji, H. N.: The Indian Ocean dipole: A physical entity, CLIVAR Exchange, 24, 15-18, 2002.

Yokoi, T., Tozuka, T., and Yamagata, T.: Seasonal Variation of the Seychelles Dome, Journal of Climate, 21, 3740–3754, doi:10.1175/2008JCLI1957.1, 2008.

Yu,W., Xiang, B., Liu, L., and Liu, N.: Understanding the origins of interannual thermocline variations in the tropical Indian Ocean, Geophysical Research Letters, 32, 24706, doi:10.1029/2005GL024327, 2005.